UNIVERSITY OF Southampton

University of Southampton Research Repository
ePrints Soton

Copyright © and Moral Rights for this thesis are retained by the author and/or other copyright owners. A copy can be downloaded for personal non-commercial research or study, without prior permission or charge. This thesis cannot be reproduced or quoted extensively from without first obtaining permission in writing from the copyright holder/s. The content must not be changed in any way or sold commercially in any format or medium without the formal permission of the copyright holders.

When referring to this work, full bibliographic details including the author, title, awarding institution and date of the thesis must be given e.g.

AUTHOR (year of submission) "Full thesis title", University of Southampton, name of the University School or Department, PhD Thesis, pagination

http://eprints.soton.ac.uk

# COMBUSTION OSCILLATIONS IN A DUCTED BURNER

by

Ian Gregory Campbell

A Thesis submitted for the degree of Doctor of Philosophy

in the Faculty of Engineering and Applied Science

Department of Aeronautics and Astronautics

University of Southampton

October 1982

University of Southampton

ABSTRACT

FACULTY OF ENGINEERING AND APPLIED SCIENCE
DEPARTMENT OF AERONAUTICS AND ASTRONAUTICS

Doctor of Philosophy

# COMBUSTION OSCILLATIONS IN A DUCTED BURNER

by I.G. Campbell

Unsteady combustion, confined within a duct, is a poorly understood and incompletely documented phenomenon. This is particularly true of the violent, low frequency combustion oscillation encountered in gas turbine reheat systems, commonly referred to as reheat buzz. This thesis describes an investigation, both experimental and theoretical, of oscillatory premixed propane-air combustion in a ducted burner. A wide range of experimental techniques is employed to provide time-resolved information on flame motion and the pressure field within the combustor.

A detailed parametric study is reported of both high frequency acoustic resonances and the large amplitude, low frequency buzz oscillation in which the effects of burner configuration, equivalence ratio and flow velocity are assessed. Important differences are observed in the dependence on these parameters of clearly identified longitudinal modes of oscillation ($\gtrsim$150 Hz) and the low frequency buzz ($\lesssim$100 Hz). These suggest important differences in the basic mechanisms which sustain these oscillations, a feature confirmed by frame-by-frame analysis of high speed cine Schlieren photographs.

A simple control volume model of low frequency oscillatory burning is developed which permits important features of the parametric study to be reproduced. Two columns of unburnt mixture and fully burnt gas are linked by a simplified flame zone. Conservation of mass and momentum, supplemented by an empirical phase relationship between pressures at the chamber inlet and exit, provide a plausible simulation without incorporating a detailed model of the unsteady heat release. Possible refinements to this model in respect of turbulent burning are suggested in the light of the insight into the flow/heat release interaction provided by the experiments.

ACKNOWLEDGEMENTS

I would like to extend my gratitude to my supervisors, Professor K.N.C. Bray, Dr. C.L. Morfey, and Dr. J.B. Moss, for their guidance, patience and encouragement through this work. I am also indebted to my colleagues for their constructive criticism and more encouragement, in particular, Dr. I.G. Shepherd and Dr. F.C. Weller.

My thanks go out to the office and technical staff of the Department of Aeronautics and Astronautics, without whose help and guidance the experimental part of this study would have been difficult to accomplish.

I would also like to thank the Science Research Council for their financial support through contract B/RG/7690.1 and Rolls Royce Derby and National Gas Turbine Establishment for their support.

Finally, my thanks goes to Mrs. Maureen Strickland for the excellent job of translating the Canadian language to English and typing this thesis.

TABLE OF CONTENTS

## LIST OF SYMBOLS

| | |
|---|---|
| $A$ | amplitude of a pressure wave ($P^-$) travelling into the mean gas flow |
| $B$ | amplitude of a pressure wave ($P^+$) travelling with the mean gas flow |
| $b$ | ratio of vee-gutter cross-sectional area to the duct cross-sectional area |
| $c$ | local speed of sound |
| $c_b$ | speed of sound in the burnt gas |
| $c_u$ | speed of sound in the unburnt gas |
| $D$ | height of the flame stabilizer |
| $f$ | frequency of oscillation |
| $G$ | arbitrary amplitude of a RMS standing pressure wave |
| $j$ | $\sqrt{-1}$ |
| $k_b$ | modified wave number in burnt gas |
| $k_u$ | modified wave number in unburnt gas |
| $L$ | total effective length of the combustion chamber (including end correction terms) |
| $L_c$ | cold duct length (measured from the combustion chamber inlet plane to the flame stabilizer) |
| $L_h$ | hot duct length (measured from the flame stabilizer to the combustion chamber exit plane) |
| $L_1$ | total length of the unburnt gas column |
| $L_2$ | total length of the burnt gas column |
| $\ell$ | total length of the flame zone |
| $M$ | local flow Mach number |
| $M_b$ | Mach number of the burnt gas flow |
| $M_u$ | Mach number of the unburnt gas flow |
| $\dot{m}_i$ | mass flow at position i |
| $\bar{\dot{m}}_i$ | mean mass flow at position i |
| $\dot{m}_i'$ | fluctuating mass flow at position i |

| | |
|---|---|
| $n$ | number of the harmonic |
| $P_i$ | static pressure at position i |
| $\bar{P}_i$ | mean static pressure at position i |
| $P_i'$ | fluctuating static pressure at position i |
| $P^+$ | pressure wave travelling with the mean flow in the duct |
| $P^-$ | pressure wave travelling against the mean flow in the duct |
| $\dot{Q}$ | heat release rate |
| $\bar{\dot{Q}}$ | mean heat release rate |
| $\dot{Q}'$ | fluctuating heat release rate |
| $S$ | duct cross-sectional area |
| $T_c$ | unburnt gas temperature |
| $T_h$ | burnt gas temperature |
| $t$ | time |
| $t_j$ | time (j'th component) |
| $U_o$ | mean inlet flow velocity |
| $\tilde{U}$ | relative amplitude of unburnt gas flow velocity fluctuations $\lvert\hat{u}_i'/\bar{u}_i\rvert$ |
| $\bar{u}$ | mean gas flow velocity |
| $u_i$ | gas flow velocity at position i |
| $\bar{u}_i$ | mean gas flow velocity at position i |
| $u_i'$ | fluctuating gas flow velocity at position i |
| $\tilde{V}$ | relative amplitude of burnt gas flow velocity fluctuations $\lvert\hat{u}_3'/\bar{u}_3\rvert$ |
| $V_b$ | burnt gas volume in $V_T$ |
| $V_T$ | total volume between position 2 and 3 (i.e., combustion zone) |
| $V_u$ | unburnt gas volume in $V_T$ |
| $V_b'$ | fluctuating burnt gas volume in $V_T$ |
| $V_u'$ | fluctuating unburnt gas volume in $V_T$ |
| $\omega$ | radian frequency of oscillation |
| $x$ | distance from combustion chamber entrance to any point in the duct |
| $\tilde{\dot{Q}}$ | relative amplitude of heat release rate fluctuations $\lvert\hat{\dot{Q}}'/\bar{\dot{Q}}\rvert$ |

| | |
|---|---|
| $y$ | distance from position 3 to any point in the burnt gas column |
| $z$ | distance from position 1 to any point in the unburnt gas column |
| $\Delta s_f$ | flame area change |
| $\Delta u_f$ | flame speed change |
| $\Delta\rho$ | gas density change |
| $\rho$ | local gas density |
| $\rho_b$ | burnt gas density |
| $\rho_u$ | unburnt gas density |
| $\nu$ | volume of the diffuser plus settling chamber |
| $\phi$ | equivalence ratio |
| $\phi_3$ | phase difference between the fluctuating velocities of position 3 relative to position 2 |
| $\phi_q$ | phase difference between the fluctuating heat release rate relative to the fluctuating velocity at position 2 |

Superscripts

| | |
|---|---|
| $\hat{\theta}$ | indicates the maximum value of quantity $\theta$ |

Subscripts

| | | |
|---|---|---|
| $\theta_i$ | i = blank | $\theta$ at an unspecified position |
| | = 1, 2, 3 | $\theta$ at position 1, 2 or 3 |
| | = f | $\theta$ at the flame front |

# LIST OF TABLES

# LIST OF FIGURES

# CHAPTER 1

# INTRODUCTION

In recent years private and industrial sectors of society have become increasingly aware and progressively less tolerant of noise production for reasons ranging from the degradation of living and working conditions through to safety hazards. In many situations, machinery or aerodynamic systems can be identified as the source, but in a number of instances combustion processes are directly or indirectly responsible.

None of these types of noise are particularly easy to control in engineering practice. However, noise produced from mechanical vibrations can often be reduced through the use of shock absorbers, vibration isolators or cyclic variation of reciprocal machinery. While aerodynamic noises are sometimes attenuated by the introduction of acoustic liners in various parts of the machinery or through the reduction of the mean flow velocity in jet streams. Unfortunately, the noise emissions from combustion processes cannot always be controlled by simple damping techniques. The high temperatures encountered in the combustion regions create a hostile environment for many possible solutions to the noise problem, with the result that work in the field of combustion noise has concentrated on studies of the fundamental processes involved in combustion noise coupling. If research in this area can identify the reasons for the noise production, then steps can be taken to design out the sources in combustors.

It is important that for combustion noise research a detailed understanding of combustion processes and their interactions with the flow and combustion chambers can be obtained in order to control and possibly eliminate some types of combustion noise.

## 1.1 Combustion and Noise

Combustion processes fall broadly into two categories; laminar and turbulent. The former type of combustion, which is not usual in practical combustors, produces little noise in comparison with the latter. Laminar burning is not however as volumetrically efficient as a turbulent flame,

so in industrial combustors to maximise the heat release in a given volume, the combustion is intentionally made turbulent, with the result that the pressure fluctuations of the turbulent burning produces noise. Moreover, if turbulent burning is confined in a combustion chamber, it is possible that the fluctuating energy released by the flame can lead to resonant pressure oscillations, sometimes of large amplitude. Thus in order to create a more efficient burner a severe noise source has been produced.

Combustion noise resulting from turbulent burning can be divided into two groups. The first is random and broadband, being directly produced by the pressure fluctuations of the turbulent combustion process. In a calculation by Bragg ( 1)* for this type of noise, the energy released by a turbo-jet, of moderate size, is approximately 60 MW, with the resulting combustion noise estimated to be 60 W. This is equivalent to hearing a 97 dB sound at 30 m from the source, or in other terms, comparable to being inside a busy subway train. In the case of the aircraft engine, the aerodynamic noise produced by the exhaust gases at take off is roughly thirty times the combustion noise, so in this situation the combustion noise is not the major problem. However, for an industrial furnace of similar power aerodynamic noises are moderate and combustion "roar" predominates. In this type of noise the energy of the pressure fluctuations is spread over the frequency spectrum with no major concentration at any particular frequency.

The second type of noise is less random, characterized by one or more dominant frequency. The combustion oscillations, which characterize this type of noise, are evident in most cases where the combustion zone is confined in a chamber or duct. The fluctuating energy released by the flame couples with the fluctuating pressure, often a chamber resonance, to set up a self-sustained combustion oscillation. In this case the acoustic energy is not broadband, but concentrated at several discrete frequencies. Two effects from this type of noise are pressure fluctuations at one or more frequencies and the possible transmission of intense pressure disturbances into nearby mechanical structures of the burner system.

---

*Numbers in brackets refer to the reference listed at the end of this study.

Mechanical vibrations in sympathy with the combustion oscillations are not unusual in combustion systems and violent pressure oscillations can induce severe stresses and fatigue in combustion chamber walls and attached mechanical components. In some instances these oscillations enhance heat transfer rates into temperatures sensitive structures causing damage through thermal loadings. Some examples of problems caused by large pressure oscillations are structural damage to the combustion chamber and exhaust systems of industrial furnaces; the cracking of rocket motor casing and splitting of attached pipe joints; and the twisting of aero-engine turbine shafts by combustion oscillations in the afterburner units of the engines. In the forementioned situations, the intended steady state combustion processes experienced pressure oscillations, which produced sympathetic vibrations in nearby mechanical structures, resulting in component damage or failure.

Emissions from the exhaust of a burner or furnace in terms of noise can be very unpleasant if undamped. Silencers and acoustic liners in the exhaust ducting can reduce high frequency oscillations to acceptable amplitude levels. Lower frequencies, however, are less easily attenuated by these methods.

Work in this thesis concentrates on the last, less random type of noise. Subsequent sections in the introductory chapter, further identify the subdivisions of this type of noise through various classifications. At the end of this survey the area directly involved in this study is reviewed with the concluding remarks of this chapter directed towards outlining the program adopted for this particular research program.

## 1.2 Classification of Combustion Instabilities

Investigations over the past few decades on combustion driven oscillations have encompassed a wide range of combustion systems. However, the various types of instabilities can be classified into three major groups as stated by Barrère (2):

1. Instabilities associated with a combustion chamber.
2. Instabilities encompassing the effects of the entire burner on the oscillation.
3. Instabilities involving only the reactants.

This classification is appropriate for solid, liquid or gaseous fuels.

The work involved in each of these groups has been both experimental and theoretical. The experimental work was designed to determine the dependence of the combustion or pressure oscillation amplitude and frequency on various flow and physical parameters of the burner design, such as inlet flow velocities, fuel-air ratio, burner rig dimensions, fuel constituents or burner component interactions. The results of the experiments gave detailed information on individual burner behaviour and data to test against theoretical models.

Theoretical work concentrated on identifying the source or sources of the oscillations and the feedback mechanism needed to sustain the instabilities. The models tried to predict the frequency, amplitude and sometimes stability ranges of the oscillations. However, problems in the understanding and incorporation of fundamental turbulent combustion-flow interactions complicates the construction of a theory. Yet a number of theoretical models have given a good account of themselves in specific areas.

In the following subsections, each class of instability is briefly examined, with a review of past research on small ducted burner instabilities.

### 1.2.1 Combustion chamber instabilities

Combustion chamber instabilities can be divided into three major groups: acoustic instability, shock wave instabilities and fluid-dynamic instabilities.

Acoustic instabilities are the most common mode of oscillation encountered in combustion chambers. These instabilities rely on the dimensions of the combustion chamber for their wavelength and the combustion process for their energy. The first recorded observation of chamber instability was by Rijke (3), who initiated an oscillation in a vertically

aligned, open-ended tube, by heating a wire gauze stretched across the diameter of the tube, a quarter of the way up the tube length. Externally heating the wire gauze using a spirit lamp, then removing the heat source, resulted in an intense sound being emitted from the tube. The intensity of the sound was noted to decrease as the wire gauze cooled. Subsequent experiments by Rijke showed that continual heating of the gauze by an electrical current produced a steady noise. Analysis of the emitted sound indicated that its frequency was nearly the fundamental organ pipe mode of the tube. Rijke postulated that a pulsing air flow was established by the heat release from the wire gauze and duct walls. The air heated by the gauze expanded and rose up the tube. On leaving the heated area of the gauze the air was cooled by the duct walls further up the tube and thus contracted. Slugs of air were heated and sequentially cooled in the tube as they rose, thus leading to sound emission from the tube. While identifying that the air movement and heat exchange were important, it was not until Rayleigh's (4) explanation that the importance of Rijke's observation became clear. Rayleigh postulated that an oscillation in the tube could be established, if heat addition to the air could be maximized at or just before the maximum amplitude of the local fluctuating pressure. The maximum heat exchange between the gauze and surrounding air depended on the motion and temperature of the flow. In the Rijke experiment, it was possible to set up a standing wave in the tube because its vertical alignment allowed air to flow past the heated gauze effecting the necessary heat exchange. The result was a feedback mechanism between the standing wave and the heated gauze. The postulate of Rayleigh's became known as the Rayleigh criterion and exists in most combustion driven oscillations.

In more recent experiments (5-8) involving combustion oscillations, the wire gauze used in the Rijke tube experiments, has been replaced by a flame stabilizer, and the initial external heating of the heat transfer element altered to a continuous energy source by the introduction of a stabilized flame. A typical experiment involves premixing fuel and air in a large mixing or plenum chamber. The mixture is then forced, often through a contraction, into a combustion chamber and ignited. The burning gas is usually stabilized in the wake of a cylindrical rod, vee-gutter or disc. The burnt gas is finally expelled from the chamber by the mean flow into the atmosphere. For most experiments, the combustion

chamber ends (both inlet and outlet) are well defined as either open or closed. The result of combustion in these chambers was the stimulation of organ pipe type oscillations that in frequency could be correlated to the length of the combustion chamber and appeared to behave in accordance with the Rayleigh criterion.

Organ pipe acoustic instabilities are not only found in small tube burners, they are also present in large industrial furnaces. Excitation of acoustic modes in one furnace (9) was found to be caused by vortex shedding from an impeller inside the burner head. Matching of the vortex shedding frequency to an acoustic chamber resonance and burner heat release, produced a strong standing wave across the breadth of the furnace. Fortunately, in this case redesigning the burner head decoupled the vortex shedding from the acoustic mode, eliminating the oscillation.

Similar acoustic modes can be excited in liquid and solid propellent combustion motors (10-13). Here mid-range frequency oscillations (100-1000 Hz) are usually the result of coupling between the longitudinal standing pressure waves along the axis of the combustion chamber and the burning propellent. Although for solid fuel motors the coupling can be with the fluctuating gas velocity at the surface of the burning propellent, not necessarily the local fluctuating pressure. In severe combustion oscillations of liquid rockets, the sinusoidal pressure waves in time become shock waves, with the result that a shock wave returning to the fuel injectors not only effects the heat release of the combustion, but can also interfere with injection of fuel into the chamber. Shock wave instabilities behave in a similar manner to longitudinal acoustic modes, but exhibit higher amplitude pressure fluctuations (12-13).

Higher frequencies (above 1000 Hz) in both solid and liquid fuel motors are attributed to radial (transverse) and circumferential modes. These modes have been found to couple strongly with the pressure-heat release interaction.

The last type of chamber instability is due to fluid-dynamic oscillations. This instability is often characterized by vortex formation at or near the flame stabilizer. In a ducted burner with a flame stabilizer , a rearward facing step, vortex formation at the trailing edge of the step dominated the flame growth (14-16); schlieren cine photographs revealed large vortices forming in the shear layer between

the burnt and unburnt gas flows. Counter rotating vortices, one in the shear layer and a second in the burnt gas zone, twist the flame into discrete pockets which are swept down the chamber by the mean flow. The sequence of events appears to be one vortex grows and detaches from the top of the trailing edge of the step, while a second vortex of reverse circulation grows and detaches from the base of the step. The two vortices follow one another in the mean flow and at one of the interfaces between the two vortices the unburnt gas is drawn into the burnt gas region. By continuous vortex shedding, pairs of these vortices form pockets of burning gas.

Reheat systems on aero-engines frequently suffer from both high and low frequency combustion instabilities (often referred to as screech and buzz, respectively) (17-18). The high frequency instability due to radial acoustic oscillations are controllable through acoustic liners built into the walls of the reheat chamber which can give substantial noise attenuation (19 ). However, because of their long wavelength, low frequency oscillations cannot be effectively attenuated by the same method. These oscillations are often associated with large amplitudes, which when imposed onto mechanical components can produce the destructive results mentioned in section 1.1. Trial and error procedures have revealed that changes in the distribution of fuel-air ratio in the flow or flame stabilizer construction reduce the amplitude of the oscillation, but do not necessarily eliminate it (20 ).

At the moment, there does not appear to be a theory which can predict this last mode of oscillation, buzz, or even enough information from experiments to isolate the parameters that contribute to the instability. A number of suggestions has been made for the mechanism ranging from acoustic standing waves and vortex shedding to fuel feed system instabilities. This region of combustion instabilities in particular is lacking in experimental data and theoretical modelling.

### 1.2.2 System instabilities

System instabilities involve the interaction of the combustion process with systems external to the combustion chamber for example fuel or air supplies, exhaust pipes, plenum chamber, etc.

Undamped oscillations in feed lines for fuel or combustible mixtures can lead to oscillations in the combustion chamber (21-23). A pressure fluctuation caused by a flow disturbance at the burner head in the combustion chamber, can feed back into the fuel supply line. If undamped, the pressure pulse will travel the length of the line to a point of reflection, then return along the same path to the burner head. The arrival of the pressure fluctuation at the burner head increases the fuel flow into the combustion chamber. If the extra fuel burns in phase with a maximum pressure fluctuation in the combustion chamber, the new pressure pulse developed by the burning of the extra fuel feeds back into the fuel line and repeats the cycle.

Similar feedback loops have been identified in industrial burners (24-27). The theoretical modelling used in these cases is broadly based on control system analysis, extending from the fuel injectors to the flue exit. Each element in the system (e.g., inlet pipes, burner nozzles, combustion chamber, exhaust stack, etc.) is connected to adjoining elements by means of a transfer function. The result is a method of calculating the unstable frequencies for a system geometry. Although the analysis can be useful, a problem arises in the specification of a transfer function for the combustion region. Much work has been done to identify this particular function (28 , 29 ), with varying degrees of success. However, the problem still remains that not enough is known about the combustion region and until there is, this type of analysis will have limitations.

Another type of system instability is that of a Helmholtz resonator (30). By analogy with a spring-mass vibrator, with the plenum chamber of the burner acting as a spring, and the gas in the combustion chamber behaving as a mass, with the additional criterion that there is sufficient area change between the cavity and combustion chamber, then oscillations can be induced. The energy feedback mechanism would involve the cavity inducing a high pressure fluctuation in the combustion chamber at the time of maximum heat release, thereby allowing for the cavity to recompress and continue the oscillation. It would not appear that this form of oscillation is prevalent in many situations, but it cannot be ignored.

System instabilities are complicated because of the numerous components that constitute a complete system, and the necessity for a complete description of the interaction of one component with another.

### 1.2.3 Reactant instability

Reactant instabilities come solely from the combustion of the reactants and not from the surrounding environment. Effects of the reactants on instabilities have been observed in solid fuel rocket motors (31), where the addition of metallic particles in the fuel attenuates high-frequency oscillations. Unfortunately, it enhances the chance of low frequency oscillations occurring.

The solid particles accumulate on the surface of the burning propellant and agglomerate into larger particles at a distance from the burning surface. By remaining on the surface of the propellant, the particles interfere with the burning rate and agglomerating at a distance from the surface they release heat away from the major combustion region. The result is a low frequency destabilization of the combustion.

Only in a few instances is this instability of any concern and for this project in particular, it is believed not to have any relevance.

## 1.3 Past Investigations on Small Ducted Burners

Investigations into combustion oscillations over the past few decades have been made using small ducted burners. Their compact size, and apparent similarity in the types of combustion oscillations experienced to those in practical furnaces and aero-engines makes them ideal laboratory experimental rigs. The investigations on these burners have concerned two phenomena, mentioned in section 1.2.1, acoustic and destructive oscillations. In the following two subsections, the results of investigations into these types of oscillations and their associated theories are examined.

### 1.3.1 Acoustic oscillations

After the work of Rijke and Rayleigh on what may be described as a pseudo, small-ducted burner, a number of investigators have concentrated on employing and improving Rayleigh's conclusions concerning Rijke's thermo-resonances. Experiments were constructed to examine the acoustic properties of the burners in more detail, while the theories became more precise in their description of the coupling between the heat source and flow pulsations.

Illustrated in Fig. 1.1 are schematic diagrams of several burner designs used in recent investigations into acoustically driven combustion oscillations. The simplest type of burner (a), reminiscent of the Rijke tube, is a length of tube or rectangular pipe through which a mixture of fuel and air flows. The downstream end of the tube is usually open to the atmosphere, while the upstream end is either connected to a large plenum chamber or is acoustically closed, by, for example a choked plate which would pass fuel and air through, but arrests acoustic waves. The combustion process takes place in the wake of a flame stabilizer set at some point in the duct (5-7). Another type of burner (b), supplies the fuel-air mixture through a perforated plate from an upstream tube into a combustion chamber. The combustible mixture is ignited and stabilized on the downstream side of the perforated plate. The burnt gas flows out of the combustion chamber into the atmosphere (21, 32). The last burner (c), consists of an outer tube, open at both ends, with a small "bunsen" burner mounted inside. The only combustion in this burner is the bunsen flame. The burnt gas exits through the outer tube to atmosphere by virtue of its buoyancy (21).

The resulting noise produced by these small burners is characterized by discrete frequencies, stimulated by acoustic resonances. The method of sustained resonance for each burner is slightly different. For example, in type (a) burner acoustic standing waves for the complete length of the duct are stimulated initially by aerodynamic noise. Since there are a number of harmonics to the fundamental mode present in the duct, it is likely that one or more mode will have maximum fluctuating pressure amplitudes in the combustion zone. The transfer of energy from the flame to the pressure field amplifies the acoustic standing waves. In time an energy balance is obtained between the energy input to the

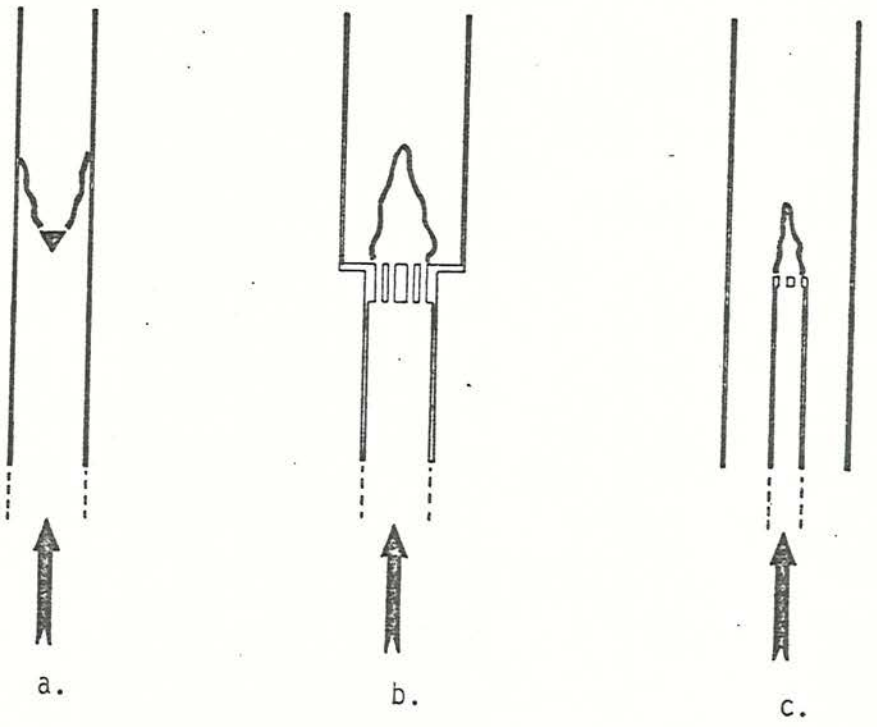


Fig. 1.1 Schematic diagrams of various burner designs

acoustic waves and the energy lost by the waves from the ends of the duct.

In burner (b), two sets of standing waves exist, one in the supply tube and another in the combustion chamber. If the solid area of the perforated plate is large compared to the open area, then the combustion chamber can behave as a single closed end pipe stimulating a quarter standing wave along its length. However, as the maximum amplitude of the fluctuating pressure will always be at the face of the perforated plate, it is possible to affect the fuel flow into the combustion chamber, thereby linking the supply pipe acoustics to the combustion chamber (21). If the solid area is small, then this system reverts to type (a), but if the area is roughly half the available area then the supply tube quarter wave and combustion chamber half wave interact, becoming intense when the frequencies of the two resonances match (6).

The last burner (c) is a combination of the previous two. Sets of standing waves exist in both the outer tube and bunsen burner. Depending on the position of the flame in the outer tube, a resonance can occur whereby the oscillations in the outer tube coincide with multiples of those in the bunsen burner. A pressure pulse in the outer tube is transmitted into the bunsen burner, where it travels the length of the chamber, reflects, and returns to impinge on the burner head. Extra fuel is forced through the head and, after a time delay, burnt. If the ignition of the extra fuel occurs at a maximum amplitude of the fluctuating pressure in the outer tube, then the resulting over-pressure amplifies the outer tube oscillations and reflects back into the bunsen burner continuing the cycles (21).

Experimental results from these burners indicated that acoustic resonances were connected to the combustion oscillations. Point measurements using microphones of the noise from the burners identified the predominant resonant frequencies. Comparisons of these frequencies to duct length indicated that for a tube burner, simple acoustic relationships for the duct length accounted for the measured frequencies (5, 6),

$$f = \frac{nc}{2L}$$

where $c$ = local speed of sound

$n$ = harmonic mode number

$L$ = total length of duct

$$= L_c + \sqrt{\frac{T_c}{T_h}}\, L_h$$

with $L_c$ = cold length of duct
$L_h$ = hot length of duct
$T_c$ = cold gas temperature
$T_h$ = hot gas temperature

Conclusive evidence of the resonant standing waves was found by measurements from a series of wall mounted pressure transducers in the combustion chamber. Examination of the spectrum from each probe and plotting the RMS pressure amplitude for a given resonant frequency revealed the profile of the standing wave (6).

General results of these burners showed that the resonant frequencies lowered as duct length increased; noise levels dropped as the equivalence ratio moved away from unity; and the noise level increased as the flow velocity increased.

Theoretical modelling of acoustic combustion oscillations follows two types of descriptions. The first is a time of travel approach, where the reciprocal of the time taken for an acoustic disturbance to travel the full length of the burner and return to the starting point is the fundamental acoustic frequency. The hot lengths in the burner are converted into scaled equivalent cold lengths. The results are reminiscent of simple acoustic resonant frequency solutions (5, 6). These have proven to be remarkably accurate in predicting frequencies, without involving the cumbersome details of combustion. However, since no emphasis is given to the combustion process and energy balances, this type of model is unable to predict the amplitudes of these disturbances.

The second type of model is based upon duct acoustics and combustion-acoustic interactions. On either side of the flame zone, the burner behaves as separate acoustic systems. In order to connect both parts of the burner around the flame, some modelling of the interaction between pressure and combustion is required. Generally, most investigators have identified the heat release fluctuations, $Q'$, as coupled to the flame area, flame speed and/or gas density changes (7, 21, 24, 32-34).

$$Q' \propto Q'(\Delta s_f, \Delta u_f, \Delta \rho)$$

$\Delta s_f$ = flame area changes
$\Delta u_f$ = flame speed changes
$\Delta \rho$ = density changes.

Not all terms are used in each model.

Using a relationship based on the above approximation in conjunction with the conservation equations (mass, momentum and energy) both sides of the flame can be coupled to complete the model. The exactness of the model depends on the ability of Q' to explain the physical combustion process. For most of these models the results are good, in predicting the resonant frequencies.

The underlining feeling acquired by examining these models is that more work is needed in producing a better understanding of heat release fluctuations and in the cases of complex burner designs, more detail in the acoustic behaviour in the various sections of the burner.

### 1.3.2 Non-acoustic oscillations

In small ducted burners of type (a), described in section 1.3.1, a second type of oscillation is sometimes present. The name of the oscillation varies from investigator to investigator, i.e., non-acoustic, reheat type, buzz, high amplitude, low frequency, etc., but the phenomena being referred to is generally a low frequency, high amplitude, combustion driven oscillation.

The experimental burners used in the various research programs alter in detail one from the others, but in general they are blow down, ducted burners of lengths ranging from 0.3 m (35) to 4.8 m (36). The fuels used are primarily propane or ethylene, mixed with air. The flame stabilizers are discs, vee-gutters or steps.

Before summarizing the results of the experiments and mentioning possible reasons for the oscillations, it is worth commenting on the frequency range that results from these experiments. The observed

frequencies that investigators have found extend from 20-500 Hz, depending on the rig. A duct of length 0.3 m produces acoustic oscillations at frequencies many times that of the non-acoustic oscillations, thus there is no ambiguity in the type of oscillation. Unfortunately, a duct of 4.8 m produces longitudinal modes of the same order as non-acoustic oscillations. Thus the data presented (36) complicates any evaluation that would identify the type of oscillation. It could be that at these low frequencies and long ducts both types coincide and therefore are indistinguishable.

High speed cine photographs (∿6000 frames per second), have shown the flame movement during these oscillations around both a vee-gutter and a step stabilizer (16, 37). At the same instant, pressure and velocity measurements in the inlet flow, upstream of the flame show that as the flame swells during part of a buzz cycle, the forward (upstream) movement of the flame accompanies a decrease in the inlet flow velocity, followed, $\pi/2$ out of phase, by a decrease in the local pressure. As the forward flame motion subsides and the flame moves back down the duct, the inlet flow velocity increases, followed by the pressure (37).

Pressure measurements in the unburnt gas region showed that increasing or decreasing the equivalence ratio of the flow away from the region 1.0-1.2, decreased both amplitude and frequency of the oscillation (35, 38). Increasing the inlet flow velocity decreased the frequency for a fixed duct geometry and equivalence ratio (35). While increasing the hot length of duct (section of duct from the stabilizer to duct exit), decreased the frequency in one investigation (39), but increased it in another (35). In these cases the frequencies ranged from 60-200 Hz, and are not really comparable, but the trends are important for future comparisons.

With each investigation, a theory was developed to explain the feedback mechanism for the oscillations. The models ranged from acoustic longitudinal standing waves to system oscillations. Jet boundary and duct longitudinal oscillation coupling was cited as one possible mechanism. The vortex formation by the pair would increase heat release, amplifying the longitudinal mode. As long as the frequency of the natural jet boundary oscillation was near that of a duct mode, then the two modes

could couple to produce the heat release fluctuation (40) through vortex shedding increasing the flame area. It was also suggested in the same investigation that a Helmholtz resonance in the burner coupling with the jet boundary oscillation could also result in an oscillation.

Interference of the flame at the stabilizer or of the fuel at the injectors by a pressure pulse has been postulated as a coupling mechanism. An over-pressure occurring in the buzz cycle will travel both up and down the length of the burner. Any pulse moving upstream can affect the flame directly on passing the stabilizer or on its return from a reflection at the end of the duct by momentarily slowing the local flow. It can also, by impinging on the fuel injectors, reduce the fuel flow into the burner, thereby causing a heat release fluctuation through the burning of that particular fuel lean slug of gas. Either method, or any variation on that theme, can give rise to a cycle oscillation and fluctuating heat release (36).

System oscillations have also been suggested as possible mechanisms. By evaluating the fluctuating flow through the various parts of the burner and relating these to the mass flow in the combustor, a fluctuating pressure and heat release can be determined. Pressure fluctuations are determined by the instantaneous mass and temperature in the combustor, while the heat release depends strictly on the mass. The method of increased burning can be through larger flame area, turbulence or vortex formation, etc. (25,41 , 42).

A further type of model is based on acoustic-flame interactions (43, 44). A flame profile is derived using the flame speed, flow velocity and pressure that satisfies the conservation equations in the combustion zone. The model examines the transmitted and reflected waves resulting from the interaction between an incident pressure disturbance and the flame. The incident wave, originating in either the hot or cold regions of the duct, is amplified for certain frequencies. The analysis derives an expression for the frequencies at which amplification will occur,

$$\frac{w\,\ell}{\bar{u}} = 2n\pi \qquad \text{for } n=1,\ 2,\ 3,\ldots$$

where $w$ = the disturbance frequency in radians

$\bar{u}$ = the mean flow velocity

$\ell$ = the flame zone length.

This proposes that the frequencies are directly dependent on the mean velocity and inversely on the flame length and on any parameter that affects these terms. The complication of this model lies in experimentally determining the flame zone length, to validate the theory.

In order to identify the region of study in this thesis, it is necessary to briefly summarize the results of section 1.3. Experimental investigations into high frequency oscillations in small ducted burners successfully established the existence of longitudinal acoustic standing waves. Simple models correlated the peak acoustic frequencies with the duct length, while more elaborate models identified in more detail possible relationships between the fluctuating pressures and heat release. The weakness of the theories lie in the theoretical understanding of the coupling between fluctuating heat release and pressure-velocity.

Low frequency oscillations still need a comprehensive theoretical and experimental program to establish the character of the disturbance. The available experimental results are from a variety of scattered programs that when combined do not show a clear picture of the oscillations, although one or two trends have been revealed for frequency with parameter changes. Little though is known about the origin of the oscillation and there is definitely no unified agreement on the mechanism for the disturbance amongst the studies.

## 1.4 Present Programme

The object of the present programme is to establish the difference between acoustic and non-acoustic combustion driven oscillations in a small ducted burner. An experimental investigation, aimed at investigating the effect of flow conditions and duct geometrical changes on combustion oscillation forms the basis of the thesis. Various methods are employed to try to establish the cycle behaviour of the flow and flame. Lastly a theoretical model of the oscillation is proposed and compared to the data.

It is felt that previous investigations have lacked a coherent experimental program to establish the oscillation behaviour. It is hoped that this programme will fulfil part of that need.

The layout of the thesis is as follows. Chapter 2 deals entirely with the experimental burner design, safety systems and air-fuel supply systems. Experimental techniques are described, as are the methods of data analysis. Chapter 3 is dedicated to presenting the experimental data for both types of oscillations. The acoustic oscillation is presented and discussed in this chapter, while the data for the non-acoustic mode is simply presented. Chapter 4 is the description of a theoretical model, based on a flapping or passive flame concept. The model incorporates some experimental data in order to close the governing set of equations. The derivation of the model is in two parts, the first describes the pressure and velocity fluctuation due to an oscillation, while the second accommodates the fluctuating heat release. Chapter 5 concentrates on using the model to predict the frequency of the oscillation and to compare it to the experimental data wherever possible.

A discussion of the model and experimental results, combined with suggestions as to future work concludes that chapter. The final chapter, the sixth, comprises concluding remarks on the programme, identifying the strengths and weaknesses of the work.

# CHAPTER 2

# EXPERIMENTAL EQUIPMENT AND TECHNIQUES

## 2.1 Introduction

The following chapter describes the combustion rig and its mode of operation, together with the diagnostic instrumentation and data acquisition techniques employed in this study. The burner configuration is described briefly with particular emphasis on those aspects having a potentially important role in sustaining combustion oscillations. Safety systems built into the burner are discussed in the context of rig operation during unstable burning.

## 2.2 Description of Apparatus

The apparatus used in this investigation is an adaptation of a blowdown ducted burner built by Lewis and Moss (45) for turbulent combustion studies. The burner was modified to allow unstable combustion to occur, mainly through configuration changes in the combustion chamber. In the following three subsections the modified experimental burner is described in terms of the working section or burner, air and fuel supply, and safety mechanisms.

### 2.2.1 Burner description

In this sub-section the experimental rig is described by the individual components that make up the burner. The description begins at the fuel and air injection point of the rig and sequentially examines each component encountered while moving along the rig in the flow direction, terminating with the duct exit. When examining the combustion chamber a brief description of the ignition system is outlined.

Figure 2.1 shows an exploded view of the burner configuration. The air and fuel are injected into the furthest upstream section of pipe. The air enters this section through a sonic orifice plate at the end of

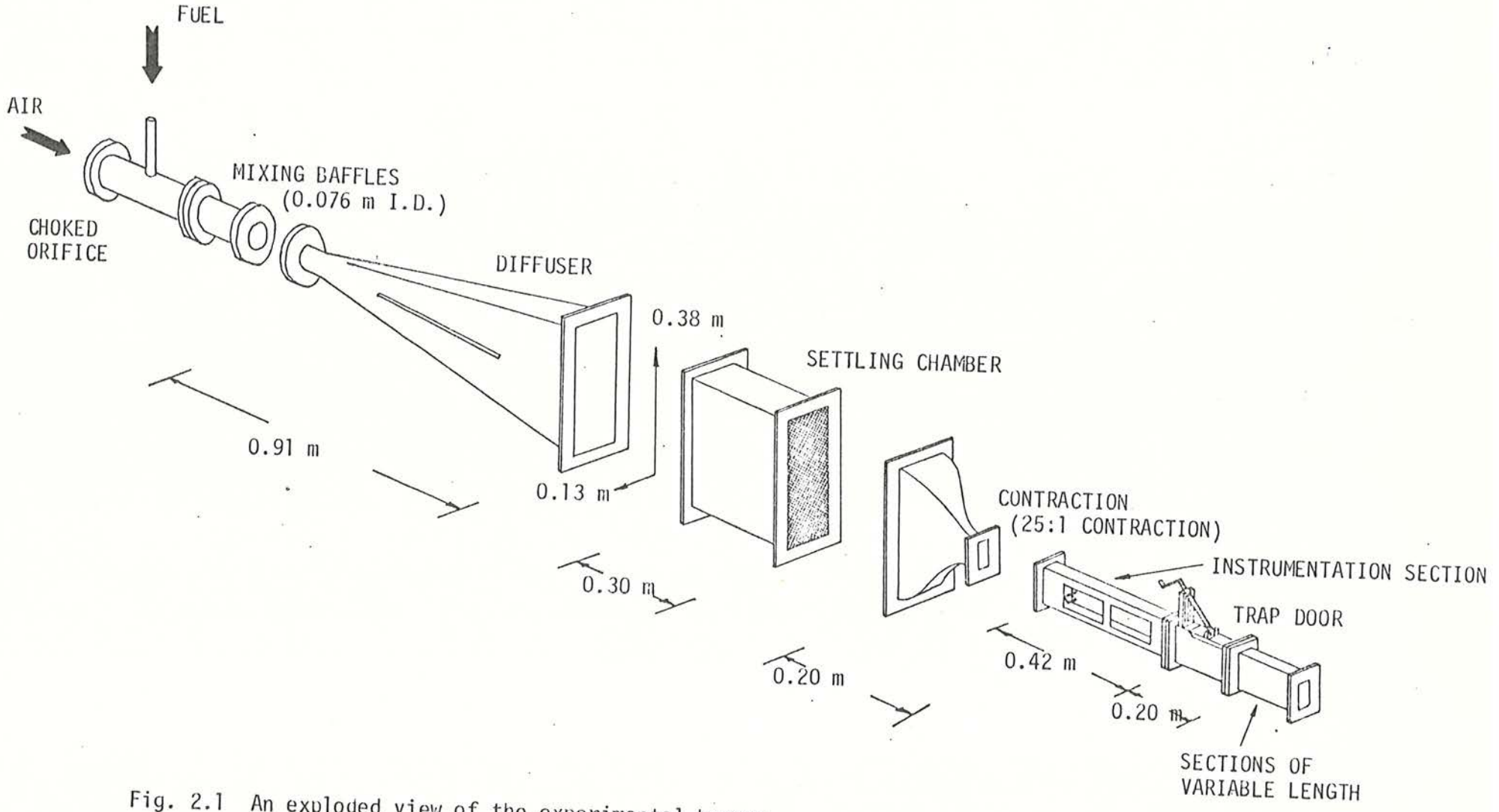


Fig. 2.1 An exploded view of the experimental burner

the pipe, while the fuel is fed in at the mid point through a tube. To enhance the mixing of the air and fuel, the next downstream section of pipe contains a set of mixing baffles, shown in Fig. 2.2a. The four plates of the baffle, perforated by various sized holes, stir the flow to ensure homogeneity of the mixture.

The turbulent flow produced by the baffles passes into a diffuser (half angle of expansion being $10^{o}$), which through its area change reduces the flow velocity by an order of magnitude and lowers the turbulence level. Along most of the length of the diffuser, a lining of 0.025 m thick, medium density, plastic foam was glued to the inside walls. The purpose of the foam was to reduce transmission of the noise generated by the mixing baffles to the combustion chamber (down stream) without impeding the gas flow. The sound attenuation by the foam was 30-40% at low frequencies < 400 Hz, but up to 80-90% at frequencies above 500 Hz (46). It was felt that a noise source upstream of the combustion chamber could cause interference with the combustion through acoustic-flame coupling.

Downstream of the diffuser is a settling chamber. Mounted inside this chamber at right angles to the flow were four fine meshed, stainless steel screens (200 grid mesh size), shown in Fig. 2.2b. The need for the screens is twofold. Firstly, the screens provide a further reduction in the turbulence scale, by flow smoothing, and secondly they act as a flame arrester should the flame leave the combustion chamber and propagate into the settling chamber.

Next downstream is a 25 to 1 contraction section. The flow is smoothly accelerated through this region into the combustion chamber. The large area reduction further reduces the level of the turbulence to less than 2% of the mean velocity. This was measured by Lee (47) using a hot wire anemometer. Because of the complicated shape of the contraction, this section had to be made from fire-retarding fiberglass, unlike the previous sections that were constructed of mild steel.

Mounted at the end of the contraction is the combustion chamber. The chamber, of internal cross-sectional area 0.075 × 0.025 m, was constructed of three pieces: an instrumentation section, a trap door section and any additional lengths. The instrumented section incorporated in its walls two pairs of schlieren quality vitreous fused silica, flush mounted

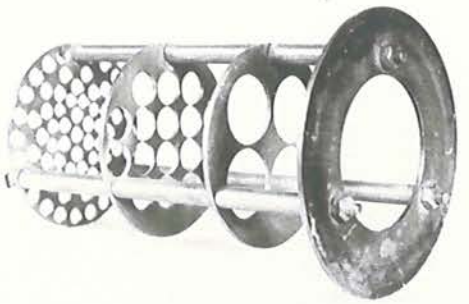

a. Mixing baffles

b. Stainless steel screens

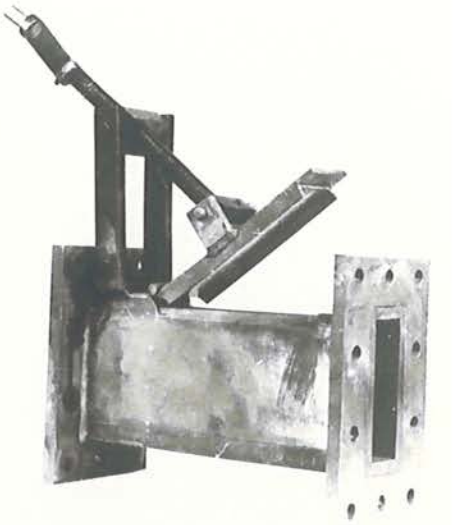

c. Adjustable trap door

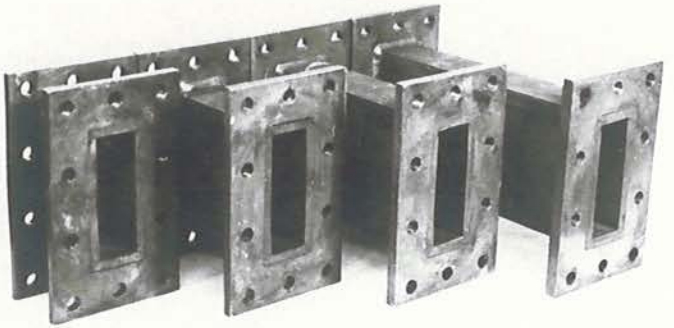

d. Duct extensions

e. Vee-gutters (flame stabilizers)

Fig. 2.2 Components of the burner

windows (0.15 × 0.075 m by 0.006 m thick). Along the top and bottom walls of the duct were six pairs of 0.0254 m diameter ports that could be blanked off by mild steel plugs or used for pressure tappings or for inserting thermocouples into the flow. This section was made of mild steel, which suffered minor distortions due to overheating during prolonged experiments of up to 2 hours duration.

The remaining two sections were built of Inconel 600, which offered substantial improvements in heat resistance compared with mild steel. An adjustable trap door section, Fig. 2.2c, allowed a hinged 0.127 m long segment of the top of the duct to be opened. This was necessary to relieve high pressure transients during ignition. Once the combustion had stabilized on the flame holder, the trap door could then be closed. The additional lengths of duct, shown in Fig. 2.2d, which varied from 0.050 to 0.203 m, could be added forward of the instrumentation section or aft of the trap door, depending on the geometry needed for an experiment.

The flame stabilizers used in the experiments were a set of five vee-gutters, Fig. 2.2e, ranging in size from 10 to 50% of the cross-sectional area of the duct. These completely spanned the duct width and were fixed to the leading edge of the first (upstream) pair of windows of the instrumentation section. The rods, visible on each vee-gutter in Fig. 2.2e, fitted into a set of holes in the glass windows, which held them securely.

The combustible flow was ignited by a high tension electrical spark generated by an automobile ignition coil connected to the electrical mains. The coil was attached to a $5 \times 10^{-4}$ m diameter tungsten wire which was inserted through an insulated plug mounted in one of the observation ports on the duct floor. Before ignition the wire was moved into a position where the tip was a few mm from the earthed flame stabilizer. To ignite the flow, a spark of approximately 10 kV was passed across the gap from the wire to the stabilizer. The sudden pressure increase due to the ignition was sometimes responsible for the flame blowing out or blowing back into the settling chamber. By opening the trap door before ignition this was usually averted. The initial flow prior to ignition was set to 16 m/s at an equivalence ratio of $\sim$1.6, with the open trap door never more than 0.50 m downstream of the flame stabilizer.

The complete rig was rigidly mounted to a vibration damped concrete block, which reduced rig vibrations induced by the combustion oscillations.

### 2.2.2 Air, fuel and exhaust systems

A schematic diagram, Fig. 2.3, shows the layout of the air and fuel delivery systems, and the exhaust ducting. The air supply for the burner came from a high pressure (1.72 $MN/m^2$) domestic source, the compressed air being stored in three 20 $m^3$ storage tanks was filled by a bank of four compressors.

Control of the air flow from the high pressure supply to the burner at near atmospheric pressure, was achieved by two pressure regulators and a sonic orifice plate. The variation of the pressure difference across the orifice plate controlled the air flow into the burner. The plate had a 0.008 m diameter hole in its centre, at which the air flow became sonic once the differential pressure across the plate was greater than 0.103 $MN/m^2$. Thus, the air flow was regulated by the control of the pressure upstream of the plate. The sonic orifice plate also created an acoustic termination point in the burner. No acoustic disturbances produced in the combustion zone or rig could travel upstream of the plate.

The pressure upstream of the orifice plate was controlled by using two Norgren pressure regulators. The upstream valve reduced the pressure from 1.72 $MN/m^2$ to 0.48 $MN/m^2$, while the downstream regulator, just ahead of the orifice plate, gave fine control of the pressure from 0 to 0.48 $MN/m^2$. This pressure range allowed the flow velocity to be varied from 10 to 50 m/s in the combustion chamber.

The fuel used in the experiments was locally supplied commercial grade propane ($C_3H_8$). The propane was stored in three 50 kg tanks outside the laboratory and fed to the burner through a network of pipes. The control of the propane flow into the rig was by a rotameter, which had an operating range of 9-90 kg/hr. A pressure regulator was mounted in the line between the tanks and the rotameter to reduce the tank pressure of 0.963 $MN/m^2$ to the working pressure of the rotameter, 0.275 $MN/m^2$. At several locations along the fuel line valves and pressure gauges were mounted to permit secure closing of the fuel line, and monitoring of the gas pressure.

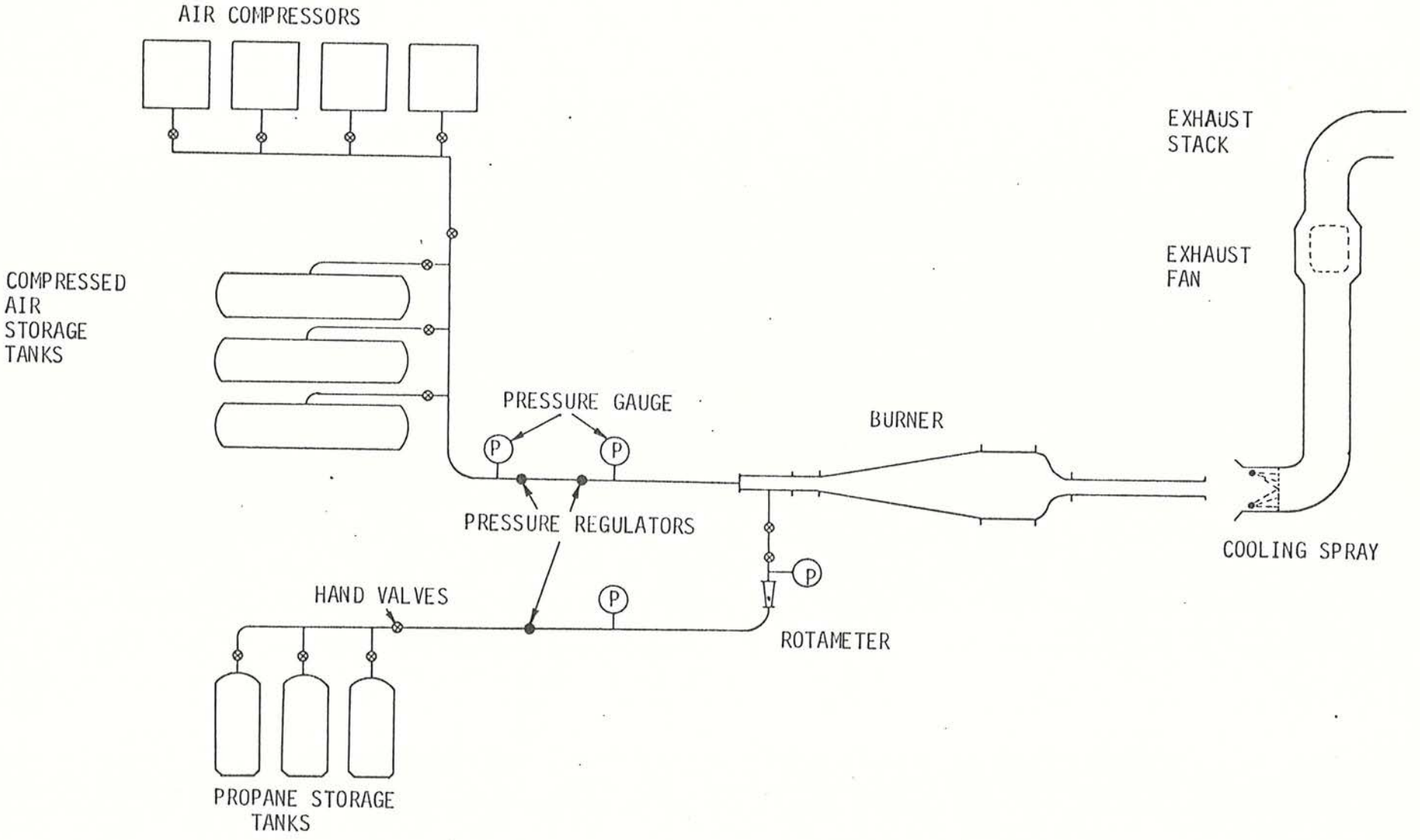


Fig. 2.3 A schematic diagram of air, fuel and exhaust systems

The calibration of the two supply systems differed. The air supply pressure was measured upstream of the orifice plate by a Standard Test gauge to an accuracy of $\pm$ 0.69 $\times$ $10^{-3}$ $MN/m^2$ and the air flow was calibrated using a 2 m, 0.075 m diameter, piece of pipe that replaced the burner for the calibration, downstream of the orifice plate. A pitot tube was traversed across the exit plane of the pipe and the air flow was calculated for a number of pressure settings. The fuel system calibration involved redirecting the propane from the rotameter into a gasometer (see Weller (48) for more information). By measuring the fill rate of the gasometer, the gas flow could be checked for several rotameter settings. The result of the calibration for both delivery systems gave confidence in the desired flow rate for a given equivalence ratio of better than 5%. Also the series mounted pressure regulators gave a < 2% instability in the air flow over long duration experiments.

The exhaust ducting, which directed the burnt gases from the combustion chamber out of the laboratory, consisted of a heat proof, acoustically lined 0.254 m internal diameter pipe. The upstream end of the exhaust system was hooded in order to help direct the fumes into the pipe. Approximately 0.30 m behind the hood, in the throat of the pipe, was mounted a water cooling spray. A perforated 0.019 m outside diameter copper tube ring was placed inside the pipe, spraying a mist of water onto the hot gases. Further up the pipe was an axial fan, which helped to extract the gases from the laboratory. With an operating temperature of < 250°C, the water cooling spray was essential for the fan's safe operation.

### 2.2.3 Safety systems

The safety mechanisms employed on the rig were used to monitor the combustion process and if necessary to extinguish the flame. Displayed in Fig. 2.4 is a schematic diagram of the location and wiring of the instruments used in the safety system.

There were two potentially hazardous situations that had to be guarded against: a flame blow off and flash back. In either case the end result was that the flame no longer burned in the combustion chamber. In a blow off, the flame detached from the flame stabilizer and was

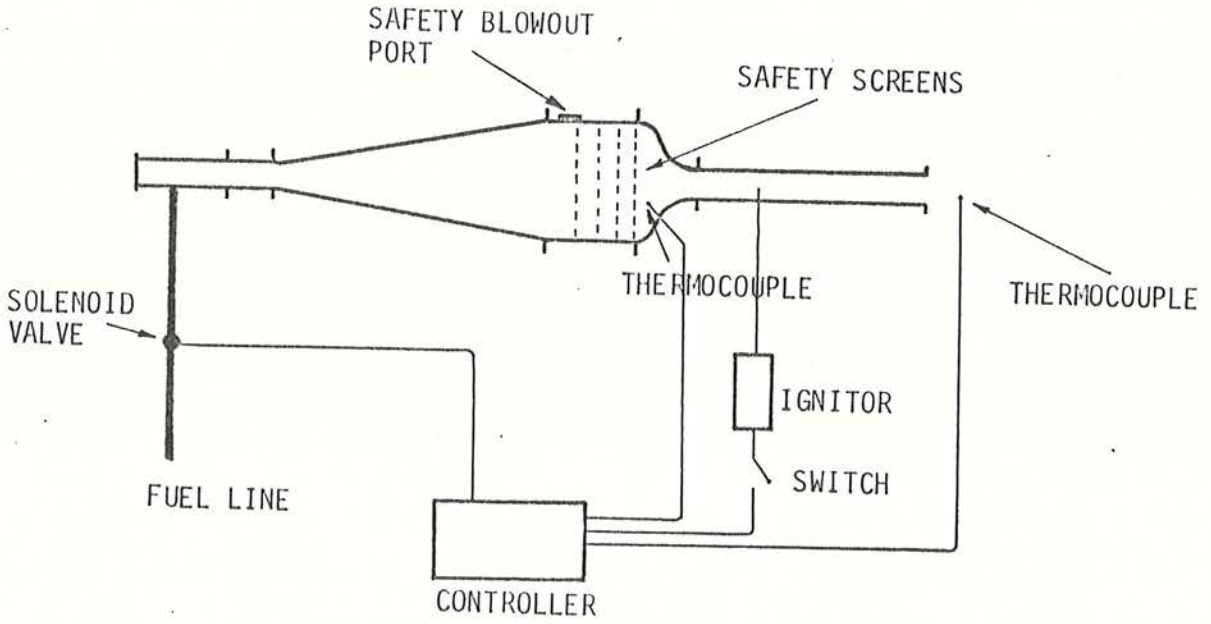


Fig. 2.4 A schematic diagram of the safety systems

extinguished upon leaving the duct, while in flash back, the flame detached from the flame stabilizer and propagated into the contraction and ultimately into the settling chamber. In these two situations the flow of propane had to be cut, to reduce the build up of unburnt fuel or to stop the combustion in a structurally weak part of the rig.

In order to safeguard against either of these situations, two sets of chromel-alumel thermocouples were mounted, one in the hot gas flow at the combustion chamber exit, and the other in the contraction. If the set in the hot gas flow registered a temperature lower than 250°C or if the other set, in the contraction, a temperature greater than 250°C, then the control unit to which the thermocouples were connected, closed a solenoid valve in the fuel line to the rig.

However, although this worked well for a blow off, the flash back case had an extra problem. Once the fuel supply was shut off, it was estimated that it took approximately 1.2 s for the gas in the rig to burn out. During the time the flame could have done substantial damage to the foam lined diffuser or any instrumentation mounted in the settling chamber.

This problem was alleviated by the set of four fine mesh stainless steel screens, used as turbulence reducers, acting as a fire break inside the settling chamber. In most cases, the flame, when it did blow back, did not penetrate the first screen and was extinguished in due course, after tripping the thermocouple safety mechanism, without damage to the rig. A further safety precaution was the placing of a blow out port in the bottom of the settling chamber, in order to release any over pressure above two atmospheres, by the bursting of a heavy paper diaphragm.

The electric ignitor was also operated from the control unit and if any of the thermocouples forced the controller to close the solenoid valve, then simultaneously the ignitor was disengaged and could not be re-used for approximately 10 s. This stopped any possible accidental re-ignition of the burner after a flame out.

## 2.3 Experimental Techniques

This section is devoted to examining the experimental techniques used in this thesis. In the following subsections, schlieren photography, water-cooled microphone probes, pressure transducers, and hot wire anemometry and thermocouples are discussed. Each type of diagnostic equipment is described in terms of the method by which it was employed and the type of analysis used in interpreting the results.

### 2.3.1 Schlieren photography

Photographic techniques were used as non-intrusive methods of obtaining some visualisation of the combustion oscillation. Unfortunately, simple high shutter speed (1/1000 s) 35 mm photographs were unable to freeze the flame motion, although these photographs did give time average information on the flame position. Spark schlieren photographs and high speed cine schlieren films were sufficient to freeze the flame motion and give detailed information. In this subsection these latter two methods of schlieren photography are described.

Both the schlieren techniques used the same basic equipment of mirrors and a knife edge, but differed in the light source and camera. Figure 2.5 is a schematic diagram of the basic pattern of the schlieren system. Because of the cramped conditions in the laboratory, a simple "z" schlieren pattern could not be set up. However, by using two plane mirrors a variation on the "z" was incorporated and successfully used.

The light from the source was focused using a lens onto a 2 $mm^2$ pin hole, which represented a pseudo-point source. The expanding light from the pin hole fell onto a concave mirror (0.203 m diameter) from a distance of 1.82 m. The reflected beam of parallel light followed the path shown in Fig. 2.5, through the windows of the instrumentation section to another concave mirror, before finally focussing onto a knife edge or graded-filter, prior to entering a lens in front of the camera. For most experiments the steep density gradients in the flame limited the use of a knife edge, as it resulted in high contrast schlieren effects. To soften the contrast a graded filter was used instead of the knife edge. For a detailed treatment of schlieren theory and uses, reference may be made to (49).

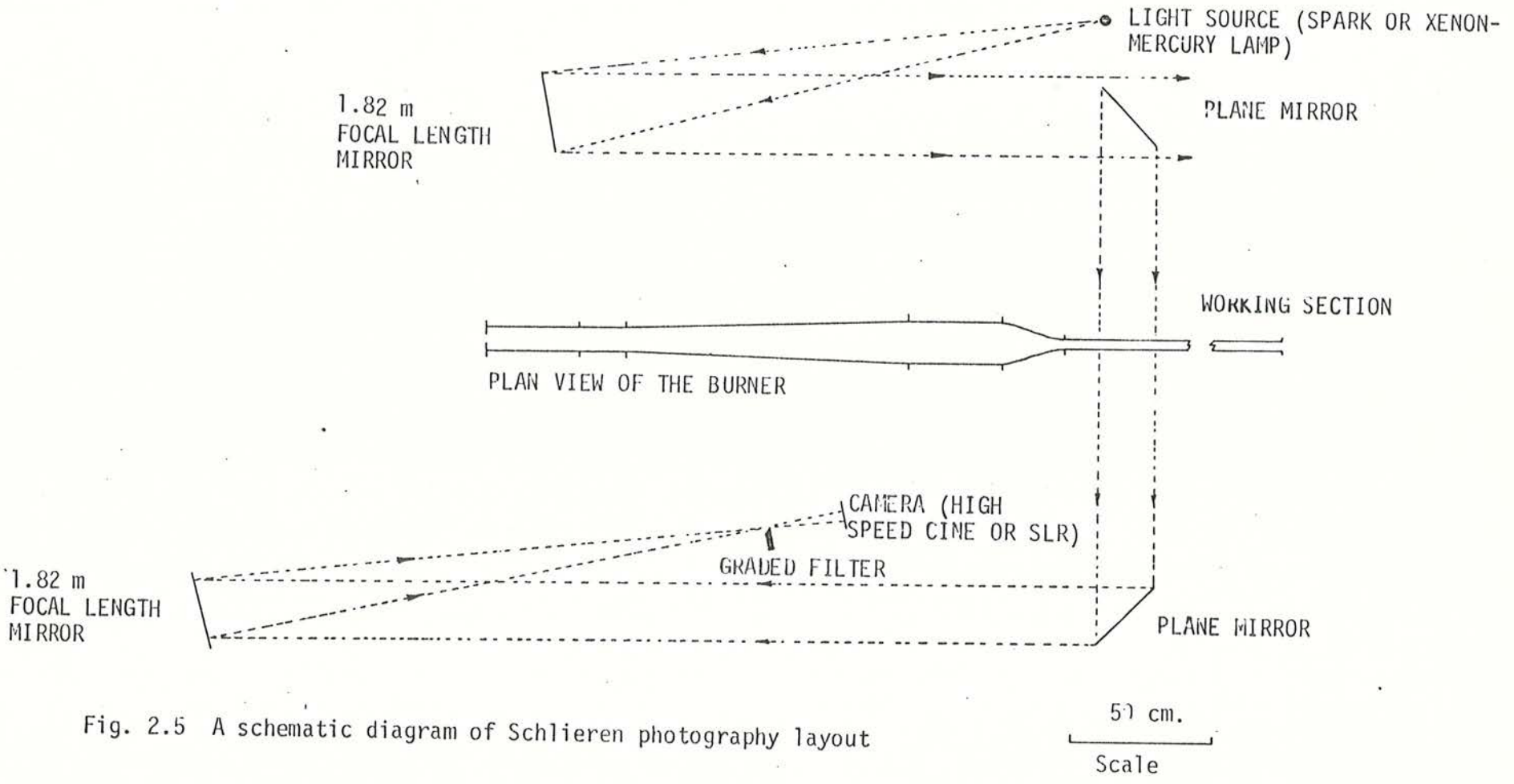


Fig. 2.5 A schematic diagram of Schlieren photography layout

To increase the amount of information available from the cine photography pressure and velocity traces were added to the film. A pressure transducer and hot wire anemometer were mounted approximately 0.075 m forward of the vee-gutter. The signals from these two devices were displayed on an oscilloscope and, through a lens mounted on the eye piece at the back of the Hyspeed camera, the images of the two oscilloscope traces were focussed onto the back of the film. The time sweep on the oscilloscope was stopped and amplitude changes of the traces were displayed as stationary vertical lines. Once the film was running through the camera, the speed of film movement introduced a new time base for the two signals.

With the photographs of the flame, and the flow velocity and pressure traces simultaneously recorded, it was possible to map the variation of flame movement with flow velocity and pressure. Unfortunately the absolute amplitudes of the two traces could not be established, because it was impossible to introduce reference lines on to the film. However, through knowledge of the mean and zero flow velocities, a rough velocity could be established within 20%.

Flame position was measured directly from the film. The method of analysis is shown in Fig. 2.6. A line, parallel to the duct walls, 0.019 m above the centre line of the duct was used as a reference. The position of any flame front that crossed this line was measured from the crossing point to the leading edge of the window frame. If there were several crossings, each was measured and monitored by frame to frame analysis.

The velocity and pressure traces were measured for each frame at the trace's intersection with the duct centre line. In all, 500 sequential frames were analysed. The data taken from the films was analysed on a PDP 11 for the individual frequency spectra of velocity, pressure and flame length, and the phase relationship between each.

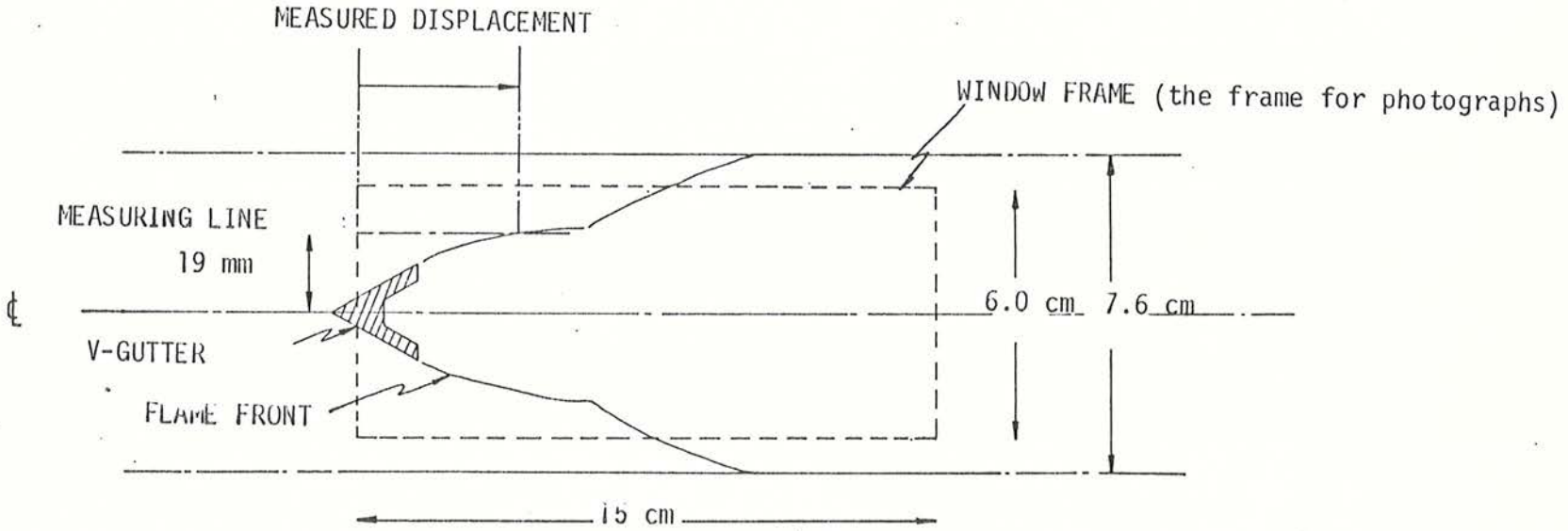


Fig. 2.6 Method of measuring the flame front position from the cine photography

Spark schlieren photographs were taken with two types of camera, a polaroid and a 35 mm single lens reflex (SLR). An argon arc spark unit was used as the light source. A 9 kV spark of 1 μs duration was discharged through an argon atmosphere. The light generated by the spark was sufficient for the use of 3000 ASA film with the Polaroid land camera, and 400 ASA (Ilford HP5) film with the power driven Nikon F3, SLR.

Since the flame was luminous, stray light from the combustion zone had to be removed. The SLR camera was set to a shutter speed of 1/125 s, and the electronic flash synchronizer was used to trigger the spark. The short duration of the spark and the high shutter speed was sufficient to eliminate the flame luminosity. However, the Polaroid camera, which was specially built for schlieren work without a lens, lacked the facilities for a high shutter speed and electronic flash control. To resolve this difficulty, a camera shutter mechanism was mounted after the graded-filter in line with the focussing lens and camera. By triggering this shutter, the Polaroid could be operated in a similar manner to the SLR.

These experiments resulted in sharp detailed images of the flame. By reference to the cine film these photographs could be ordered into a sequence of events for a single buzz cycle, even though the photographs were taken many cycles apart.

The cine schlieren technique lacked the fine detail of the spark schlieren but had the advantage of producing up to 100 sequential photographs of a single buzz cycle. The framing rate for the clinic was set at 5000 frames per second, which is equivalent to an effective shutter speed of 1/12,500 s. However, even at these speeds, a mean flow velocity in the flame of 20 m/s results in movements of the flame front of $\sim$2 mm during each photograph. This is sufficient to result in a slight blurring of the flame on the films.

The light source for this technique was a 200 watt xenon-mercury lamp. The continuous source was placed in the same location as the spark source, while a Hyspeed camera Model H10/16 replaced the SLR. The film used by the camera was Ilford 16 mm (HP5) 400 ASA 30.5 m in length, although when developing the film it had to be uprated to 800 ASA. At 5000 fps the film was exposed in approximately 1.25 s, although due to run up time to steady speed, only the last half of the film was framed at the proper rate. The results of the cine film made possible a frame by frame analysis of a complete cycle of buzz oscillation.

### 2.3.2 Water cooled microphone probe

The purpose of the water cooled microphone probe was to investigate acoustic standing waves in the combustion chamber. Records of the pressure fluctuations at discrete points along the length of the combustion chamber were analysed by a spectrum analyser at specific frequencies. The amplitude change of the pressure signal with duct position, allowed the identification of the standing waves.

The probe, Fig. 2.7, was designed around a Muirhead ½" microphone probe, type 2115. The needle nose of the probe was detached and the body containing the microphone (Bruel and Kjaer (B & K) 4134 microphone) connected to a 3.175 mm O.D. stainless steel tube by a similar sized plastic tube. The stainless steel tube connected the microphone to the region where the pressure was to be sampled in the same manner as the static part of a pitot-static pressure probe. Surrounding the tube was a water jacket made from two concetric tubes of 6.35 and 9.52 mm O.D. At the microphone end of the probe the tube ends connected into a block and cold water was forced down between the 3.175 and 6.35 mm tubes at 1.37 $MN/m^2$ along the length of the probe and back between the 9.52 and 6.35 mm tubes. This provided the cooling for the probe when it was in the flame zone.

The probe, when in use, lay on the floor of the duct with the hole of the centre tube oriented normal and away from the duct floor. To measure the pressure field in the burner, the probe was inserted into the duct via the combustion chamber exit. The microphone was set back away from the exhaust plane and protected from radiation from the flame and duct by a sheet-metal shield, with further cooling provided by a flow of compressed air inside the shield. The microphone, shield and probe end were mounted on an optical rail, allowing the probe to be traversed along the axis of the duct on the combustion chamber floor.

The data acquisition from the probe was made at discrete points in the duct, usually at 1 or 2 cm intervals, starting 10 cm ahead of the contraction-combustion chamber junction. At each location the pressure fluctuations measured by the microphone were recorded on a Hewlett-Packard 3960 tape recorder (set to a speed 3.75 ips that cut off frequencies above 1250 Hz). The recorded data was then analysed on either an Hewlett-Packard 3582A or 5420A spectrum analyzer. The spectrum for each sample was

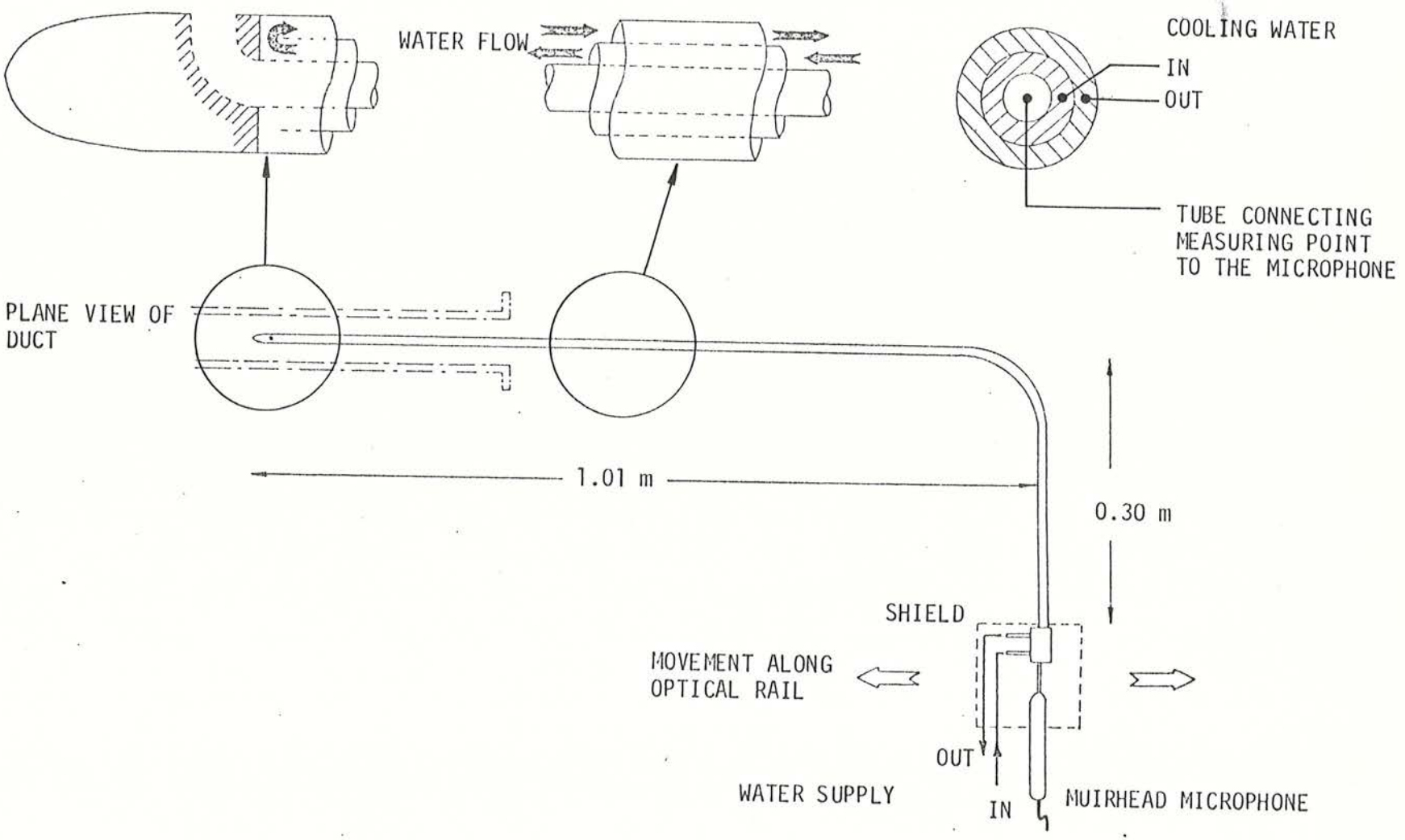


Fig. 2.7 Schematic diagram of water cooled microphone probe

transferred through an IEEE interface to a Commodore 3032 micro computer and stored on a floppy disc.

In order to use this data to identify standing waves, the spectra for each measuring point in a traverse was recalled by the micro computer from disc and the amplitude of the pressure signal at selected frequencies recorded. At a specific frequency, the RMS pressure amplitude was plotted against duct length. The RMS pressure amplitude was normalized by the maximum amplitude of the plot, the reason for this will be explained at the end of this section. If a standing wave was present at the selected frequency, then a rectified sine wave would appear in the plot.

No calibration of the microphone probe was necessary when operated in this manner as the acoustic distortion of a signal arising from the tube geometry did not affect the final results. Each frequency in any signal was affected in the same way, thus normalizing the amplitudes of a plot at a specific frequency by the maximum amplitude, standardized the effects deriving from the tube.

A further problem was encountered when the probes' outside diameter was increased from 6.35 to 9.52 mm. The smaller probe was initially and successfully used in non-buzzing experiments. However, as the duct length increased, the amount of cooling water flowing through the probe was insufficient, and the capacity of the water pump was not enough to alleviate the problem. A new larger diameter probe was constructed that overcame the cooling problem, but however caused another. As the diameter of the probe increased, the blockage of the probe rose from 1.5% to 3.5% of the chamber cross-sectional area. In a non-buzzing experiment the probe had no effect on the combustion, but once buzzing occurred, the probe reduced the buzz amplitude when it was near the flame stabilizer. To resolve this situation, a pressure transducer was maintained at a fixed location adjacent to the vee-gutter and the pressure at this point was recorded simultaneously with probe measurements. Treating the pressure transducers spectra in the same way as the probes', then dividing the two normalized plots, a modified pressure plot was developed that removed the effects of the probe diameter.

### 2.3.3 Pressure transducer

Kistler 7031, piezo-electric pressure transducers were used to measure the fluctuating pressure in the combustion chamber from fixed positions along the walls. Used in conjunction with the transducers were Kistler 566 charge amplifiers and a purpose-built bank of linear amplifiers, with 1, 10, 20, 50 or 100-fold amplification.

The transducers were mounted in a special metal casing and suspended from a tubed plug in one of six ports on the instrumentation section of the duct by a 3 mm O.D. rubber tube, shown in Fig. 2.8. Isolating the transducers from direct contact to the duct reduced the rig vibrations from being transmitted to the acceleration-sensitive pressure gauges. Tests and calculations indicated that the natural frequencies of vibration for the pressure transducer housing on the rubber tubing were approximately 5.6 and 13 Hz. The length of tube from the inside wall of the chamber to the face of the pressure transducer, roughly 7 cm, attenuated frequencies above 1000 Hz. Calculations indicated that the amplitude would be reduced by 1.7 dB at 1000 Hz, and would reduce further at high frequencies. Within the frequency range of interest, 30 to 1000 Hz, these two limitations were acceptable. A further limiting factor above 1000 Hz was the onset of the harmonic of acoustic standing waves, $\sim$1850 Hz, that occurred in the tube of the transducer mounting.

To check the calibration of the transducer against the manufacturer's specifications, the transducer in the complete mounting was connected to a Bruel and Kjaer piston phone calibrator and tested. The transducer signal was analysed by an HP 3582A spectrum analyzer and found to be within 1 dB of the 124 dB generated signal at 1000 Hz, which was within the accuracy of the analyser.

During experiments the pressure signals were recorded on an HP 3960 tape recorder, and later analysed on either an HP 3582A or 5420A spectrum analyzer, using a Hanning filter band pass. The resulting spectra frequency span of 0 Hz to 250, 1000 or 2500 Hz in 256 points were transferred through an IEEE connection to a Commodore 3032 micro computer and stored on floppy disc. The amplitude of the fluctuating pressure was measured on an RMS sound pressure level in terms of decibels (dB), with respect to a reference pressure of $2 \times 10^{-5}$ N/m$^2$ (referred to as the threshold of hearing at 1000 Hz) or as an RMS gauge pressure (N/m$^2$).

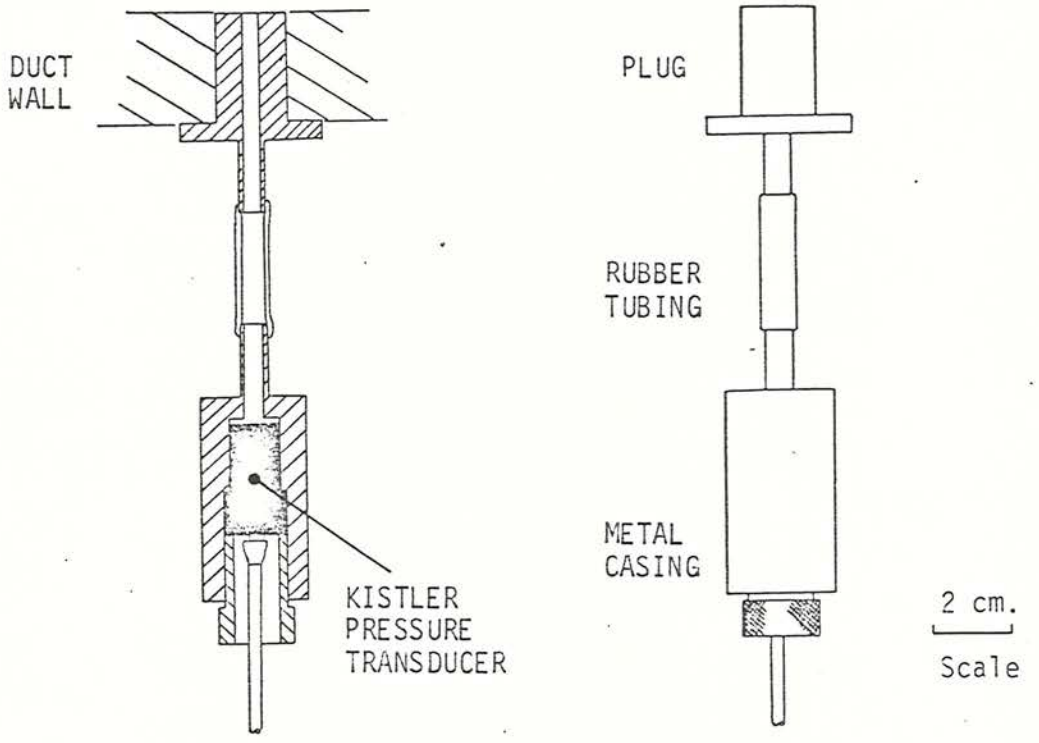


Fig. 2.8 Cross-section and schematic diagram of pressure transducer housing

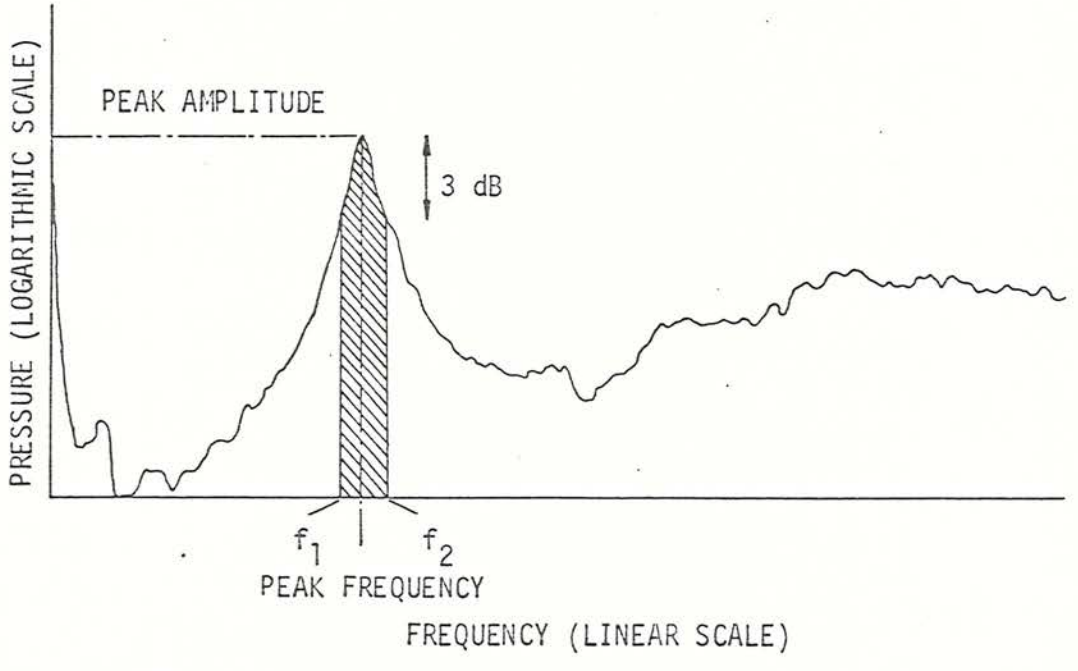


Fig. 2.9 Half power level in a pressure spectrum of a low frequency oscillation

In the next chapter, acoustic pressure signals are quoted in terms of frequency (Hz) and corresponding amplitude, while buzz data are quoted in terms of peak amplitude and frequency band, for the buzz frequency. Displayed in Fig. 2.9 is a pressure spectrum, showing a buzz peak. As a measure of the cycle variation, the breadth of the peak is measured in terms of a frequency band $(f_2 - f_1)$ 3 dB down from the maximum amplitude, referred to as the half power level.

The Kistler pressure transducer can only measure dynamic pressures, thus to obtain static pressures, methyl alcohol or water manometers were used. These measurements were obtained through the upper set of observation ports or by the use of the water cooled microphone probe, with the tube to the manometer replacing the microphone.

### 2.4.4 Hot wire anemometry and thermocouples

Flow velocity fluctuations in the unburnt gas were measured using a constant temperature hot wire anemometer (ISVR Type 201B). These measurements were made in conjunction with pressure transducer measurements at the same position shown in Fig. 2.10, for two separate experiments. One involved superimposing the velocity and pressure oscilloscope traces on the high speed cine schlieren, as described in section 2.4.2. The other was the use in the simultaneous determination of the velocity fluctuation, directly from the hot wire anemometer and indirectly from the pressure fluctuations (refer to section 2.4.3).

Sketched in Fig. 2.11 are two views of the hot wire anemometry probe mounted through a plug for insertion into the instrumentation section of the duct. The wire stretched across the two horns of the probe is a 5 μm diameter piece of tungsten. Only the middle 2 mm of the 5 mm of tungsten is exposed, the remainder is covered in a layer of copper.

Calibration of the hot wire was performed before each run against the known mean flow velocity in the duct. The operating details of this particular hot wire anemometer are outlined by Lee (47). The velocity was analysed, in the same manner as the pressure, by using an HP spectrum analyser for the fluctuating component and an HP 3721A correlator or Prosser Scientific Instruments A1301D RMS voltmeter for the mean. The spectrum of the signals was transferred to a Commodore 3032 micro computer and stored.

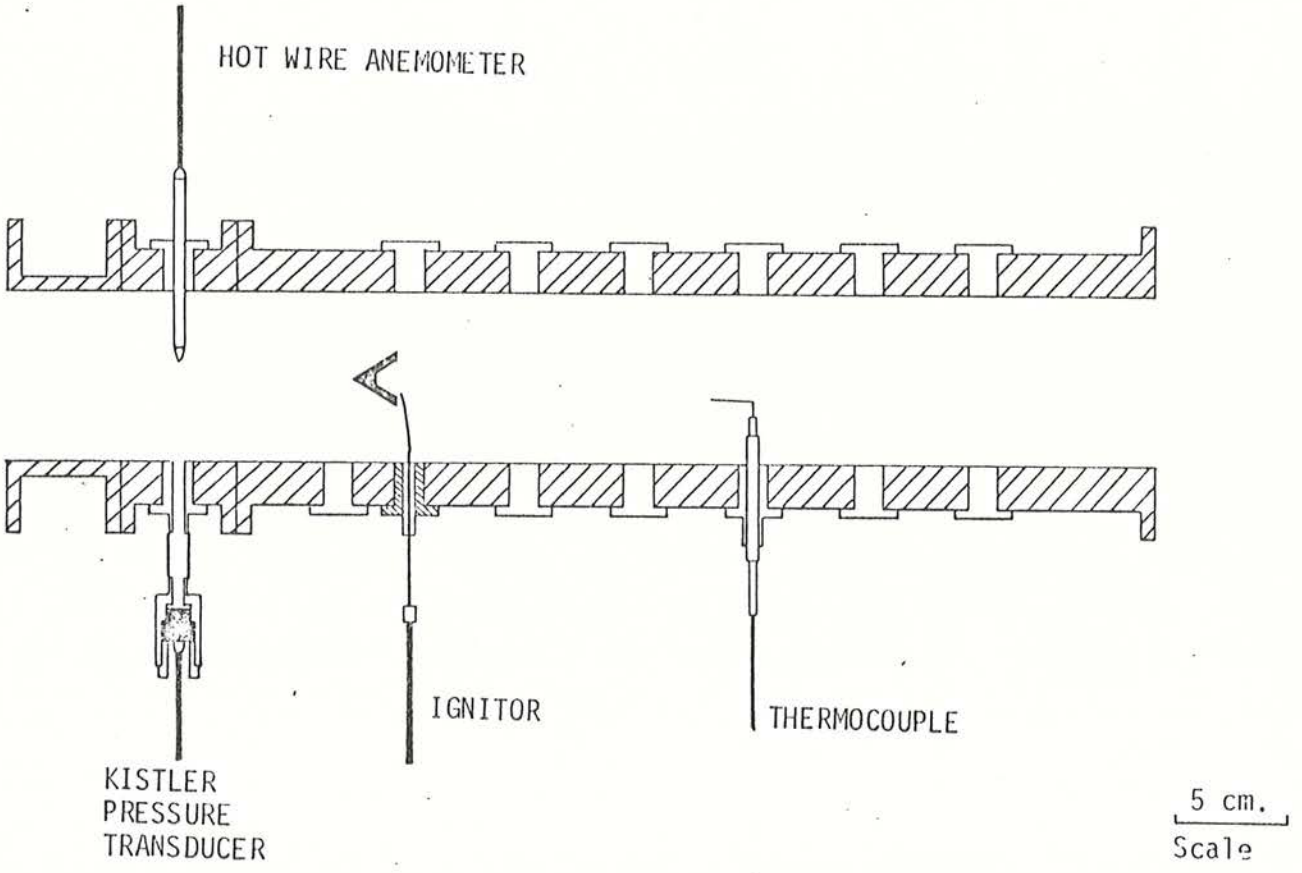


Fig. 2.10 Cross-sectional diagram of the burner showing the relative positions of measuring probes (hot-wire anemometer, pressure transducer and thermocouple)

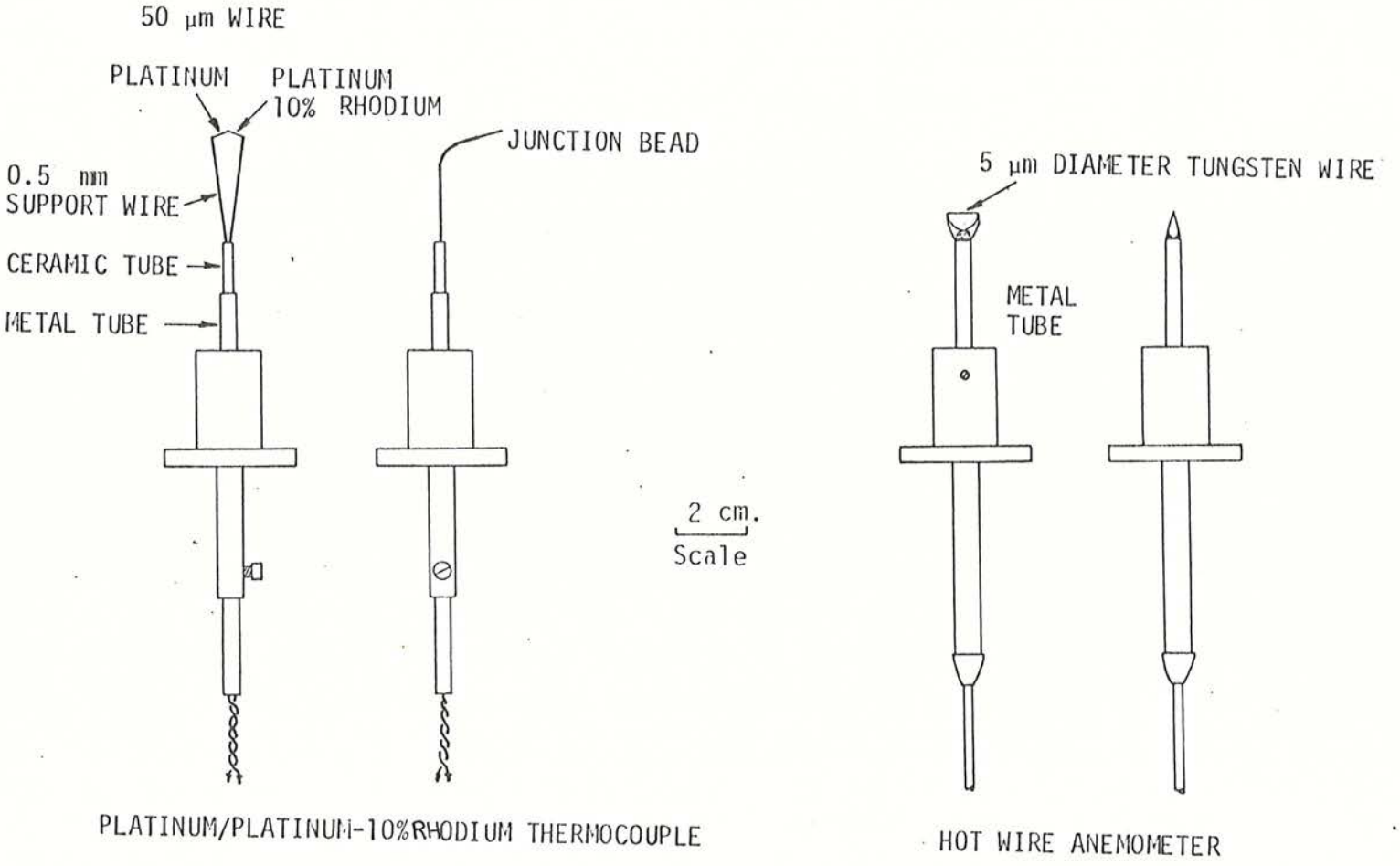


Fig. 2.11 Two views of hot wire anemometer and thermocouple probes

A platinum/platinum-10%rhodium, 50 micron thermocouple, shown in Fig. 2.11, was used to measure the frequency spectrum of the temperature fluctuations in the flame brush during non-buzzing experiments. The tip of the probe was covered in silicon oxide to reduce the catalytic effects between the platinum and combustible mixture. Simultaneously, pressure fluctuations were recorded further upstream at the vee-gutter. The relative positioning of the probes is shown in Fig. 2.10. The object of these measurements was to establish a correlation between pressure fluctuations and events in the flame brush. No attempt was made to quantify the burnt gas temperatures using this probe, nor use the probe in a buzzing flame.

The analysis of the temperature signal is the same as for the pressure transducer outlined in section 2.4.3. For more information on this type of thermocouple and supporting electronics reference may be made to (50).

# CHAPTER 3

## 3.1 Introduction

The experimental aspects of this investigation provide both a basic physical understanding of flame behaviour in conditions of unstable burning, and detailed measurements for the development and validation of a theoretical model. The experiments are designed and operated in a manner necessary to separate and investigate individually acoustic and non-acoustic combustion driven oscillations.

In the subsequent sections, acoustic and non-acoustic oscillations in the pressure field and flame motion are examined by sets of intrusive and non-intrusive experiments. Pressure signals derived from wall mounted pressure transducers are the basic experimental techniques employed. Characteristics of the oscillation are determined from frequency and amplitude changes in the pressure spectra due to alterations in the physical parameters of the rig and flow (i.e., inlet velocity, equivalence ratio, vee-gutter size, etc.). High speed cine schlieren photography allows visual examination of the flame movement with respect to the duct inlet velocity and pressure.

## 3.2 Investigation of Acoustic Properties of the Rig

Examination of a typical pressure spectrum, Fig. 3.1, recorded in the combustion chamber during large amplitude combustion oscillations, reveals a number of discrete peaks. The five major peaks, labelled A to E can be associated with two different phenomena in confined combustion. The higher frequencies, C to E, can be identified with longitudinal organ pipe oscillations in the combustion chamber. The lower frequencies, A and B, are referred to as "buzz"* in the literature, a poorly understood phenomena.

---

*The term "buzz" is used in the remainder of the thesis to describe low frequency, combustion oscillations

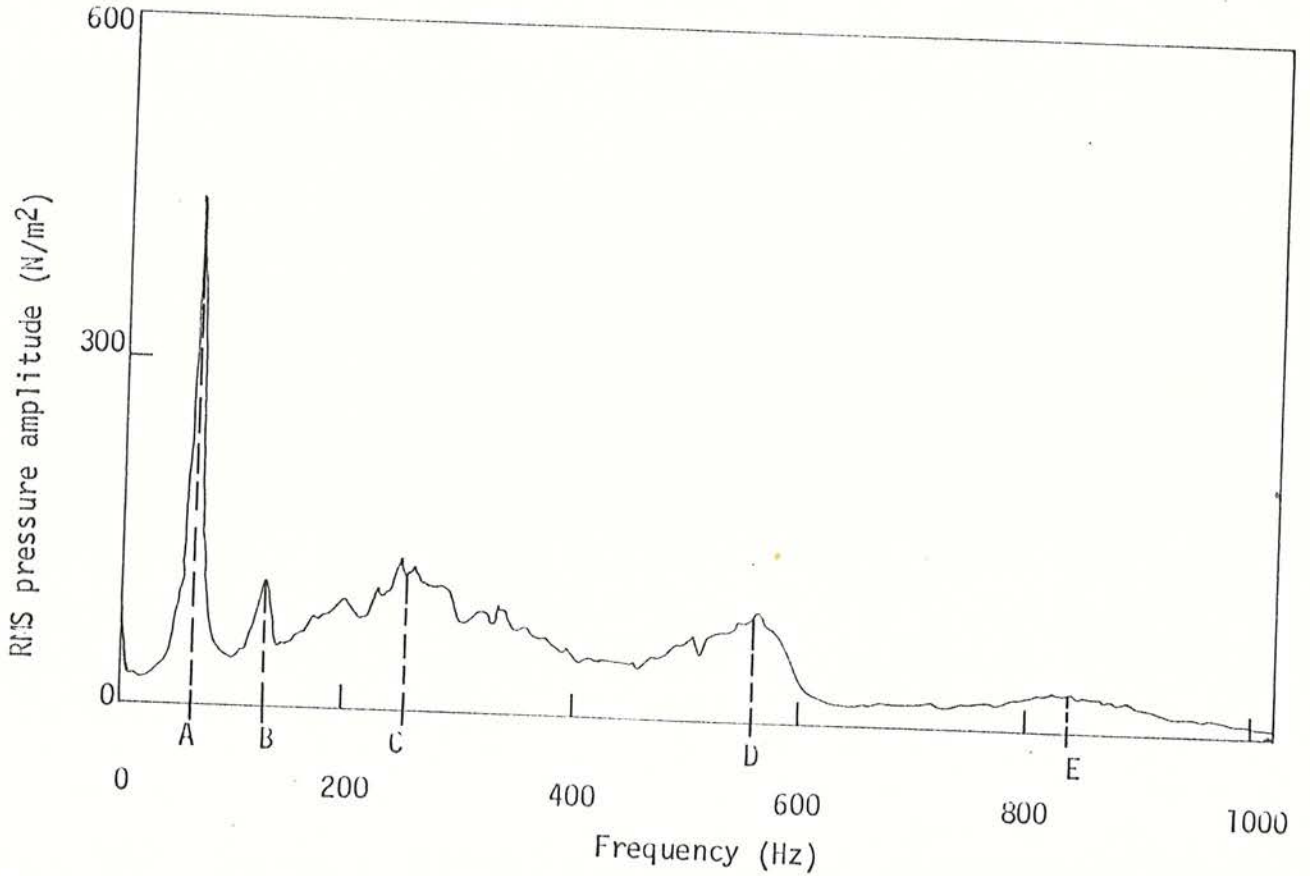


Fig. 3.1 Pressure spectrum for a large amplitude combustion oscillation ($L_c$ = 0.20 m, $L_h$ = 0.66 m, $U_o$ = 20 m/s, 30% blockage, $\phi$ = 1.15)*

*In all subsequent plots the conditions of the experiment will be listed as follows; $L_c$ = cold duct length, $L_h$ = hot duct length, $U_o$ = inlet flow velocity, vee-gutter blockage and $\phi$ = equivalence ratio.

A number of previous investigators (5,6) have examined organ pipe combustion oscillations in burners, and their work has established the properties of these oscillations well. In this thesis the experimental work on organ pipe combustion oscillation is used to demonstrate their existence in the burner and their effect on the flame, but does not undertake new fundamental work in this area. In the following subsections, the higher frequencies are presented through experiments using pressure, temperature and microphone probe measurements. Microphone traverses were used to examine the profile of the RMS pressure fluctuations at the resonant frequencies along the duct. Pressure transducers and thermocouples measured the resonant frequencies in the pressure field and the effect of the pressure on the flame structure.

This section closes with a discussion of the acoustic oscillations in the duct.

Having identified the longitudinal oscillations in the burner in section 3.2, the lower frequencies of buzz, which cannot be reconciled with the longitudinal resonance modes, are examined experimentally in section 3.3.

### 3.2.1 Water cooled microphone probe traverse

The objective of the microphone traverses was to examine the profile of the RMS pressure fluctuations of the longitudinal standing waves along the combustion chamber. In cold flows the longitudinal resonant frequencies, as well as RMS pressure fluctuation profile, can be determined theoretically for particular duct geometries (discussed in Appendix A). The microphone method was established in hot flows by examining first the known resonances in a cold flow, then applying it to the combusting flow to identify similar profiles at the duct resonances.

The results of the microphone traverses are separated into two sections, one dealing with cold air flow and the other combusting flows. The cold flow traverse gives an example of the method, in addition to some interesting noise sources, while the traverse in combusting flows examines the acoustic standing waves of the combustion driven oscillations.

3.2.1.1 Cold flow

The acoustic resonances (organ pipe modes) in the duct can be excited by, for example, turbulent flow, an internal noise source or a combusting flow. In the simple situation of blowing cold air down the combustion chamber, the aerodynamic noise created by the flow is sufficient to excite the first and sometimes higher harmonics of the longitudinal acoustic modes for a particular duct length. As an example of the microphone traverse method in this situation, a 6.25 mm diameter microphone probe was traversed down the length of a 0.40 m combustion chamber taking pressure measurements at 1 cm intervals. Five centimetres from the inlet plane of the duct was mounted a flame stabilizer (20% blockage vee-gutter). The air flow in the duct was set at 20 m/s. The data recorded for this experiment was analysed by the method described in section 2.3.2 and the results of the normalized RMS pressure fluctuations for three frequencies are displayed in Fig. 3.2, against a scaled schematic diagram of the combustion chamber.

In the plot of the 60 Hz oscillation, the large pressure fluctuation at the duct inlet decays to approximately zero at the duct exit, indicating that a noise source exists upstream of the duct somewhere in the settling chamber. The zero pressure fluctuation at the duct exit is due to the acoustic properties of an open ended duct (see Appendix A for an explanation of these properties), while the large pressure fluctuation at the inlet can only be due to an external upstream source. Had the noise source been internal to the chamber, then the pressure fluctuations would have been zero at both ends of the duct. For the moment this observation of the possible location of the low frequency signal is not important in the acoustic context. However, when examining the low frequency combustion oscillations this point will be recalled for discussion.

The next frequency, 260 Hz, is the result of vortex shedding off the vee-gutter. In all cold flow experiments with a flame stabilizer in place, vortex shedding was observed in the pressure signals and the frequency determined to within 10% from the relationship:

$$\text{frequency} = \frac{0.21\ \bar{u}_v}{D} \qquad (3.1)$$

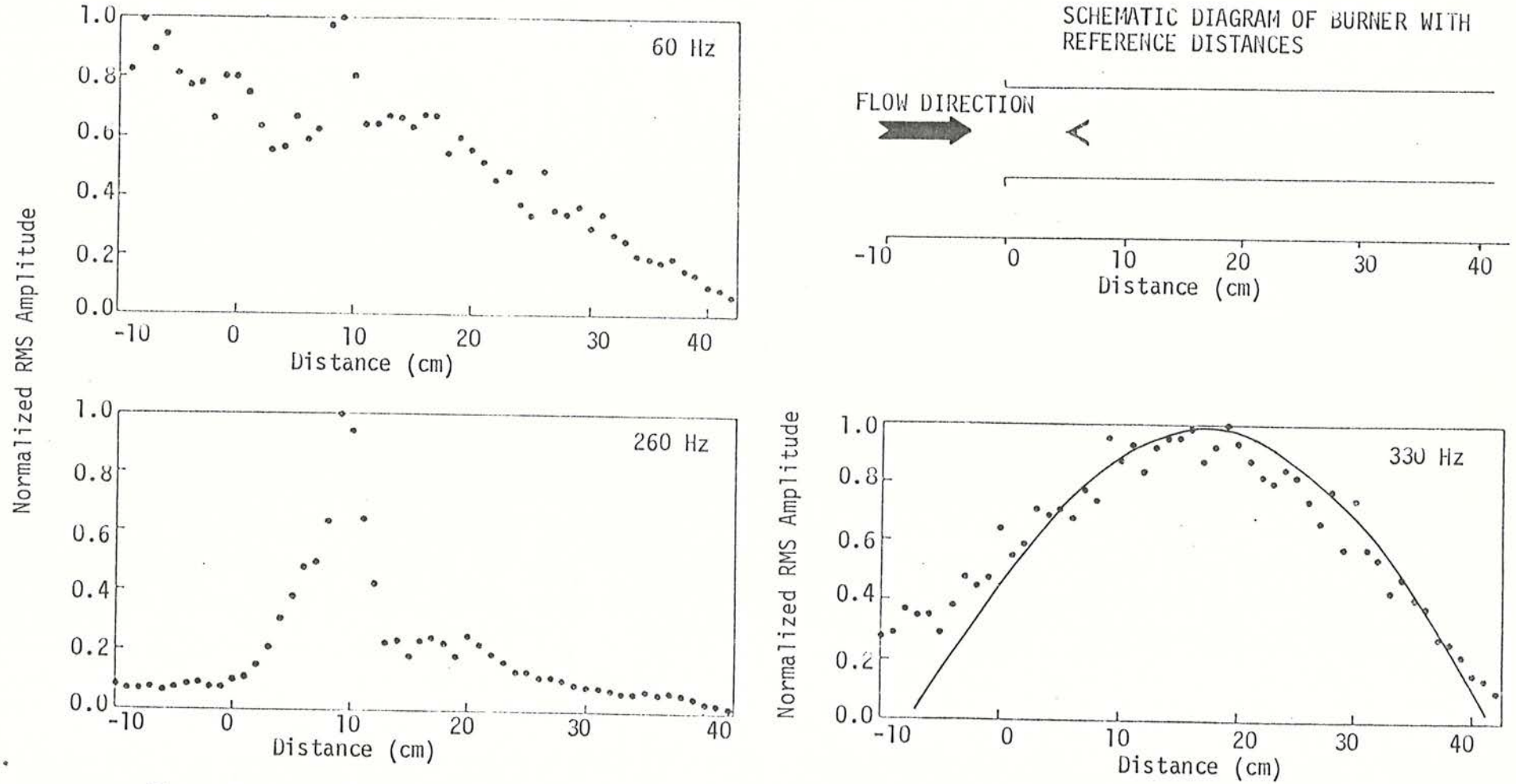


Fig. 3.2 Normalized RMS pressure fluctuation amplitudes versus position in the combustion chamber, for pressure fluctuations centred at 60, 260 and 330 Hz ($L_c$ = 0.05 m, $L_h$ = 0.36 m, $U_o$ = 20 m/s, 20% blockage, $\phi$ = 0.0).

where $\bar{u}_v$ = mean flow velocity around the flame stabilizer
D = height of the flame stabilizer

given in Schlichting (51). During these experiments as well as those of combusting flows, the Reynolds number of the inlet flow based on the hydraulic diameter (52) of the duct was approximately $10^5$. The influence of the vortex shedding on the fluctuating pressure appeared to be localized around the vee-gutter.

The remaining plot of Fig. 3.2 for the 330 Hz signal, shows the profile of a longitudinal standing wave. For the above duct geometry and flow conditions the calculated resonant frequency is 343 Hz (fundamental mode), using the expression

$$\text{frequency} = \frac{c(1 - M^2)n}{2L} \tag{3.2}$$

where c = local speed of sound
M = flow Mach number
n = number of the harmonic (i.e., 1, 2, 3,...)
L = duct length (including end correction terms)

(the derivation of this expression is given in Appendix A).

Plotted against the data points is the theoretical line for the RMS pressure fluctuation of the first harmonic (shown in Appendix A). The profile of the pressure signal is roughly a half sine wave, beginning with zero pressure fluctuation 7 cm upstream of the duct-contraction junction with a similar termination 1 to 2 cm downstream of the duct exit.

In this particular experiment the higher order harmonics could not be obtained, through either lack of sufficient internal excitation or masking, possibly due to the vortex shedding from the flame stabilizer, as it seems that the pressure node for the second harmonic lies near the flame stabilizer.

3.2.1.2 Combusting flow

In an experiment using a short combustion chamber ($L_h$ < 0.50 m)* with a combusting flow, it was possible to excite several organ pipe modes. As an example, in a duct 0.55 m in length ($L_c$ = 0.20 m and $L_h$ = 0.35 m) a water cooled microphone was traversed down the combustion at 1 cm sampling intervals. The results of the analysis for four frequency scans (60, 340, 660, 1000 Hz) are plotted in Fig. 3.3. The discussion of the first plot, 60 Hz, is deferred until the next section, on low frequency oscillations, but it is worth noting that the source of this signal is no longer due to upstream noise as in the cold flow case, but rather due to a source in the combusting flow region of the duct. To give a scale to the peak amplitude of the 60 Hz signal compared to the other frequencies, this signal is at least 10 dB lower than the 100-110 dB sound pressure level of the others.

The second frequency, 340 Hz, represents the first harmonic for this rig geometry. The plot shows the normalized RMS pressure fluctuations beginning close to zero at approximately 7 cm before the entrance to the combustion chamber and terminating with the same amplitude, 1 to 2 cm beyond the duct exit. Between these two points the shape of the curve is a sine wave, which is stretched in the burnt gas region, because of an increase in the local sound speed. The two lengths of the starting points, 7 cm and 2 cm, were common to most of the microphone traverse experiments and were felt to be the experimental end correction terms.

The other two plots, 660 and 1000 Hz, the second and third harmonics respectively, show the expected resonant standing wave profiles. In both plots, the rectified sine wave of the pressure fluctuation lengthened in

---

*As a standard definition used throughout the remainder of the thesis, the combustion chamber is divided into two lengths, $L_c$ and $L_h$. The length $L_c$ is the distance from the junction of the contraction and combustion chamber to the flame stabilizer, and $L_h$ is the length from the stabilizer to the duct exit.

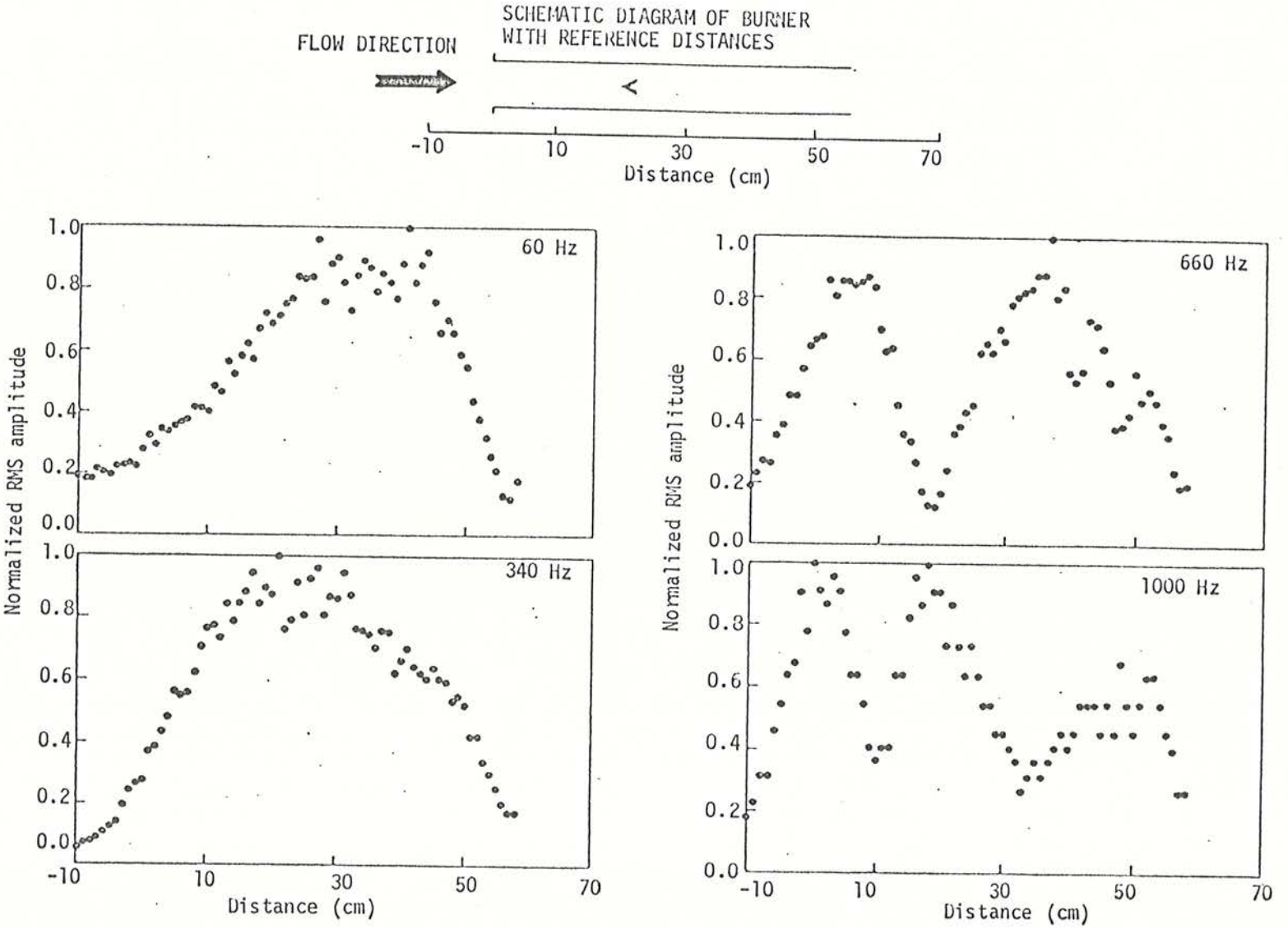


Fig. 3.3 Normalised RMS pressure fluctuation amplitudes versus position in the combustion chamber, for pressure fluctuations centred at 60, 340, 660 and 1000 Hz.
($L_c$ = 0.20 m, $L_h$ = 0.35 m, $U_o$ = 20 m/s, 30% blockage, $\phi$ = 1.15)

the burnt gas region. The transition from cold to hot flow, through a "mean" flame position is approximately 6 to 8 cm downstream of the flame stabilizer. The 1000 Hz signal shows the attenuation effects of the microphone probe, by the fact that there are approximately only 25 voltage levels in the spectrum analyser to represent the full-scale normalized pressure fluctuation.

Similar resonant conditions are present in a duct of sufficient length ($L_h > 0.50$ m) to induce buzzing of the flame. Using the same measuring and analysis techniques as before, with the addition of a wall mounted pressure transducer just upstream of the vee-gutter, a traverse of an 0.81 m duct was made ($L_c = 0.20$ m and $L_h = 0.61$ m). The probe traverse extended from 6 cm upstream of the duct-contraction junction, to 70 cm downstream of the junction. The remainder of the duct could not be traversed because of physical constraints in the laboratory. At 2 cm intervals pressure samples from the microphone probe and simultaneous measurements from the fixed pressure transducer were recorded.

Plotted in Fig. 3.4 are two sets of results of the analysis pertaining to the traverse, one dealing with the normalised RMS pressure fluctuations along the duct for the first and second harmonic resonances, 280 and 560 Hz respectively, while the other shows the phase shift of the standing wave, identified as the phase difference between the two recorded pressure signals. Both normalized pressure fluctuations exhibit a rectified sine wave superimposed on background noise, this being most obvious in the 560 Hz signal. The normalized pressure traverse at 280 Hz shows the significant change in length of the half sine wave in the burnt gas region ($\gtrsim$ 30 cm along the duct from the junction). From the phase information at 280 Hz, pressure downstream tended to lead the upstream pressure by progressive amounts, until at the two ends of the chamber the phase difference is approximately $70^{\circ}$. The same sort of phase trend is visible in the 560 Hz plot, but superimposed on a "step" phase shift of $180^{\circ}$ at approximately 30 cm.

The 60 Hz signal of this traverse will not be considered in this section, but will be displayed and discussed in the section concerning buzz oscillations (section 3.3.2).

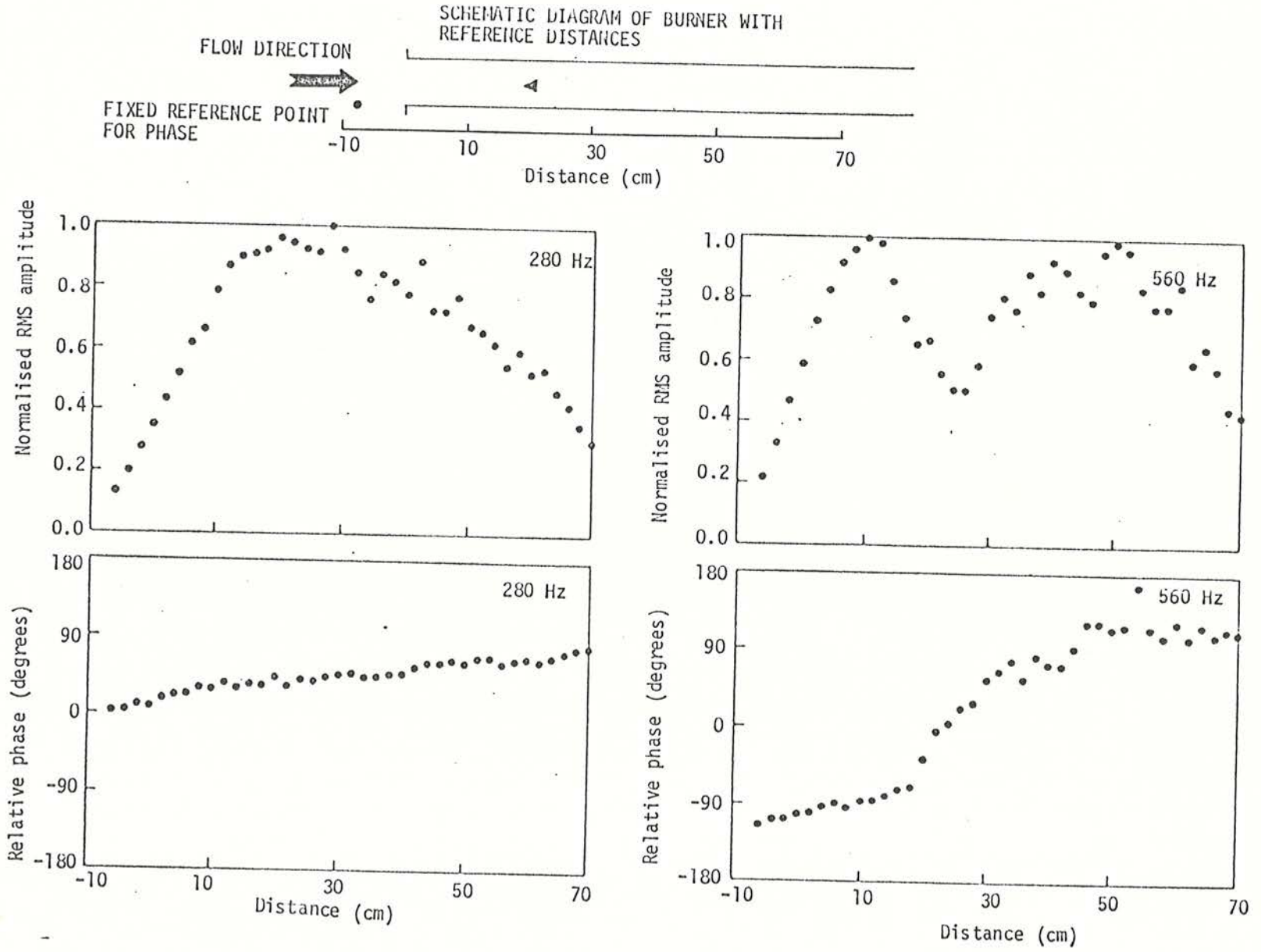


Fig. 3.4 Normalised RMS pressure fluctuation ampliutdes and phase differences versus position in the combustion chamber for pressure fluctuations centred at 280 and 560 Hz.
($L_c$ = 0.20 m, $L_h$ = 0.61 m, $U_o$ = 20 m/s, 30% blockage, $\phi$ = 1.15).

### 3.2.2 Pressure and temperature measurements

A method of investigating longitudinal acoustic modes in the duct, complementary to the water cooled microphone, was through the use of two fixed position measuring probes: a pressure transducer and a platinum/platinum-10%rhodium thermocouple. The two static probes were used together only during non-buzzing combustion experiments as the thermocouple lacked water cooling and was liable to melt if engulfed for prolonged periods (tenths of a second) in burnt gas. However, as long as only the tip of the thermocouple protruded into the flame brush, intermittent unburnt gas slugs cooled the platinum sufficiently to ensure no damage.

The pressure transducer measured the fluctuating pressure at one location in the duct. From a fixed position it is not possible to determine the peak amplitude of a longitudinal wave, but it is sufficient to identify the resonant frequencies. The object of these experiments was to identify any coupling between the acoustic modes of the duct and flame front fluctuations, obtained from measured temperature fluctuations associated with flame movement. Shown in Fig. 3.5 are the relative probe positions used in these experiments, and Fig. 3.6 shows typical spectra from the two probes.

The spectra of Fig. 3.6 are for a chamber of $L_c$ = 0.45 m, $L_h$ = 0.36 m, with a flow of 20 m/s at an equivalence ratio of 1.15 and a vee-gutter blockage of 30%. From the spectra, two frequencies are common to both signals. The pressure signal contains fluctuations from the first, second and third duct resonances, while the temperature signal shows that the flame "bubbles" at two discrete frequencies which correlate with the first and third harmonics in the pressure signal. The "missing" second pressure harmonic in the temperature spectrum does not seem to have been stimulated.

This point will be discussed in the concluding comments of section 3.2.5. The two other peaks of both spectra indicates that there appears to be a coupling between the pressure and flame movement.

Further indications that there is coupling between the flame fluctuations and the pressure fluctuations can be seen by plotting the peak frequencies from both signals from an experiment that involved

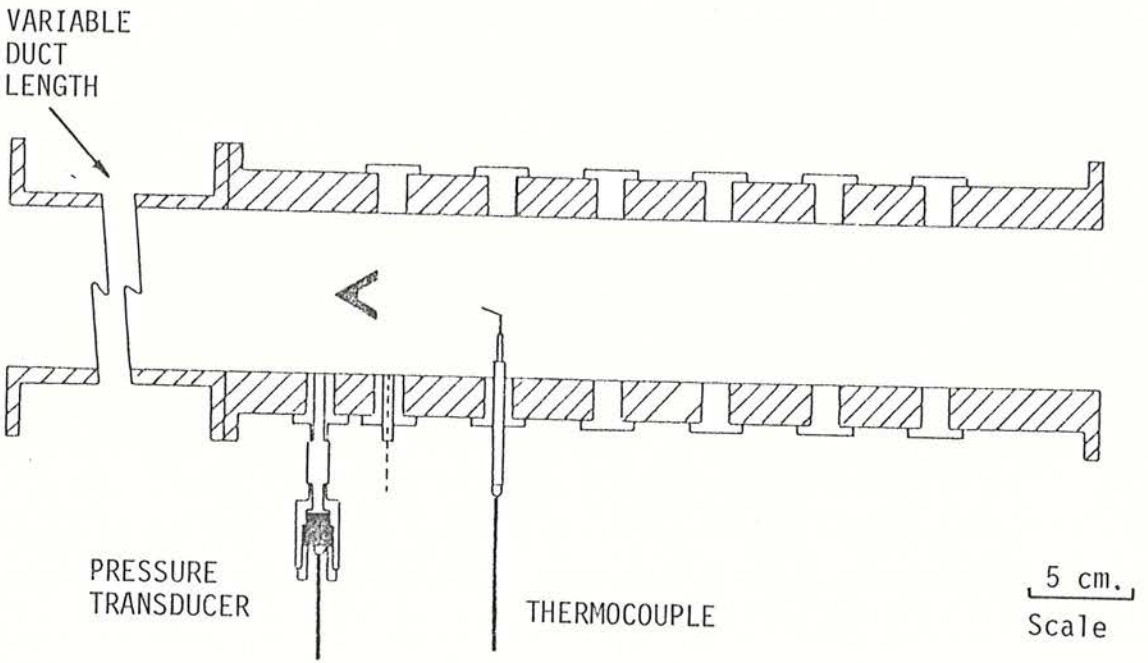


Fig. 3.5 Relative position of pressure transducer and thermocouple in the combustion chamber.

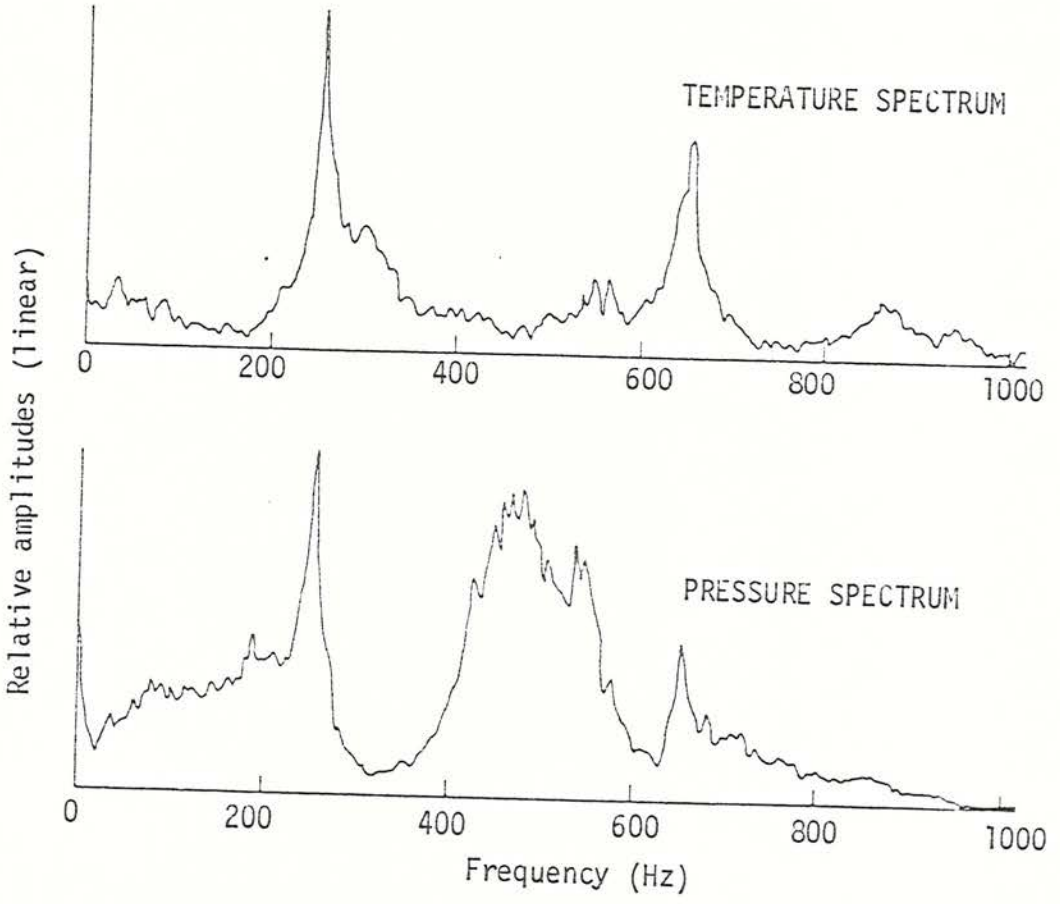


Fig. 3.6 Spectra for pressure and temperature measurements in non-buzzing combustion flow.
($L_c$ = 0.45 m, $L_h$ = 0.36 m, $U_o$ = 20 m/s, 30% blockage, $\phi$ = 1.15)

changes in cold duct length ($L_c$). The experimental conditions were the same as those mentioned above, except that $L_c$ ranged from 0.05 to 0.55 m.

Figure 3.7 shows the effects on the peak frequencies of changing the duct length on both the temperature and pressure fluctuations. As $L_c$ increases, the frequencies of the fluctuations decrease. In most cases the peak pressure and temperature fluctuations were at the same frequencies. However, in some cases, for example at $L_c$ = 0.05 m, one or more harmonics recorded by the pressure transducer were not reflected in the temperature oscillations. Plotted as solid lines against the data points are the theoretical predictions of the frequencies for the first and second longitudinal duct harmonics.

Extending the burnt gas length into the region of low frequency oscillations, the acoustic pressure oscillations were still present. For a duct of $L_h$ = 0.76 m, $L_c$ was varied from 0.05 m to 0.55 m, and only pressure measurements made. Displayed in Fig. 3.8 are the predominent frequencies of the pressure signal measured for varying $L_c$; however, the low frequencies of the buzz oscillation present in the signal are not plotted.

### 3.2.3 Photographs

Spark schlieren photographs of the flame show visually the form of a flame oscillation, Fig. 3.9. For a duct of cold length ($L_c$) = 0.05 m and hot length ($L_h$) = 0.35 m, the flame can be seen to "bubble" at approximately 1000 Hz, (photographs A and B). Although photograph A shows little in the way of a pronounced oscillation, a time average frequency measurement of a thermocouple signal for the flow reveals a 1000 Hz oscillation. The 1000 Hz is close to the second harmonic of the pressure oscillations for the duct.

To extend the use of such photographs, a 5 cm diameter loudspeaker was inserted into the settling chamber through the blowout safety port and driven at 1000 Hz. The result was again a "bubbling" of the flame at 1000 Hz (photographs C and D). The loudspeaker was then tuned to 1600 Hz, with the result that the flame responded and "bubbled" at the

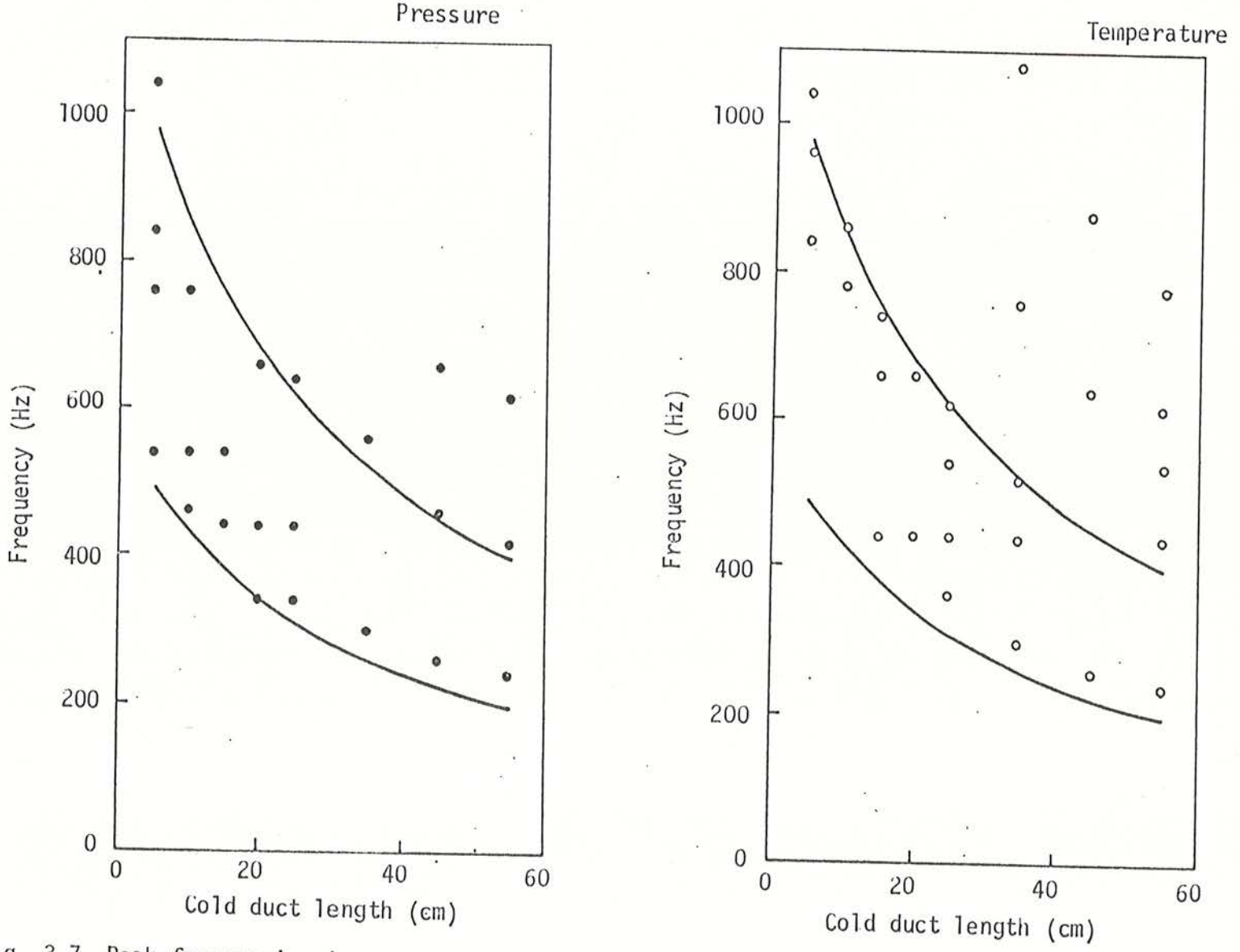


Fig. 3.7 Peak frequencies in pressure and temperature spectra for various cold duct lengths ($L_c$). ($L_h$ = 0.36 m, $U_o$ = 20 m/s, 30% blockage, $\phi$ = 1.15)

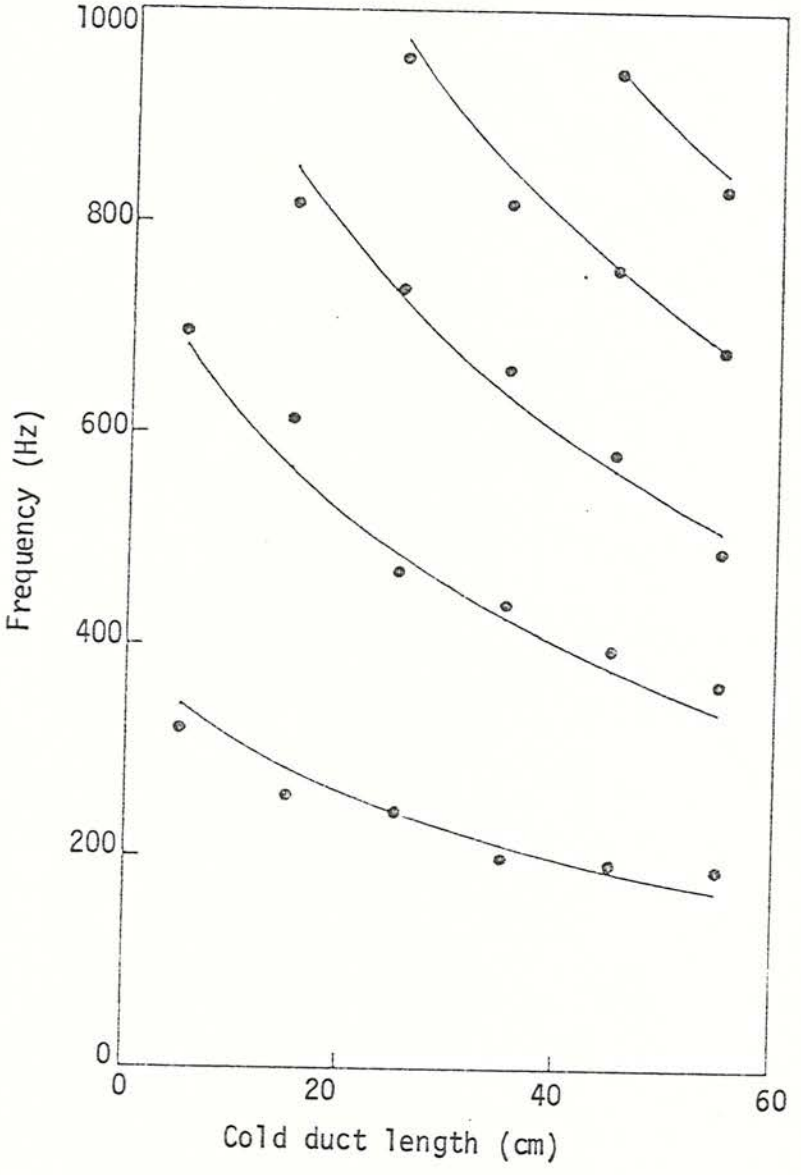


Fig. 3.8 Peak frequencies in pressure spectrum for various cold duct lengths ($L_c$)
($L_h$ = 0.76 m, $U_o$ = 20 m/s, 30% blockage, $\phi$ = 1.15).

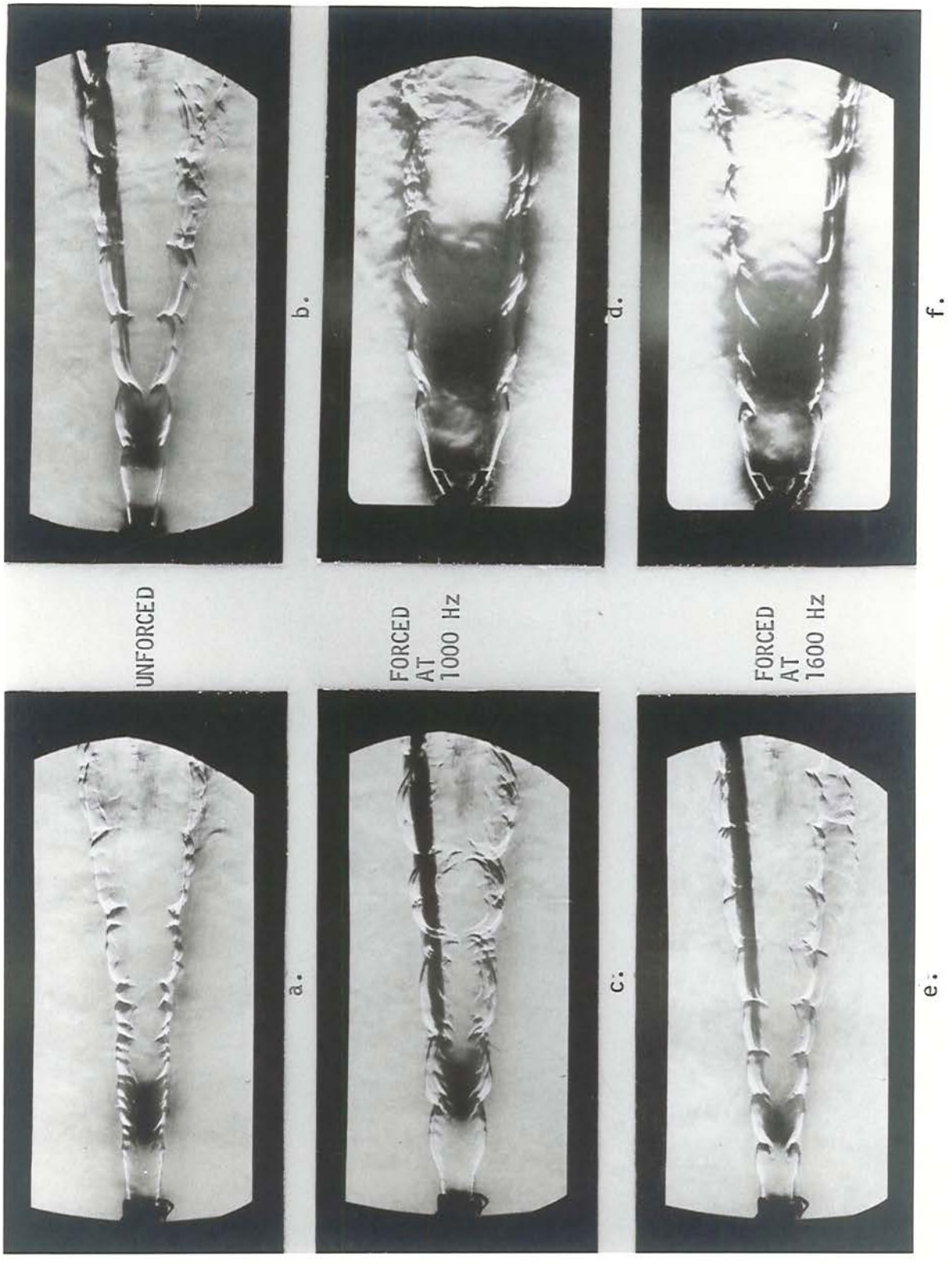


Fig. 3.9 Spark schlieren photographs of a non-buzzing flame subjected to upstream noise of a single frequency.
($L_c$ = 0.05 m, $L_h$ = 0.36 m, $U_o$ = 20 m/s, $\phi$ = 1.0)
(blockage: a - 10%, b - (rod) 6%, c - 10%, d - 20%, e - 10%, f - 20%)

new frequency (photographs E and F). It is clear that the flame couples to the pressure field, but not necessarily at every frequency: for example, the flame did not follow a 500 Hz signal from the loudspeaker. The apparent vortex formation off the vee-gutter would indicate that the pressure oscillations or the resulting velocity fluctuations cause the flow to alter sinusoidally in the region of the stabilizer.

### 3.2.4 Acoustic oscillations summary

The results of the previous subsections indicate the existence of organ pipe oscillations in the combustion chamber in cold, hot or buzzing combustion flows. The frequency and RMS pressure profile of the cold flow resonant standing waves match those predicted by theory and so similar experimental results in combusting flows would again indicate the presence of longitudinal resonant oscillations.

An interesting result of the high frequency oscillation was the flame "bubbling" revealed through photographs and temperature fluctuations. To explain this phenomena, the pressure and velocity fluctuations due to the longitudinal standing waves are examined. If viewed from the flame stabilizer towards the upstream open end of the combustion chamber, the RMS fluctuating pressure amplitude can be expressed as

$$P_{rms} = \left| G \sin \frac{\omega x}{c(1 - M^2)} \right| \tag{3.4}$$

where $x$ is measured from the duct inlet to any location in the cold region of the duct, and $G$ is an arbitrary amplitude. The corresponding velocity fluctuation that accompanies the pressure is,

$$U_{rms} = \left| \frac{G}{\rho c} \cos \frac{\omega x}{c(1 - M^2)} \right| \tag{3.5}$$

The velocity has a maximum where the pressure fluctuations are a minimum and vice versa. If, with the standing waves, the situation arises that at the flame stabilizer the RMS pressure fluctuations are a maximum, then the RMS velocity fluctuation will be at a minimum. With

minimum velocity fluctuations at the trailing edge of the vee-gutter, the flow around the stabilizer is not affected, which could lead to a lack of visible response in the flame shape simply because the flame has no forcing disturbance on it. To test this idea, calculations can be done to determine the nodal positions of the fluctuating velocity for the given condition in the experiment of Fig. 3.7. Approximate calculations show that two duct geometries ($L_c$ = 5 and 10 cm) have a velocity node near the vee-gutter for the first harmonic, while another ($L_c$ = 45 cm) has one in the second harmonic. Re-examining Fig. 3.7, shows that at these three cold lengths although the pressure recorded a peak amplitude for the harmonics, the thermocouple registered nothing. It would appear then that the fluctuations of the flame, visible in the photographs of Fig. 3.9 are determined by the location of velocity nodes for the duct standing waves. The strength of these fluctuations will depend on the pressure field, vee-gutter position and energy transmitted to the pressure field from the combustion process.

Referring back to Fig. 3.1: the higher frequencies C to E are attributable to the first three harmonics of the duct. The measured frequencies from these pressure peaks were 248 (c), 556 (D) and 825 Hz (E), while using the simple approximate expression for the longitudinal modes derived in Appendix A give calculated values at 265, 531 and 797 Hz for the three harmonics.

While confidence has been gained in identifying the high frequencies in the duct, a problem remained in the source of the low frequencies, A and B, of Fig. 3.1. These oscillations did not conform to the longitudinal resonances of the higher frequencies by virtue of the long wavelengths for the low frequencies. In the following section 3.3, experiments were performed to establish the parameters that affected the low frequencies and the characteristics of the oscillations.

## 3.3 Investigation of Low Frequency Oscillations

In the following section the behaviour of the flame is examined by means of high speed schlieren cine, water-cooled microphone probes and pressure transducers, in order to establish some physical appreciation of low frequency combustion oscillations. The previous section involved identifying the higher (C to E) of a pressure spectrum, Fig. 3.1. These oscillations were attributed to organ pipe modes, but the lower frequencies (A and B) do not appear to comply with the same mechanism.

### 3.3.1 Schlieren photography

In order to gain an appreciable physical insight into the movements of the flame during low frequency oscillations, schlieren photography was used. When low frequency disturbances were absent, the mean flow in the duct was steady and the flame shape broadly constant as shown in the spark schlieren photograph of Fig. 3.10. The flame brush is made up of a number of flame "bursts", and although the photograph was obtained with a microsecond exposure, it is representative of the flame at any instant in time. Once low frequency oscillations commence, the quiescent behaviour gives way to a violent cyclic pulsation of the flame.

Spark schlieren photographs give sharp images of the flame but do not resolve the complete flame movement. High speed schlieren cine reveals the cyclical character of the unstable behaviour with slightly reduced resolution. Displayed in Fig. 3.11 is a sequence of 18 photographs taken at 1 ms intervals (representing every fifth frame from the cine film). The flow in each photograph is from left to right as portrayed in the accompanying duct schematic. Initially the flame resembles the quiescent flow of photograph Fig. 3.10, and remains that way until 5 ms. At this point, the flame starts to swell, filling progressively more of the duct cross-sectional area several centimetres behind the vee-gutter. By 8 ms the swelling is quite pronounced and the smaller scale structures, produced by the fluctuating velocity field at the stabilizer accompanying the pressure standing waves, begin to coalesce. This "bunching" phenomenon is obvious by 11 ms. At this point the flame has swept forward to its maximum upstream position, then from 12 ms onward the flame starts

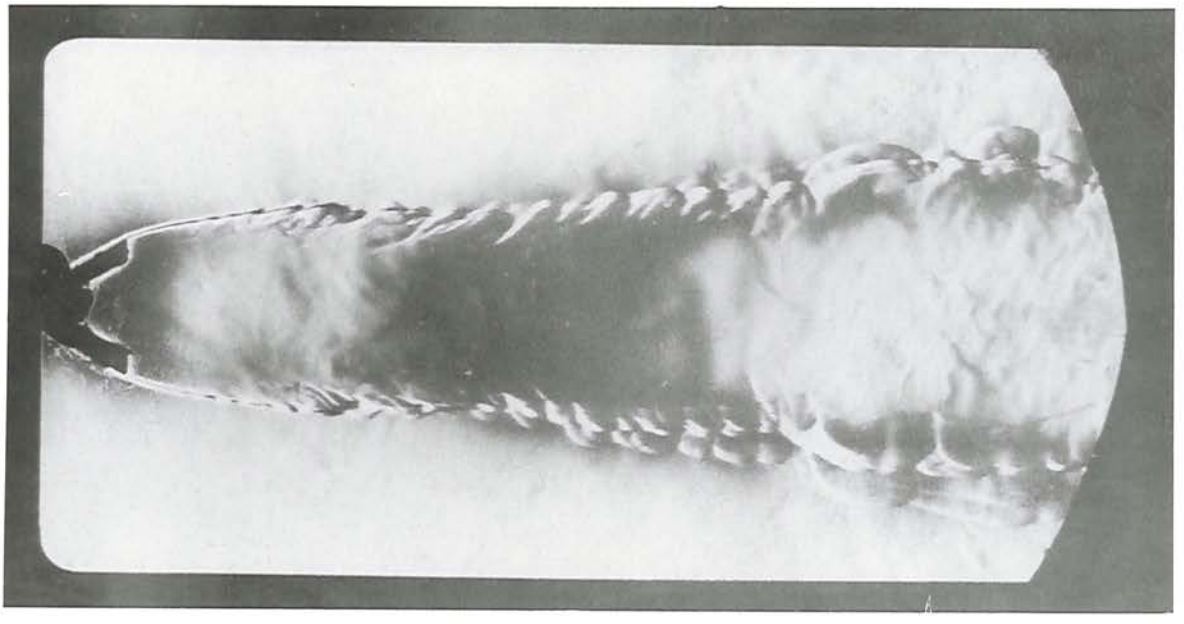

Fig. 3.10 Spark schlieren photograph of a non-buzzing flame. ($L_c$ = 0.05 m, $L_h$ = 0.36 m, $U_o$ = 20 m/s, 20% blockage, $\phi$ = 1.0).

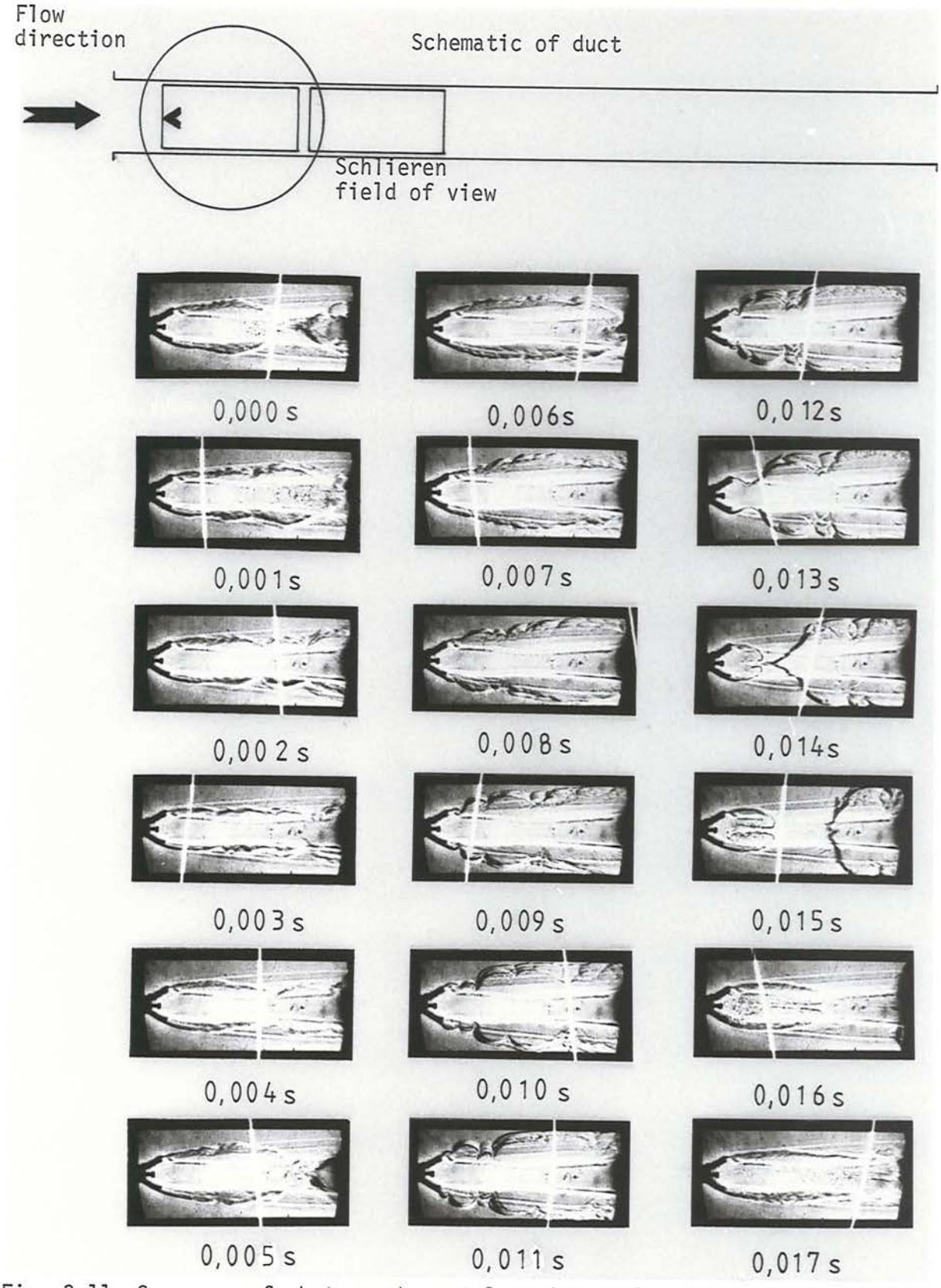


Fig. 3.11 Sequence of photographs, at 1 ms intervals, from a high speed cine schlieren film of low frequency flame motion. Oscilloscope trace of pressure superimposed.
($L_c$ = 0.05 m, $L_h$ = 0.81 m, $U_o$ = 20 m/s, 30% blockage, $\phi$ = 1.15).

to move downstream. Accompanying this initial downstream movement of the flow, a starting vortex is shed by the vee-gutter. For this particular oscillation, the vortex was strong enough to produce a pronounced necking in of the flame, separating the main body of burning gas from that recirculating immediately behind the vee-gutter, leaving a small burning kernel in the vee-gutter wake. The separation of the two flame fronts continues to 15 ms. The kernel continues to grow, resuming the quiescent flame shape and thereafter the cycle is repeated. Whilst this cycle is representative, there are variations from cycle to cycle in the period and the flame motion.

The oscillation amplitude illustrated in these photographs was comparatively modest. A lower amplitude oscillation would cause the flame to simply flicker, with slight swelling during the forward motion of the flame in the cycle. On the other hand, a large amplitude oscillation could cause the flame to propagate upstream during the swelling and travel in the quiescent flow ahead of the vee-gutter. A sequence of photographs at 1 ms intervals, Fig. 3.12, shows this process occurring. The flame has managed to circumvent the flame stabilizer and propagate into the undisturbed inlet flow. The flame movement is finally arrested and blown back downstream, past the vee-gutter. This sequence, like the other series of photographs is cyclically repeated with slight cycle variation.

In the case of strong oscillations, where the flame has either reached or passed the flame stabilizer, the receding flame front during the latter part of the cycle produces a strong starting vortex. In some circumstances successive small vortical disturbances propagate off of the vee-gutter. The initial, and sometimes sole starting vortex in a cycle is responsible for the first low frequency, frequency A in Fig. 3.1, while it is likely that subsequent vortices in a cycle produce the second peak, frequency B.

To gain further understanding of the flame behaviour, velocity and pressure traces were superimposed on the film (described in section 2.3.1) in an attempt to correlate these pieces of information with flame motion. The hot wire anemometer and pressure transducer were mounted diametrically opposite one another 7.6 cm upstream of the flame stabilizer, shown in a representative sketch of a section of the duct, Fig. 2.10. The inability to illuminate multiple traces used for calibration on the film meant that neither pressure nor velocity signals could be ideally calibrated. The

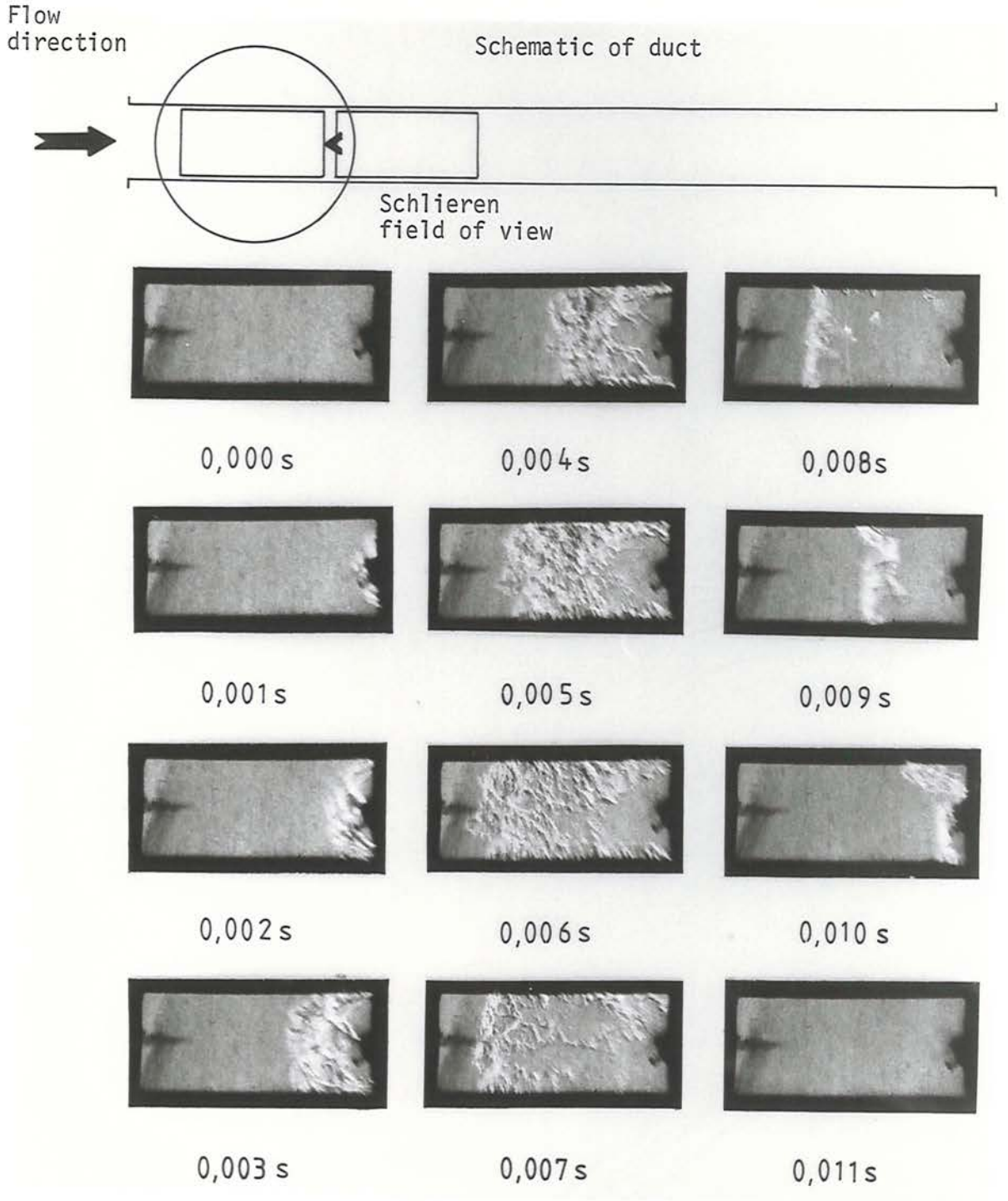


Fig. 3.12 Sequence of photographs, at 1 ms intervals, from a high speed cine schlieren film of low frequency flame motion, upstream of the flame stabilizer.
($L_c$ = 0.20 m, $L_h$ = 0.71 m, $U_o$ = 20 m/s, 20% blockage, $\phi$ = 1.15)

velocity trace from the hot wire anemometer could be calibrated to within 20% of the mean flow using the knowledge of mean and zero velocities from the trace.

The frame by frame analysis of pressure, velocity and flame length (which is termed in section 2.4.1 as any flame front that cuts an imaginary datum line 1.9 cm above the centreline of the duct and measured as the length from the leading window edge to the intersection of flame and this line) is displayed in Fig. 3.13. The abscissa for the figure is the frame count or an equivalent time series of 0.2 ms per frame. The top part of Fig. 3.13 is the uncalibrated pressure signal, which represents the superpositioning of a high frequency acoustic pressure signal on the low frequency signal.

The middle part of the figure is the quasi-calibrated velocity trace. Measuring ahead of the flame stabilizer the velocity ranged from 0 to 40 m/s. In the region of the 35'th to 50'th frame there might have been flow reversal where the mean flow travels back towards the settling chamber, but a single hot wire probe is unable to resolve this condition. Analysis of the data on a PDP 11 shows that between the pressure and velocity signal there is a $82\frac{1}{2}^{o}$ phase shift, with velocity leading pressure, although this is not completely clear from the figure. The velocity trace clearly shows the effect of low frequency oscillation, and the irregularity of the cycles.

The last plot in Fig. 3.13 is the flame position relative to the vee-gutter over the first 50 frames, while the flow velocity approaches 0 m/s, the flame is swelling and approaching the vee-gutter at a speed of approximately 5 m/s. The upstream motion of the flame is finally arrested and by the 60'th frame, the flame is moving back down the duct at a velocity calculated from the flame position, of 40 m/s. From the 70'th to 200'th frame no large oscillations occur with the result that the flame does not move forward but rather bubbles, due to acoustic excitation sending flame "bursts" down the duct at velocities ranging from 20 to 40 m/s (represented by individual lines). The analysis on the PDP 11 indicates that the large scale flame movement lags the velocity by $\sim 15\frac{1}{2}^{o}$.

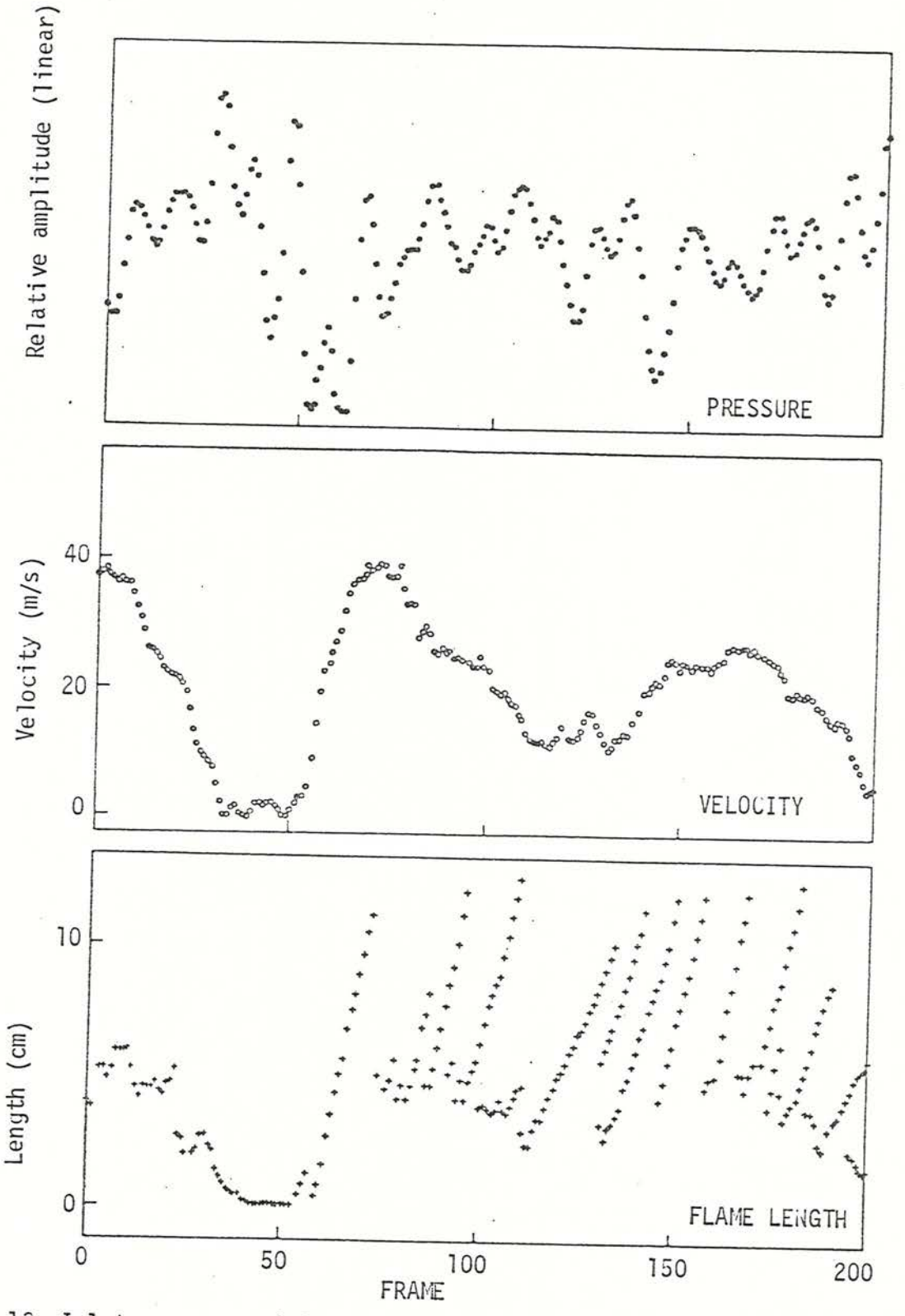


Fig. 3.13 Inlet pressure, inlet flow velocity and flame length measurements from a high speed cine schlieren film per individual photographic frames (1 frame = 1/5000 s)
($L_c$ = 0.25 m, $L_h$ = 0.86 m, $U_o$ = 20 m/s, 30% blockage, $\phi$ = 1.15).

Using the results from both the cine film and spark photographs of Fig. 3.11, a more comprehensive description of the buzz cycle is possible. During the initial quiescent period of burning (0 - 5 ms), the flow begins to decelerate as the upstream pressure in the duct reaches a peak, whilst the flame shape is largely undisturbed. From 6-10 ms, during flame swelling the pressure reaches its peak and the upstream velocity approaches its lowest value. In the time period 10-12 ms the flow velocity reaches its minimum, whilst the pressure starts falling. The flame appears to be stationary during this period at its maximum upstream movement. From 12 to 16 ms the pressure registers its lowest value, whilst the upstream velocity starts to increase through a rapid acceleration and the flame front begins to move down the combustion chamber. During this period the flame necks, splitting into two sections. Several milliseconds after the maximum velocity and rising pressure the flame regains its original shape and the cycle repeats.

To assign some typical values to this process: the velocity fluctuates between a maximum of 40 m/s and minimum of 0 m/s for a mean flow of 20 m/s. During the period of rapid flow acceleration (12-16 ms), the flame was estimated (from velocity calculations) to experience an acceleration of the order of 7500 $m/s^2$. The mean velocity of the flame front after the high acceleration was calculated from its positional changes, to be 40 m/s. The amplitude of the pressure oscillations (sound pressure level) of the low frequency during these cycles was estimated (from velocity fluctuations) to be 145-155 dB, relative to a reference pressure of $2 \times 10^{-5}$ $N/m^2$.

An interesting calculation can be made utilizing the flame front movement observations. In the region where the flame is approaching the vee-gutter (10 to 40'th frames in Fig. 3.13) the flame front is moving into an oncoming flow at an approximate relative velocity of 10 to 20 m/s, whilst from 40 to 70'th frames the flame front is moving relative to the approach flow at approximately 1 to 2 m/s. This suggests that the flame speed is changing during the buzz cycle which could have a pronounced effect on the combustion rate.

### 3.3.2 Water-cooled microphone traverse

In section 3.2.1, the microphone traverse of the acoustic resonant frequencies in the combusting flow, clearly showed the standing wave profiles along the duct. However, the 60 Hz signal, which could not be associated with a standing wave, had quite different traverse profiles. Reviewing the two 60 Hz plots of the cold flow, Fig. 3.2, and non-buzzing combustion flow, Fig. 3.3, a comparison can now be made to the 64 Hz traverse for a buzz flow, Fig. 3.14.

The difference between the three traverses revolves around the source of the low frequency signal. In the cold flow experiment, the source appeared to be upstream of the combustion chamber, probably originating at the mixing baffles, as there was no identifiable source of low frequency noise in the working section. This differed from the non-buzzing combustion flow, where the source appeared to be in the flame brush. Although some noise still appeared to derive from outside the duct, because of the non-zero signal at the duct entrance in Fig. 3.3, a larger portion of sound came from the burning zone. It is probable that this signal was part of broadband noise being emitted by the combustion process. The behaviour of the fluctuating pressure at the open ends of the duct is reminiscent of open ended organ pipes seen in the other frequencies plotted in Fig. 3.3. However, any noise generated in the duct would be expected to terminate in a similar manner. The spectrum for this type of combustion measured by a fixed transducer would show peaks at the acoustic resonances for the chamber dimensions, but there is no discernible peak in the low frequency regime.

In contrast to non-buzzing combustion, single point pressure spectra of buzzing combustion shows a definite peak in the low frequency, as well as the acoustic modes. The microphone traverse of the fluctuating pressure at 64 Hz, shows the combustion region as being the noise source. It is probably that it is in this region that high heat release rates are responsible for the over pressures that induce low frequency oscillations. Conjecture as to the possible mechanism of these oscillations will be left until Chapter 5. To either side of the burning zone, the noise reduces to a node at either end of the duct, similar to that of non-buzzing combustion.

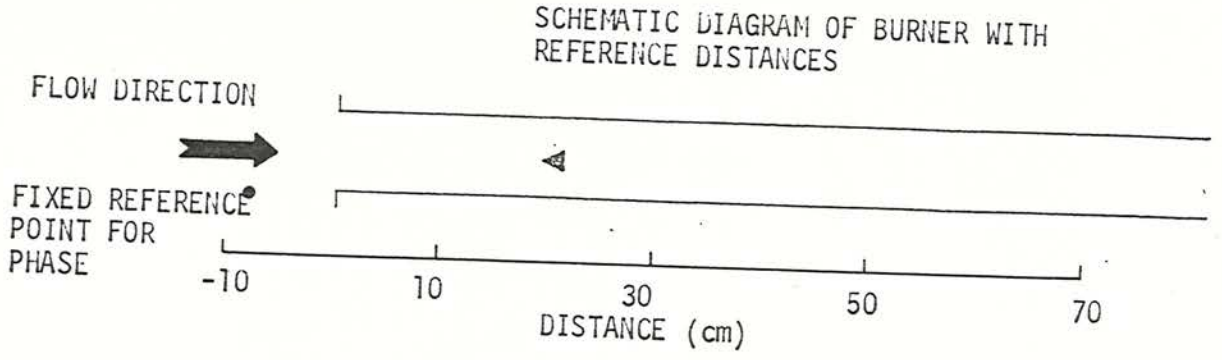


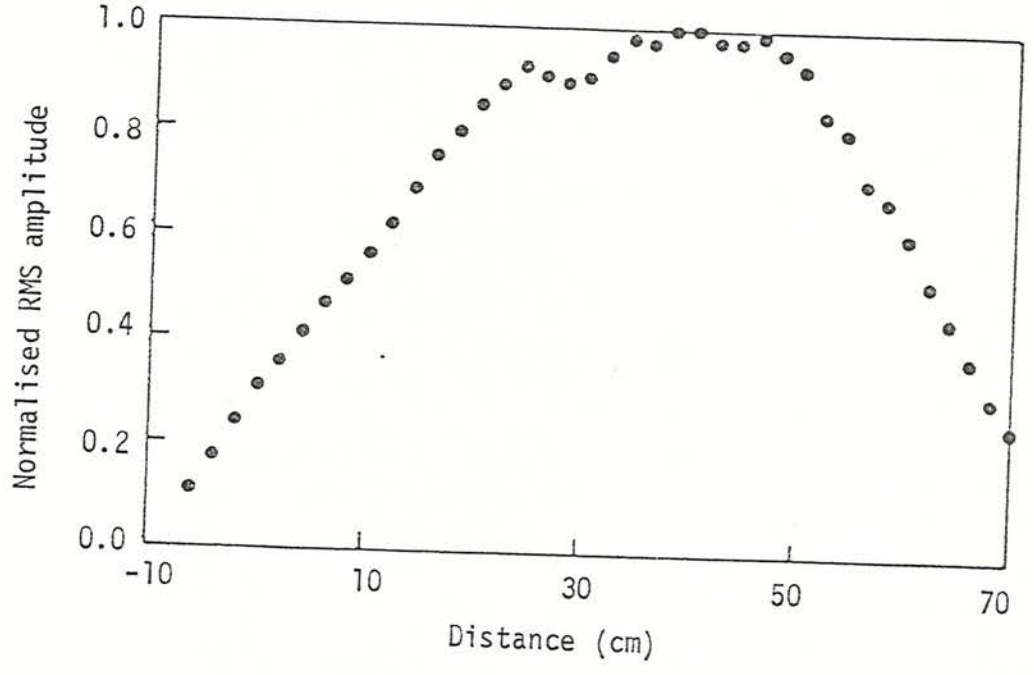


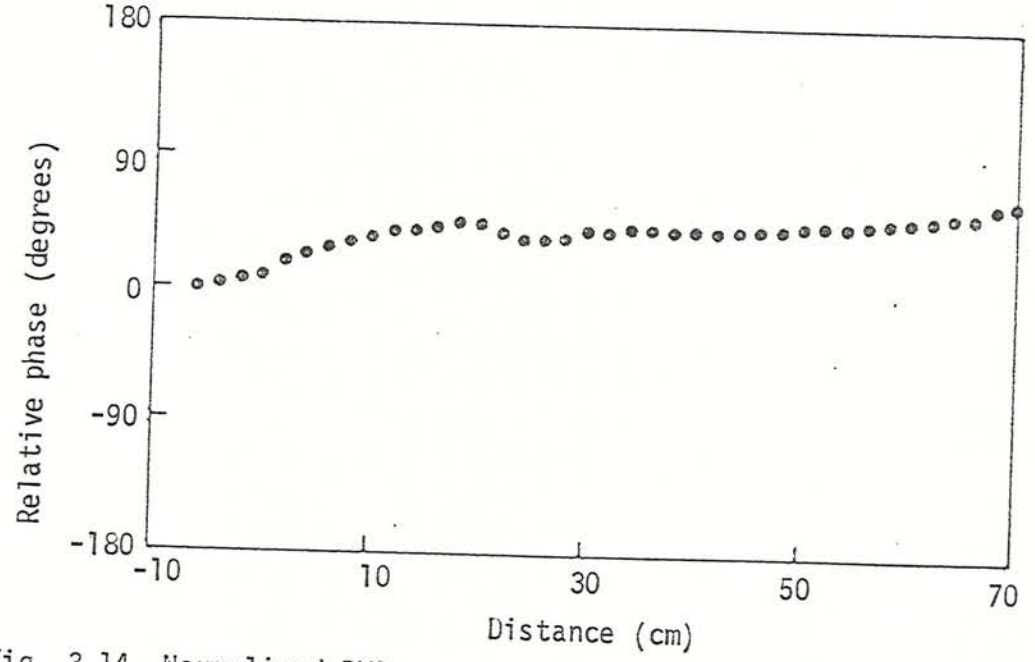


Fig. 3.14 Normalized RMS pressure fluctuations and phase differences versus position in the combustion chamber, for pressure fluctuations centred at 64 Hz ($L_c$ = 0.20 m, $L_h$ = 0.61 m, $U_o$ = 20 m/s, 30% blockage, $\phi$ = 1.15).

The phase relationship between a fixed pressure transducer and the microphone shows an increase in phase moving down the duct, with the downstream pressure fluctuations leading the upstream pressure fluctuations, Fig. 3.14.

### 3.3.3 Pressure measurements

In this subsection the effects of changing the duct configuration and flow conditions on the frequency and amplitude of the low frequency oscillations are examined. A pressure transducer was wall mounted 2 cm upstream of the flame stabilizer, as shown previously in Fig. 3.5, and remained in this relative position to the vee-gutter for all the experiments. Using the HP 3582A spectrum analyser, the pressure signal was determined to an accuracy in frequency of 1 Hz and amplitude of 0.2 dB.

The frequencies measured during separate experiments are generally repeatable to within 5%, whilst the amplitudes were found to vary significantly between the same groups of experiments because of leaks from seals between sections of the combustion chamber and from asbestos packing around the windows. If the pressure in the combustion chamber was released due to a leak, the frequency of the oscillation dropped by several Hertz, while the amplitude decreased by up to 10-15 dB. This meant that care had to be taken in assembling the chamber for each experiment. However, regardless of the painstaking methods applied to assembling the burner, leaks inevitably occurred and several runs had to be repeated. Viewed in this light, sets of results from experiments that encompassed large changes in duct configuration should be compared with caution.

During the course of experiments lasting many hundreds of seconds, the duct heated up significantly before reaching a steady state condition with the walls of the chamber ultimately glowing cherry red (approximately $900^{\circ}C$). Between the time of ignition and obtaining steady-state conditions, the amplitude and frequency of the buzz oscillation rose. Plotted in Fig. 3.15 against time from ignition are the results of amplitude and frequency measurements for four experiments that involved various hot lengths ($L_h$). For the experiment in which $L_h$ was 0.56 m, the buzz

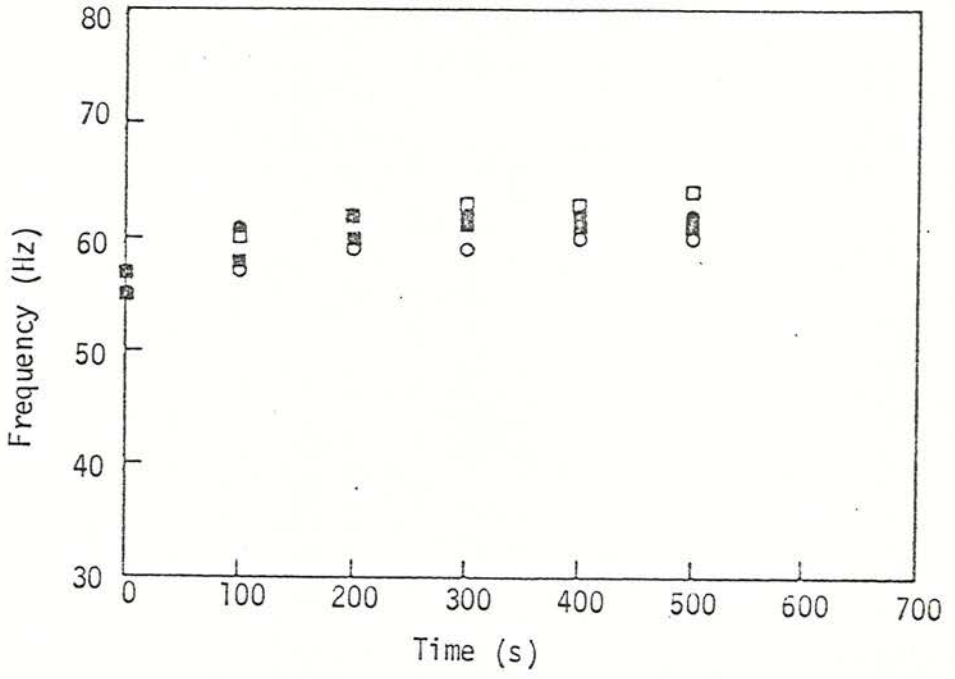


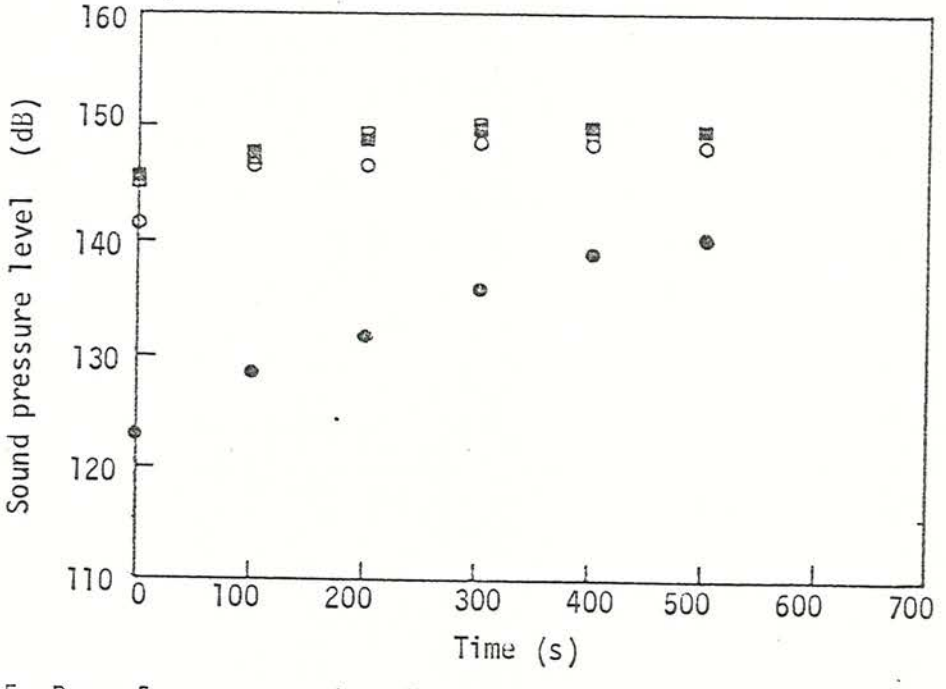


Fig. 3.15 Buzz frequency and peak amplitude versus time following ignition (closing of the trap door) for various hot duct lengths ($L_h$). ($L_c$ = 0.20 m, $U_o$ = 20 m/s, 30% blockage, $\phi$ = 1.15)
($L_h$: □ = 0.86 m, ■ = 0.76 m, ○ = 0.66 m, ● = 0.56 m)

frequency rose from 55 to 60 Hz over 600 s, while the accompanying peak amplitude of the sound pressure level increased from 124 to 142 dB. Experiments of longer hot lengths showed similar changes in frequency and amplitude, but to a lesser degree.

After 300 to 400 s the walls of the duct had usually warmed up sufficiently for the amplitude and frequency to stabilize. Thus, as a standard experimental procedure for the other parameters investigated, the combustion chamber was allowed to equilibrate to this steady state before making measurements of the pressure. A spectrum analyser was used on line during most experiments, so that changes in the buzz amplitude could be monitored directly and detection of the equilibrium state simplified.

Fixing the duct configuration with $L_c$ and $L_h$ at 0.05 m and 0.66 m respectively, the inlet velocity was varied from 20 to 50 m/s in 5 m/s steps. The results of this experiment, displayed in Fig. 3.16, show that the buzz frequency increases roughly linearly with increasing velocity. The corresponding half power limits, plotted on the same graph, indicate a broadening of the peak and larger cycle to cycle variation of the oscillation with increasing frequency. The peak amplitude, however, decreased over the velocity range, showing a decrease of 13.7 dB for a 30 m/s velocity increase. The amplitude at 20 m/s was sufficiently large to cause visible and substantial flame movement around the flame stabilizer. At higher flow rates the power contained in the oscillating flow was spread out over a range of frequencies and not concentrated under a narrow band as at lower velocities. However, the total energy density contained in the spectrum over the half power bandwidth was highest at low flow rates and dropped with increasing flow. In fact the peak amplitude was a good indication of the energy density for the buzz data and will be discussed in the remainder of the thesis instead of the energy.

In experiments involving equivalence ratio changes, the duct geometry was fixed at $L_c = 0.05$ m, and $L_h = 0.18$ m whilst the equivalent ratio was increased from 0.95 to 1.4 in steps of 0.05. The results shown in Fig. 3.17, display the same trends in peak broadening with decreasing peak amplitude as found in the velocity data. Both frequency and amplitude behave similarly, exhibiting an initial rise with increasing equivalence

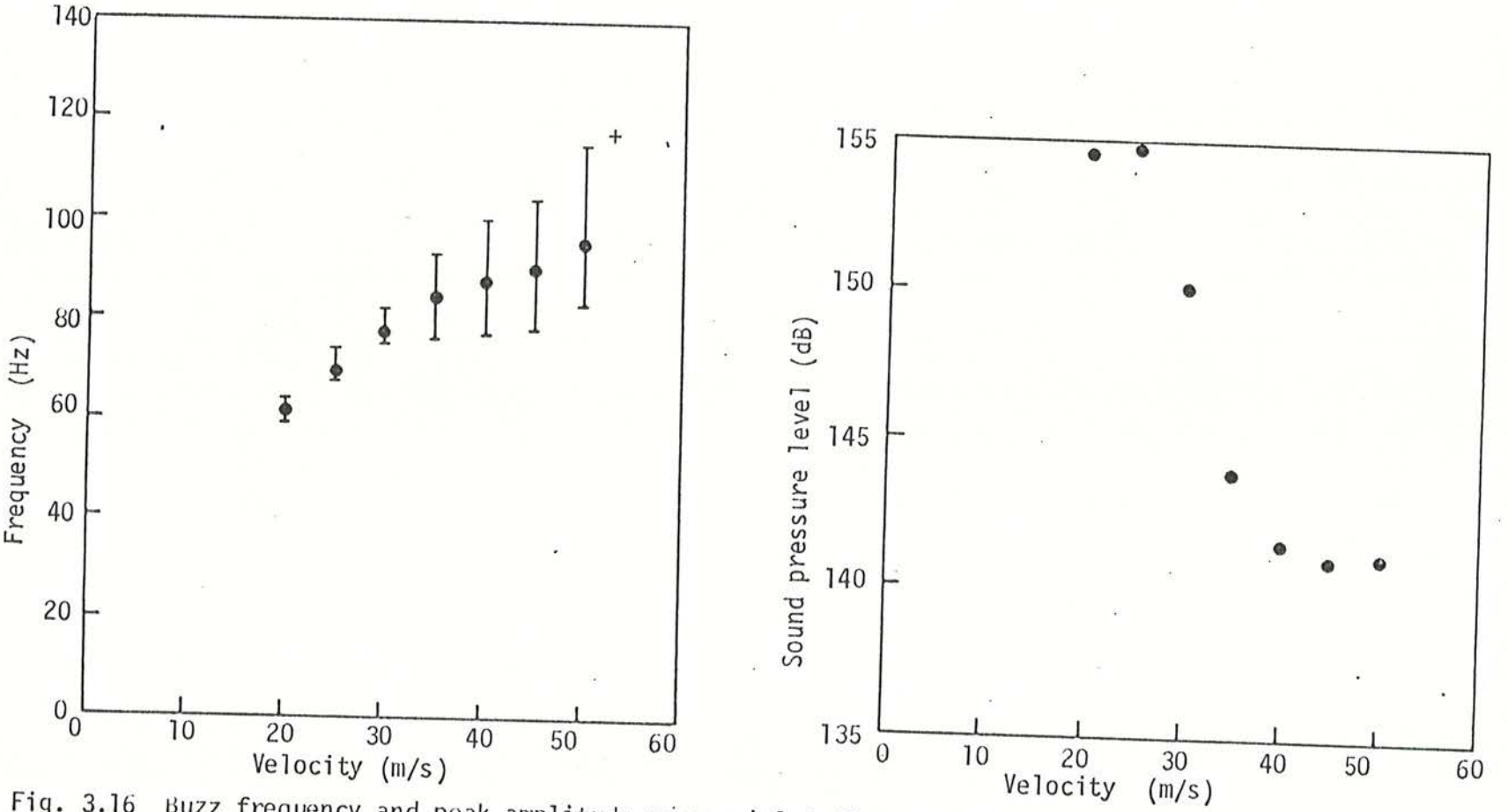


Fig. 3.16 Buzz frequency and peak amplitude versus inlet flow velocity.
($L_c$ = 0.05 m, $L_h$ = 0.66 m, 30% blockage, $\phi$ = 1.15)

+bars represent half power levels in all subsequent frequency plots.

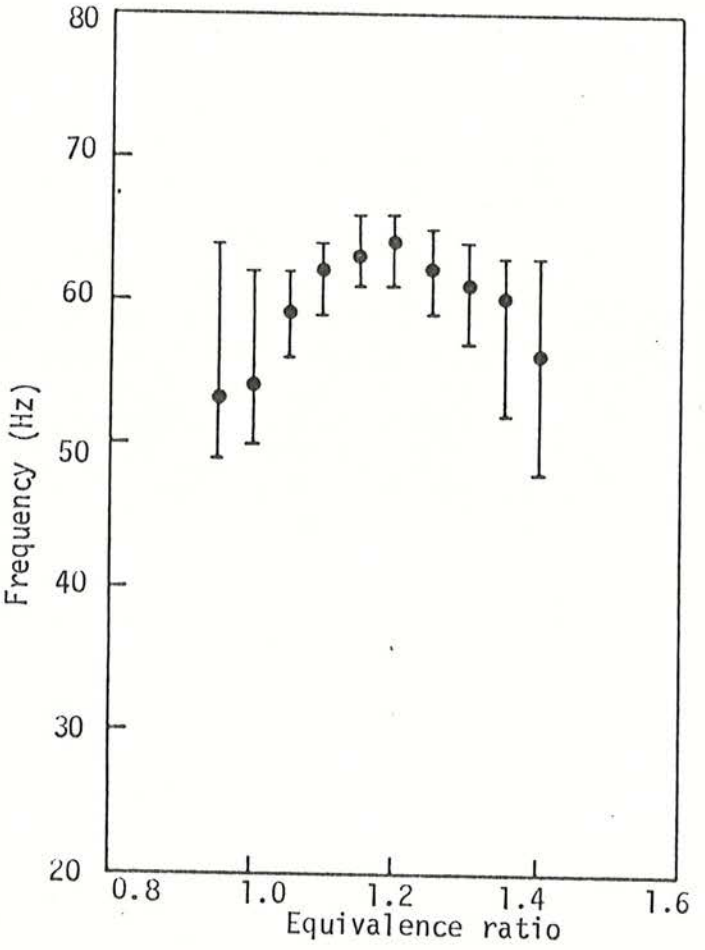


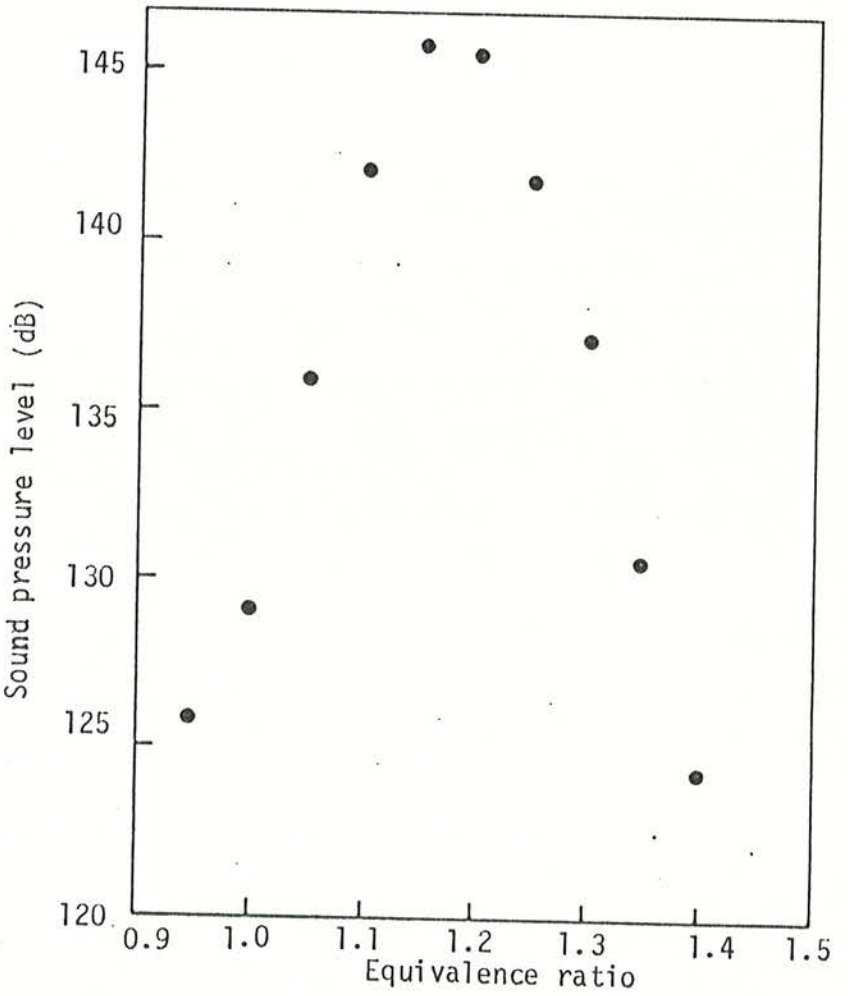


Fig. 3.17 Buzz frequency and peak amplitude versus equivalence ratio ($L_c$ = 0.05 m, $L_h$ = 0.81 m, $U_o$ = 20 m/s, 30% blockage)

ratio, peaking at $\phi \sim 1.2$ and subsequently decreasing with further equivalence ratio increases. The frequency changed by 11 Hz and peak amplitude by 22 dB, over the range of equivalence ratios. By decreasing the heat release, the peak amplitude reduced to a level, not shown on the graph, where below $\phi \sim 0.9$ or above $\phi \sim 1.4$, buzz oscillations could not be identified from background noise in the pressure spectrum.

The above tests did not involve duct geometry changes, only flow condition variations. To investigate the duct parameters, both vee-gutter size and duct lengths were changed. In the experiments with different vee-gutters, the duct lengths were fixed with $L_c$ and $L_h$ being 0.05 m and 0.66 m respectively, the flow velocity was set at 20 m/s for an equivalence ratio of 1.15. The size of the vee-gutters are characterized in percentage blockage of the cross-sectional area of the duct. Five different sizes were used ranging from 10 to 50% blockage in 10% steps. For tests involving duct geometry changes the flow was maintained at 20 m/s with an equivalence ratio of 1.15. Where changes in the cold length are reported, the hot length was fixed at 0.559 m and 0.863 m, with a 30% blockage flame stabilizer. Changes in the hot length are made with a fixed cold length of 0.20 m.

The effects of these duct changes on the buzz frequency and peak amplitude are summarized in table 3.1 and individually displayed in Figs. 3.18 to 3.21. Increasing the vee-gutter blockage increased the frequency, but the peak amplitude rose to a maximum at 30% blockage and then decreased, as shown in Fig. 3.18. At 10% blockage the peak amplitude and energy density were less than at 30% blockage, yet visually the flame movement was more noticeable for 10% blockage. At 50% blockage metal windows were used in place of the glass for safety reasons and this entailed all the tests being re-run with metal windows, so no observations of the flame were possible at this blockage.

For the experiments involving cold length changes, the frequency generally decreased with increasing $L_c$, although the amplitude variation was quite different. In a test where $L_h = 0.55$ m, the peak amplitude rose from 128 to 140 dB with an increase in $L_c$ from 0.05 to 0.35 m, then subsequently decreased to 136 dB as $L_c$ increased further to 0.56 m (see Fig. 3.19). With $L_h$ set at 0.86 m, however, the amplitude rose

Velocity (m/s)

| | 20 | 25 | 30 | 35 | 40 | 45 | 50 | |
|---|---|---|---|---|---|---|---|---|
| Frequency | 62 | 71 | 78 | 86 | 92 | 93 | 95 | hz |

Blockage (%)

| | 10 | 20 | 30 | 40 | 50 | |
|---|---|---|---|---|---|---|
| Frequency | 45 | 50 | 58 | 62 | 75 | hz |

Equivalence Ratio

| | 0.95 | 1.0 | 1.05 | 1.1 | 1.15 | 1.2 | 1.25 | 1.3 | 1.35 | 1.4 | |
|---|---|---|---|---|---|---|---|---|---|---|---|
| Frequency | 53 | 54 | 59 | 62 | 63 | 64 | 62 | 61 | 60 | 56 | hz |

Cold Duct Length (cm)

| Hot Duct Length (cm) | | 5.0 | 15.2 | 25.4 | 35.5 | 45.7 | 55.9 | |
|---|---|---|---|---|---|---|---|---|
| Frequency | 55.8 | 59 | 60 | 57 | 55 | 49 | 51 | hz |
| | 86.4 | 64 | 62 | 60 | 60 | 57 | 55 | |

Velocity (m/s)

| | 20 | 25 | 30 | 35 | 40 | 45 | 50 | |
|---|---|---|---|---|---|---|---|---|
| Amplitude | 154.3 | 154.5 | 148.9 | 143.7 | 141.3 | 140.7 | 141.0 | db |

Blockage (%)

| | 10 | 20 | 30 | 40 | 50 | |
|---|---|---|---|---|---|---|
| Amplitude | 125.7 | 135.2 | 140.2 | 133.2 | 121.7 | db |

Equivalence Ratio

| | 0.95 | 1.0 | 1.05 | 1.1 | 1.15 | 1.2 | 1.25 | 1.3 | 1.35 | 1.4 | |
|---|---|---|---|---|---|---|---|---|---|---|---|
| Amplitude | 125.6 | 129.0 | 135.8 | 141.9 | 145.6 | 145.3 | 141.6 | 136.9 | 130.4 | 121.1 | db |

Cold Duct Length (cm)

| Hot Duct Length (cm) | | 5.0 | 15.2 | 25.4 | 35.5 | 45.7 | 55.9 | |
|---|---|---|---|---|---|---|---|---|
| Amplitude | 55.8 | 127.9 | 128.9 | 137.4 | 139.8 | 136.6 | 135.6 | db |
| | 86.4 | 146.6 | 151.2 | 153.3 | 148.7 | 145.1 | 142.7 | |

Table 3.1 Tabulated values of buzz frequency and peak amplitude for inlet flow velocity, vee-gutter blockage, equivalenceratio and cold duct length changes.

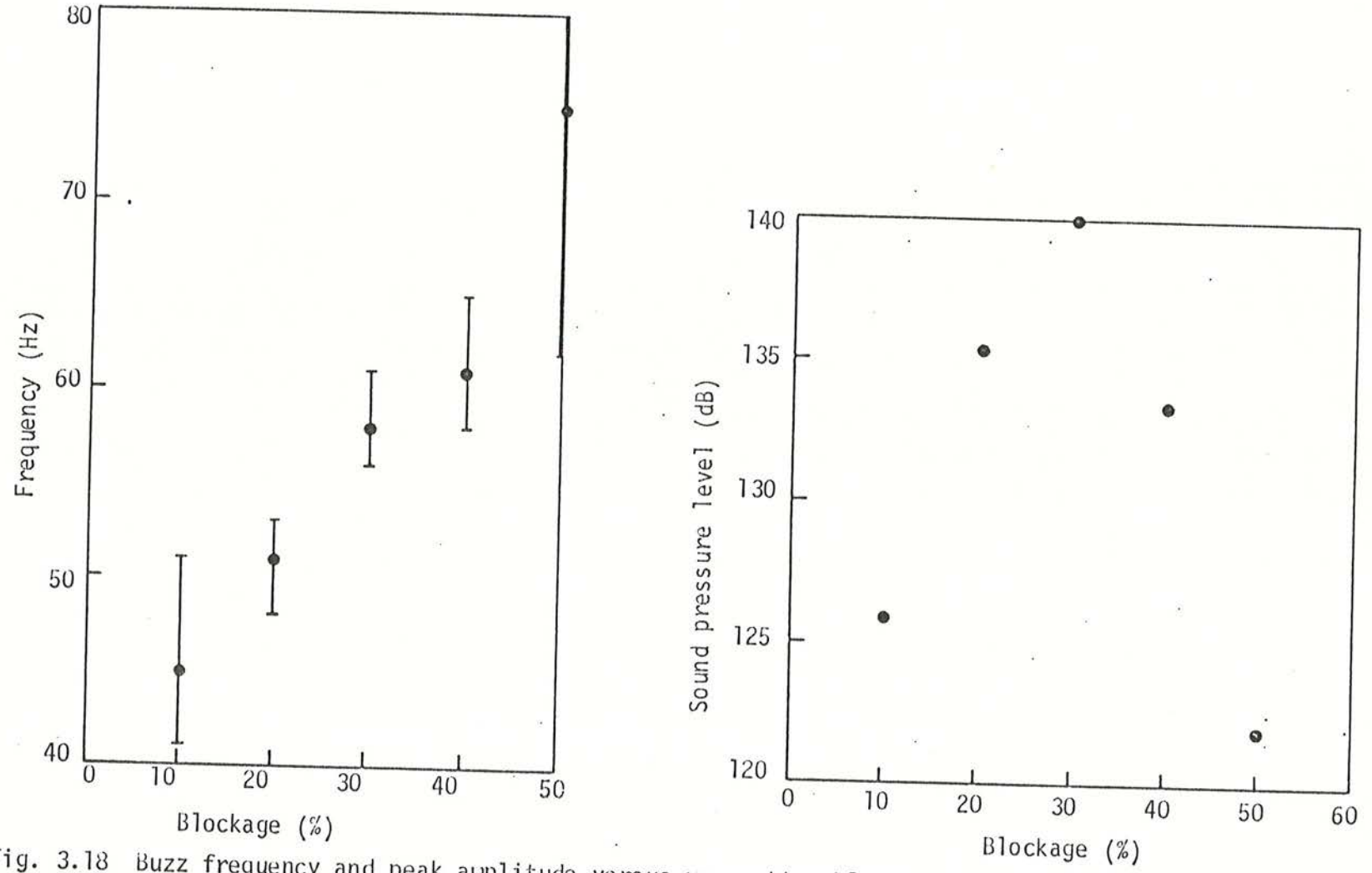


Fig. 3.18 Buzz frequency and peak amplitude versus vee-gutter blockage ($L_c$ = 0.05 m, $L_h$ = 0.66 m, $U_o$ = 20 m/s, $\phi$ = 1.15)

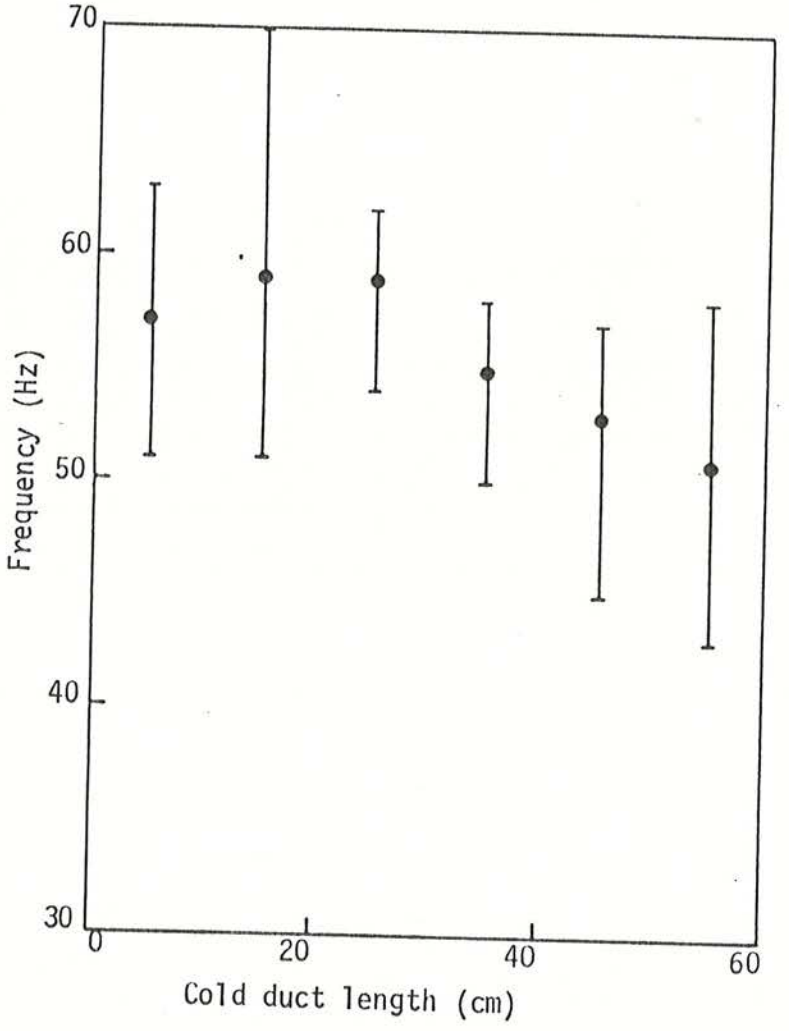


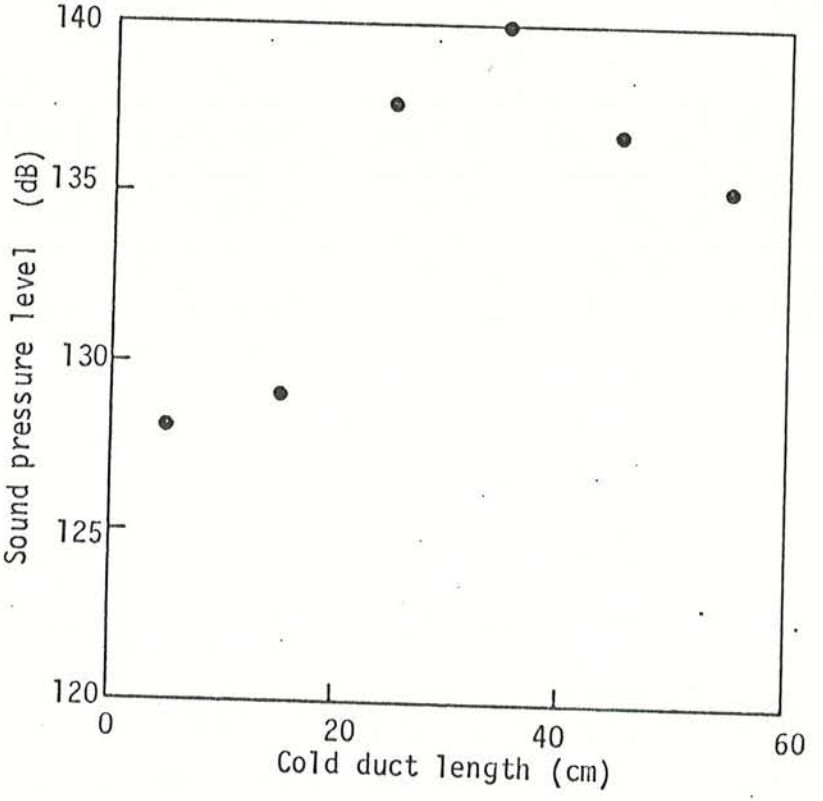


Fig. 3.19 Buzz frequency and peak amplitude versus cold duct length ($L_c$)
($L_h$ = 0.56 m, $U_o$ = 20 m/s, 30% blockage, $\phi$ = 1.15)

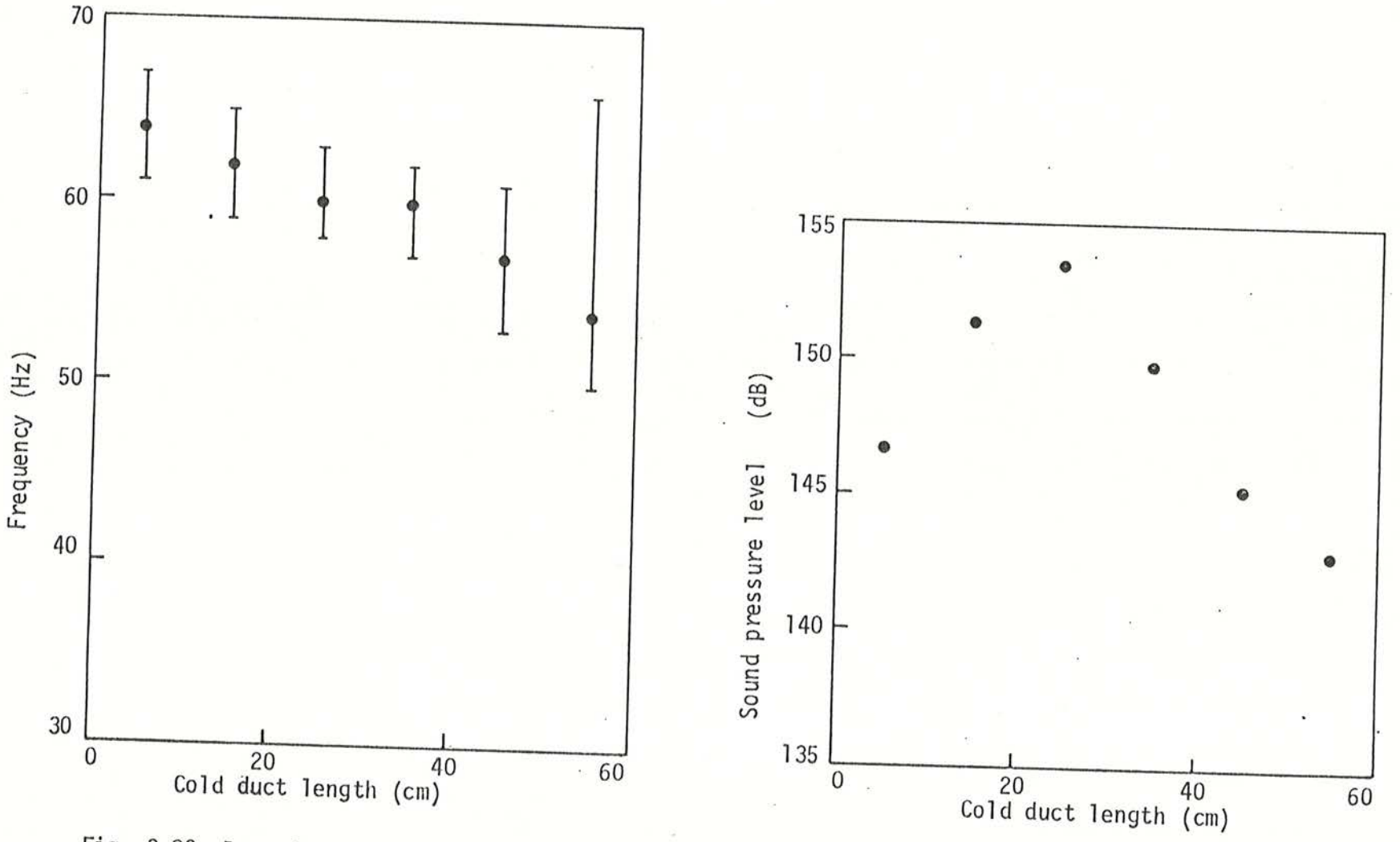


Fig. 3.20 Buzz frequency and peak amplitude versus cold duct length ($L_c$). ($L_h$ = 0.86 m, $U_o$ = 20 m/s, 30% blockage, $\phi$ = 1.15).

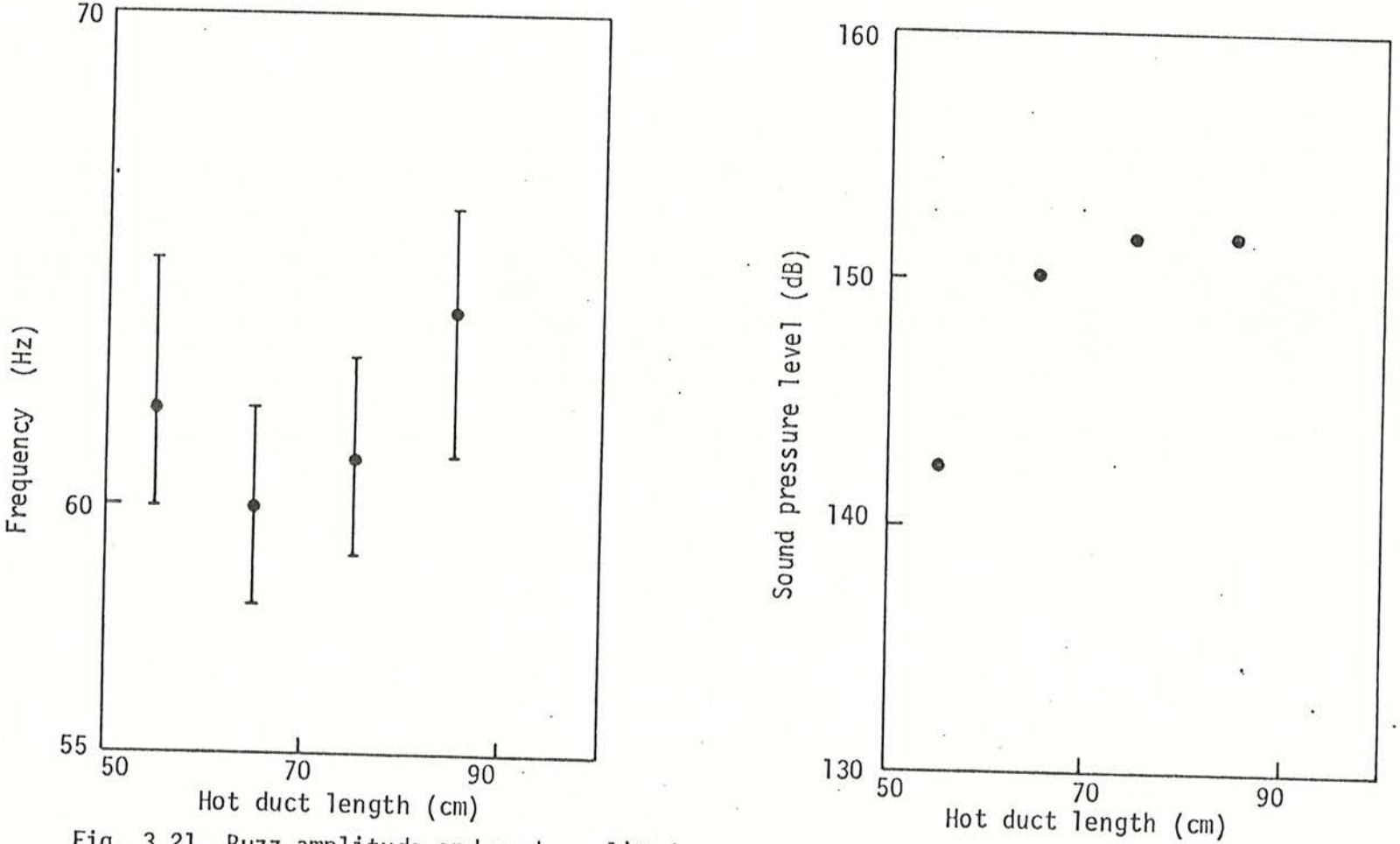


Fig. 3.21 Buzz amplitude and peak amplitude versus hot duct length ($L_h$)
($L_c$ = 0.20 m, $U_o$ = 20 m/s, 30% blockage, $\phi$ = 1.15)

from 147 to 153 dB with the peak at $L_c$ = 0.25 m, then decreased to 143 dB as $L_c$ was further increased, Fig. 3.20.

When the cold length was fixed and the hot length varied, Fig. 3.21, the effect on amplitude and frequency was different. Fixing $L_c$ at 0.20 m and varying $L_h$ from 0.56 to 0.86 m, the frequency initially fell and subsequently rose with increasing $L_h$. The peak amplitude rose continuously from 142 dB to a levelling peak at 157 dB over the $L_h$ range.

The combination of the above experimental results outlined the changes that could occur to the low frequency oscillation with changes to the experimental rig and flow. The frequency of the oscillation could be increased by the following:

- increases in the inlet flow velocity
- increases in vee-gutter blockage
- maximizing the heat release through the equivalence ratio
- decreases in the cold length ($L_c$) of the duct.

While the peak amplitude could be decreased by:

- increases in the inlet flow velocity
- minimizing the heat release (but retaining combustion)
- decreases in the vee-gutter blockage
- decreases in both hot and cold duct lengths ($L_h$ and $L_c$).

These results gave information concerning the effect of each parameter on buzz which is useful in hypothesising a possible mechanism for buzz and in the longer term in testing models of the oscillation, as will be done in Chapter 5.

### 3.3.4 Upstream noise sources

In the preceding subsections, the experiments have concentrated on combustion zone behaviour. It is, however, possible to envisage a simple controlling mechanism for the oscillations involving an upstream noise source or resonator in the rig. A series of experiments were conceived to investigate this possibility.

### 3.3.4.1 Helmholtz resonator

Hakluytt and others (40,30) have suggested that a Helmholtz resonator is capable of driving the flame oscillation. This experimental rig contains the basic elements needed to excite such a resonance, with the settling chamber as the enclosed volume and the duct as the throat with a driven mass. An equation for the frequency of natural oscillation can be readily derived (53) in the form,

$$f = \frac{c}{2\pi}\sqrt{\frac{S}{L\upsilon}} \qquad (3.6)$$

where $c$ = sound speed in the throat

$S$ = cross-sectional area of the duct

$L$ = effective length of the duct

$\upsilon$ = diffuserplus settling chamber volume

To investigate the Helmholtz resonance in the rig without combustion or flow, a piston was mounted in the floor of the settling chamber, through the safety blow out port, and driven by an external vibrator (98N, 400 series Ling Dynamics Systems), whilst a Muirhead probe microphone (Type H-112) was mounted in the outlet of the duct. By vibrating the piston using a frequency generator (Farnell Type LFM2) and power amplifier, the response of the duct to individual driving frequencies could be measured. The peak signals were recorded by the microphone at the frequencies specified by the above equation ($\pm$ 5%). This result indicated that the rig behaved in accordance with a simple Helmholtz resonator, and that if the Helmholtz resonator was to drive the flame, it might be expected to do so in a manner according to the above equation (3.6).

Since changes in the duct length had already been observed to alter the buzz frequency, it seemed more appropriate to examine the effect of changing the upstream volume. To this end, a series of experiments were carried out in which the settling chamber was either left in place, removed or doubled in size for a particular duct geometry. Conditions of the experiments were $L_c$ and $L_h$ of 0.50 m and 0.71 m, respectively, inlet flow velocity of 20 m/s at an equivalence ratio of 1.15. The

results of the buzz frequencies against Helmholtz volume are plotted in Fig. 3.22, showing that large changes in volume produce very small changes in frequency, < 10%. The amplitude change over the three volumes was 2 dB at 144 dB peak amplitude. The measured frequencies were two or three times greater than those calculated from equation (3.6).

The piston used in the Helmholtz experiments was driven during a buzz experiment at a number of frequencies near that of the buzz oscillation. The analysis of the effect of the induced single frequency was monitored by a combination of a wall mounted pressure transducer near the vee-gutter and an on-line spectrum analyzer. The signal derived from the driven oscillator was clearly visible in the pressure spectrum in the combustion chamber. The peak amplitude of the induced vibration was usually 5 to 10 dB lower than the buzz amplitude. Changing the piston frequency above or below the buzz oscillation produced no visible effect on buzz. Both signals could co-exist within several Hertz without effect. This indicated that an upstream noise source did not affect the buzz oscillation.

Similarly, the upstream volume did not appear to be excited as a Helmholtz resonator when there was combustion in the duct.

### 3.3.4.2 Mixing baffle noise

A further possible noise source examined was that of the mixing baffles. These were known to produce significant noise levels, when air was passed through the four perforated plates.

A wall mounted pressure transducer was placed 12 cm downstream of the baffles in a 25 cm extension piece of pipe placed between the mixing baffles and inlet to the diffuser. At a flow of 20 m/s a discrete peak appeared in the noise spectra from the transducer at approximately 70 Hz. This frequency did not appear to change with flow velocity or combustion chamber length. Although it seemed to originate from the baffles, the question this prompted was 'how far would this disturbance influence downstream sections of the rig?'.

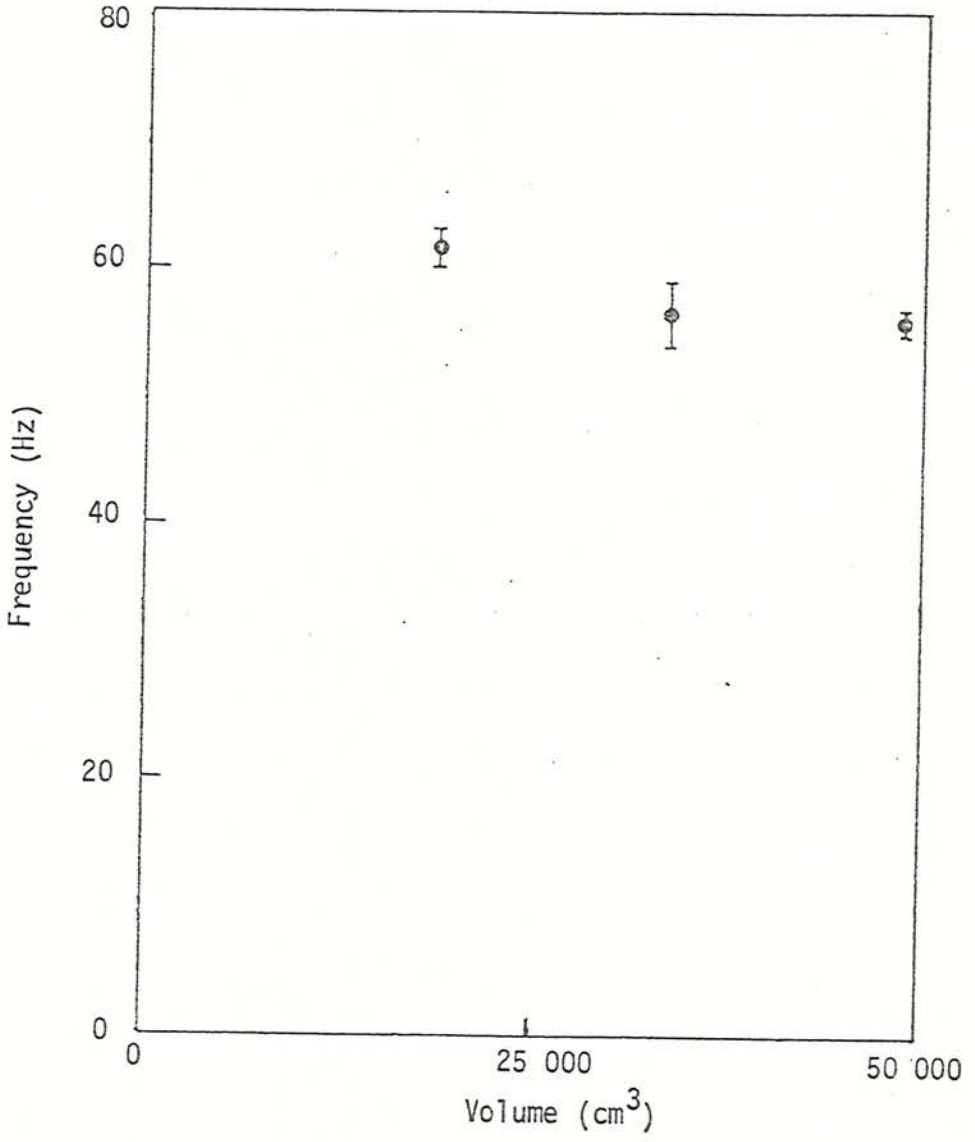


Fig. 3.22 Buzz frequency versus settling chamber-diffuser volume ($L_c$ = 0.05 m, $L_h$ = 0.71 m, $U_o$ = 20 m/s, 30% blockage, $\phi$ = 1.15).

Since previous experiments, involving noise measurements in cold flow at the entrance of the combustion chamber, had shown only low amplitude noise at 70 Hz, it was assumed that most of the noise from the baffle was dissipated in the settling chamber. As a test of the noise transmission down the rig, the baffles were replaced by a specially constructed loudspeaker and housing. White noise was transmitted down the duct from the loudspeaker. The sound pressure level measured by a Muirhead microphone probe in front of the loudspeaker was compared with that measured with the same probe in the duct at the other end of the rig. The results, Fig. 3.23, indicate that an approximate 20 dB attenuation of the signal occurred at 70 Hz, but at 40 Hz the attenuation was only 5 dB. Higher frequencies were subjected to 20-30 dB attenuation by the rig, most likely due to the foam on the walls of the diffuser.

The conclusions drawn from this exericse were that noise generated in the upstream part of the rig, i.e., orifice plate or mixing baffles, was strongly attenuated by the diffuser-settling chamber. Thus noise generated directly by the baffles would not have a noticeable influence in the combustion chamber.

### 3.3.4.3 Standing waves

The results of the previous section 3.3.4.2 indicate that noise generated by the baffles was attenuated by the settling chamber. However, because of the lengths involved in the upstream sections of the rig, it could be possible to produce standing waves in these regions that would couple with the combustion process in the duct.

Two microphone traverses were made: one in the diffuser during a buzz experiment and a second in the settling chamber during an air run. The results of both traverses indicated that there were three pronounced standing waves at 116, 240 and 330 Hz, with a strong signal at 72 Hz. The microphone traverse in the cold air flow (without a chamber) are displayed in Fig. 3.24. The 72 Hz signal appears to start in the region of the choked plate or mixing baffles and terminates at the contraction. The other three frequencies appear to start at the baffles and terminate

The upstream section of the experimental rig.

Schematic diagram of rig and microphone measurement locations

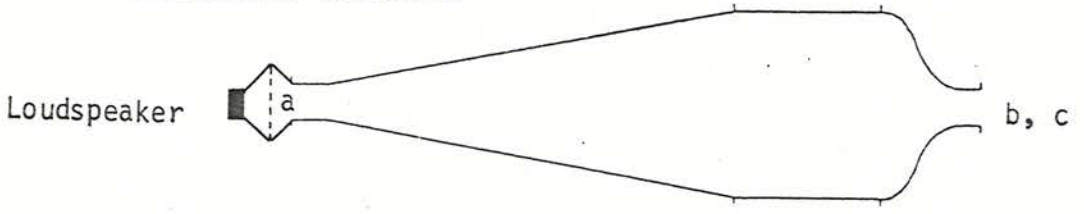


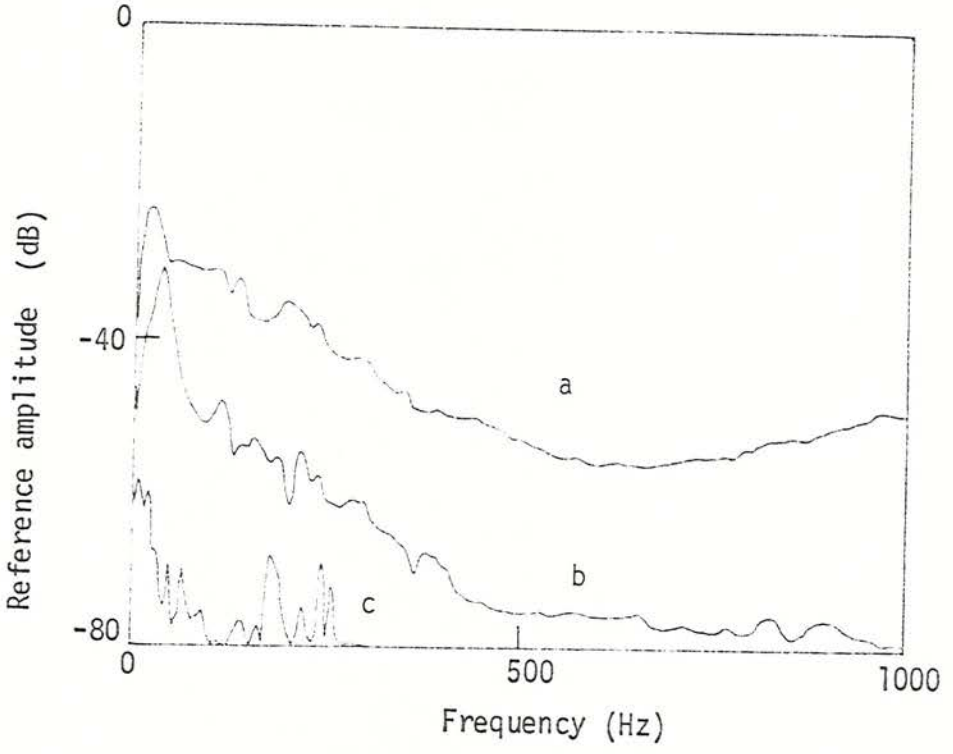


Fig. 3.23 Pressure spectra for a. noise source at rig entrance;
b. transmitted noise in combustion chamber;
c. reference level in combustion chamber with no noise.

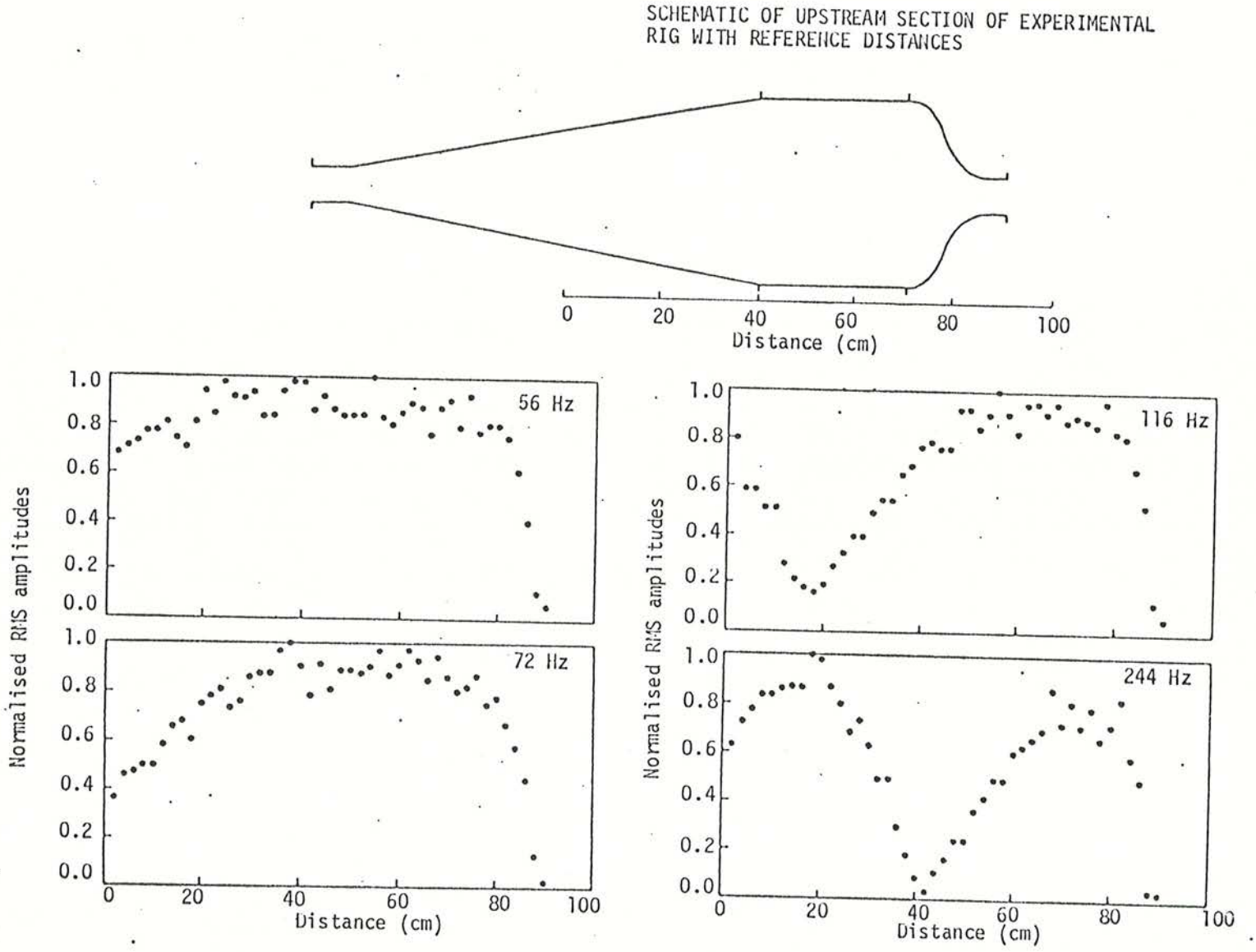


Fig. 3.24 Normalized RMS pressure fluctuation amplitudes versus position in upstream section of the experimental rig, for pressure fluctuations centred at 56, 72, 116 and 244 Hz ($L_c$ = 0 m, $L_h$ = 0 m, $U_o$ = 20 m/s, $\phi$ = 0.0).

at the contraction, representing the first through third harmonics of the rig. These signals, as well defined as they are, did not propagate in any strength into the duct, for they were not recorded with any strength in the pressure spectrum in the combustion chamber during combusting flows, although they were noted at times in the cold flow. Thus there is little reason to suspect, by virtue of the high frequency and low transmitted strength to the combustion chamber, that the standing waves of the settling chamber have any significance to the low frequency buzz.

### 3.4 Summary

The results of the experiments discussed in the previous subsections offers some distinction between acoustic and non-acoustic behaviour of the combustion oscillations. They also identify several noise sources inherent in various parts of the rig.

Outside the combustion chamber, the upstream section of the burner was subjected to noise from the air flow through the mixing baffles and sonic orifice plate. The lengthy geometry of the expansion and settling chambers allowed mid-frequency (< 500 Hz) standing waves to be established in the region from the sonic orifice plate or mixing baffles to the contraction. Higher frequency (> 500 Hz) noise was not evident in the upper sections possibly due to attenuation of the foam lining in the diffuser. In general, noise emitted in the upper sections of the rig were significantly attenuated before reaching the combustion chamber, thus reducing any possible influence these noises would have on the combustion process.

The large volume upstream of the working section could be stimulated through external excitation to behave in the manner of a Helmholtz resonator. Yet on its own, there did not appear to be any stimulation of this type of resonances, as both buzz and acoustic frequencies were much higher than would have been expected from a Helmholtz resonator.

The combustion chamber possessed similar acoustic behaviour in the manner of standing waves. Whether in cold, hot or buzzing combustion flow conditions, strong standing waves were excited, that spanned the

region from the contraction to the duct exit. The velocity fluctuations associated with the pressure standing waves in the region of the flame stabilizer affected the combustion flow and produced a bubbling phenomena in the brush of the flame. As long as the hot length of duct was kept below 0.50 m, the flame was only subjected to bubbling due to acoustic waves.

However, if the hot duct length was extended beyond this valve, then the character of the flame oscillation changed. The high frequency flame oscillations continued, but with a low frequency oscillation superimposed. From high speed cine photographs, the low frequency flame motion and its relationship to the upstream flow velocity and pressure were apparent. The fluctuating velocity and pressure relationship was consistent with those of a simple open ended pipe, with velocity leading pressure by approximately $90^{o}$. The flame motion appeared to be in phase with the upstream velocity, for the flame propagated forwards as the flow velocity fell, and moved downstream as the velocity increased. During the forward progress of the flame during a cycle it would at times engulf the vee-gutter filling most of the duct with burnt gas, and then moved down the duct leaving only a wisp of flame behind the flame stabilizer.

Probe microphone traverses of the duct during buzzing combustion showed that a noise source appeared to lay in the wake of the vee-gutter over a 10 to 30 cm region. Outside this "source" area, the generated noise behaved acoustically at either end of the duct. The source seemed to be dependent on the surroundings, for after ignition the buzz oscillation increased in amplitude and frequency over the first few hundred seconds before stabilizing. It is probable that the walls of the duct play an integral part in the heat release rates, since they have to reach an equilibrium temperature before the oscillation stabilizes. Also any pressure release in the hot region of the combustion chamber due to leaks decreased the buzz oscillation in amplitude and frequency.

Changing the physical parameters of the duct or the flow conditions, altered the behaviour of the low frequency oscillation. Increasing the hot length of the duct increased the amplitude of the pressure signal, while having little effect on the frequency. The amplitude of flame motion became very large for long duct lengths. Cold length increases,

reduced the frequency and produced an initial amplitude increase followed by a decrease. With increasing vee-gutter blockage, the frequency increased, whilst the amplitude initially rose then fell.

Flow changes showed that raising the inlet flow velocity increased the frequency of oscillation, but decreased the amplitude. Equivalence ratio increases produced similar effects in both frequency and pressure amplitude; moving the equivalence ratio above or below 1.15 decreased both.

In general the upstream sections of the rig had their own acoustic behaviour, which did not appear to influence the flame in the combustion chamber. Whereas the acoustic standing waves in the duct directly influenced the flame in terms of forcing oscillations in the flame structure, the low frequency oscillations had a separate identity to the acoustic waves and reacted to duct changes differently from the acoustic oscillations.

# CHAPTER 4

## 4.1 Introduction

In this chapter, a simple fluid-mechanical model of the low frequency oscillation is described. The formulation of the model involves mass and momentum balances between three interacting control volumes, shown schematically in Fig. 4.1. The upstream and downstream volumes represent wholly unburnt and burnt gas columns, respectively. In between these two well defined regions is the combustion volume, which contains both unburnt and fully burnt gas, and in which the whole of the combustion process takes place.

The theory is split into two parts, one dealing with the combustion zone, and the other with the upstream and downstream control volumes. The combustion zone theory explores a simple heat release model based on the mass flow across its two connecting boundaries with the unburnt and burnt gas columns. The other portion of the theory connects the unburnt and burnt gas control volumes across the flame zone, using the velocity and pressure of these two volumes at the boundaries of the combustion zone.

In all three regions, the oscillations are assumed to be of small amplitude, thus allowing the equations to be linearized. Because the model does not include an energy balance for the oscillations, it cannot predict the frequency or amplitude of the oscillation. The resulting set of equations is incomplete and must be supplemented by certain additional information, which may be either experimental data or an extra modelling assumption concerning the interaction between the heat release and flow. With this addition, the model can predict the oscillation frequency, amplitude ratios and phases of the pressure and velocity fluctuations in the different sections of the duct. Comparison of its predictions with experimental data allows alternative modelling assumptions to be tested.

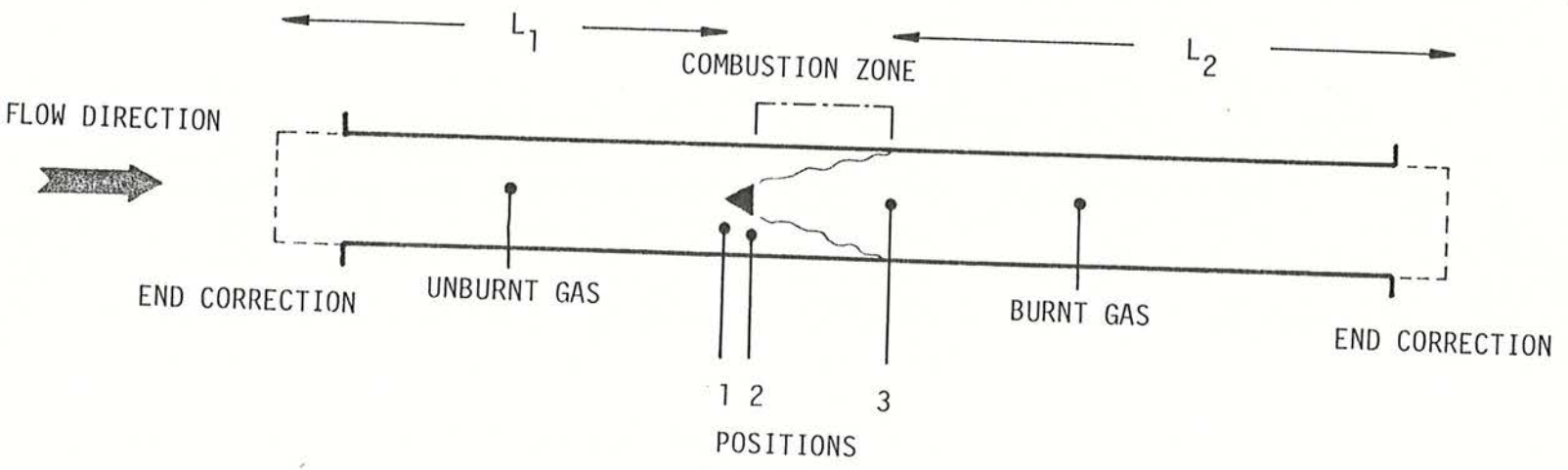


Fig. 4.1 Schematic diagram of the combustion chamber showing the positions and lengths used in the theoretical model.

Following a description of the assumptions underlying the model, this chapter contains two sections concerning fluctuations in the velocity-pressure on both sides of the flame, and heat release.

## 4.2 Assumptions for the Model

A complete physical description of the processes involved in oscillatory combusion is at present too complex to build into a model. To reduce the complexity of the combustion model, the flame is assumed to involve fast chemistry or global reactions. The laminar flame thickness, which is of the order of 0.1 to 1.0 mm, is small compared to the dimensions of the turbulent burning zone ($\sim$2 to 20 cm). In this model the gas in the duct is regarded as either completely burnt or unburnt, with the burning region between the two flows reduced to one or more surfaces of thickness comparable to that of a laminar flame.

The flow is assumed to be one-dimensional and adiabatic. Strictly speaking the flow is neither, for the flow is two-dimensional around the vee-gutter and combustion zone, and energy is lost to the walls as they heat up to $\sim$900$^{o}$C during a run, thereby radiating and conducting energy into the surroundings. However, in the completely burnt and unburnt gas volumes the flow is reasonably one-dimensional, and for adiabaticity, in comparison to the heat released by the flame, the heat losses represent a small fraction (< 5%) of the total energy.

The Mach number of the flow is low (0.06 to 0.38), thus the flow would be expected to experience only small compressibility effects. In addition, the amplitude of the low frequency (40 to 200 Hz) fluctuating pressure is small (< 1%) compared to the static pressure of the flow. Thus as a simplification, the flow is assumed to be incompressible in both burnt and unburnt regions.

The model contains three control volumes. The region ahead of the vee-gutter (upstream length), with the flow moving from left to right in Fig. 4.1, represents the unburnt gas section. The leading edge of the vee-gutter defines positions. A cold length, $L_1$, is then defined as the distance from position 1 to the contraction. The exact location of this

upstream boundary of the control volume in the contraction is determined from acoustic measurements. It is assumed to be 7 cm upstream of the duct-contraction junction. As the trailing edge of the vee-gutter is position 2 and position 3 is the control volume where all the combustion is assumed to occur. Position 3 is designated as the flame impingement point on the top and bottom walls of the duct. This position is variable, as it depends on the inlet velocity and flame shape. Downstream of position 3 is the wholly burnt gas region. The hot gas length, $L_2$, includes the length from position 3 to the open end of the duct, plus an additional length due to acoustic effects at the open end.

These three regions form the basic control volumes of the model. Further physical and flow parameters will be described as they are introduced into the theory.

## 4.3 Pressure and Velocity Fluctuations - Theory

The first part of the formulation of the model is to examine the relationship between the velocity and the pressure in the cold section of the duct with a similar relationship for the hot section. This is done through the use of the continuity and momentum equations between position 2 to position 3. The theory for the heat release in the included region is described in the following section 4.4.

In the region ahead of position 1, the fluctuating pressure-velocity relationship is assumed to be acoustic, namely (54):

$$\frac{p'}{u'} = -j\rho_u c_u \tan k_u(L_1 - z) \qquad (4.1)$$

where $p'$ = fluctuating pressure
$u'$ = fluctuating velocity
$j = \sqrt{-1}$
$\rho_u$ = unburnt gas density
$c_u$ = local sound speed in the unburnt gas

$\omega = 2\pi f$, where $f$ is the frequency of the oscillation

$k_u = \omega/c_u(1 - M_u^2)$

$L_1$ = total length of the unburnt gas region

$z$ = distance from position 2 to any point in the unburnt gas column

$M_u$ = Mach number of the unburnt gas flow.

Equation 4.1 describes the acoustic impedance looking upstream into the cold flow, from position 1; the $90^o$ phase shift $(-j)$ in the equation results from the definition of the direction of the flow. The sign convention adopted for this model is that flow from the duct inlet to outlet in Fig. 4.1 is taken as positive for all regions. This sign designation changes the phase from the usual acoustic definition of pressure leading velocity by $90^o$ at an open tube end to pressure lagging velocity by $90^o$. Since low frequencies are being investigated, the term $\tan k_u(L_1 - z) \simeq k_u(L_1 - z)$, and this simplifies the equation 4.1 to

$$\frac{p'}{u'} = -j\rho_u\omega\frac{(L_1 - z)}{(1 - M_u^2)} \tag{4.2}$$

Experiments by the author and Lee (47), using simultaneous pressure and hot wire measurements in a buzz rig have confirmed the $90^o$ phase lag predicted by this equation.

The fluctuating velocity can be expressed,

$$u' = \bar{u}\tilde{U}\cos(\omega t) \tag{4.3}$$

where $\bar{u}$ = mean gas flow velocity

$\tilde{U}$ = relative amplitude of unburnt gas velocity fluctuation, $|\hat{u}'/\bar{u}|$.

Inserting the expression for fluctuating velocity into equation 4.2 at position 1 ($z = 0$), the fluctuating pressure becomes

$$p_1' = \rho_u\omega\bar{u}_1\tilde{U}\frac{L_1}{(1 - M_u^2)}\cos(\omega t - \frac{\pi}{2}) \tag{4.4}$$

To calculate conditions at the trailing edge of the vee-gutter from those at the front, Bernoulli's equation is used. The only assumption made here is that the downstream face of the flame stabilizer has no fluctuating

pressure component on it. Because the pressure on the upstream face does fluctuate, the effect of this assumption is to maximize the fluctuating drag of the vee-gutter. Using Bernoulli's equations yields:

$$p_1 + \tfrac{1}{2}\rho_u u_1^2 = p_2 + \tfrac{1}{2}\rho_u u_2^2.$$

Decomposing the pressure and velocity in this equation into mean and fluctuating components by the substitutions,

$$p = \bar{p} + p'$$
$$u = \bar{u} + u'$$

where $\bar{p}$, $\bar{u}$ = mean pressure and velocity

$p'$, $u'$ = fluctuating pressure and velocity

and separating the mean and fluctuating contributions gives

$$\bar{p}_1 + \tfrac{1}{2}\rho_u \bar{u}_1^2 = \bar{p}_2 + \tfrac{1}{2}\rho_u \bar{u}_2^2$$

and
$$p_1' + \tfrac{1}{2}\rho_u(2\bar{u}_1 u_1' + u_1'^2) = p_2' + \tfrac{1}{2}\rho_u(2\bar{u}_2 u_2' + u_2'^2) \qquad (4.5)$$

The mean part of the Bernoulli equation gives the mean pressure and velocity changes that occur around the vee-gutter, while equation 4.5 shows the corresponding results for the fluctuating components. It is this last equation which is of interest for investigating the low frequency oscillations. Adhering to the assumption of small oscillations, the terms containing $(u')^2$ are neglected, giving,

$$p_1' + \rho_u \bar{u}_1 u_1' = p_2' + \rho_u \bar{u}_2 u_2' \qquad (4.6)$$

By continuity the mean and fluctuating velocities at the trailing edge of the vee-gutter are

$$\bar{u}_2 = \frac{\bar{u}_1}{(1 - b)}$$

$$u_2' = \frac{u_1'}{(1 - b)}$$

where b is defined as the ratio of the vee-gutter cross-sectional area to that of the duct, this ratio is termed the blockage ratio. Substituting these into equation 4.6 yields

$$p_2' = p_1' + \rho_u \bar{u}_1 u_1' \left[1 - \frac{1}{(1-b)^2}\right] \qquad (4.7)$$

Note that the length of the vee-gutter is neglected in the pressure changes. For the moment the expressions for $p_1'$ and $u_1'$ are not substituted into equation 4.7, to allow for simpler manipulation of the expressions in later stages.

Having specified the fluctuating pressure and velocity at the upstream face of the combustion control volume (position 2), the transition across the combustion zone is achieved using the momentum balance equation. The properties at the inlet to the combustion zone can be related to those at the outlet (position 3) giving,

$$(1-b)\left[p_2 + \rho_u u_2^2\right] + b\bar{p}_2 = p_3 + \rho_b u_3^2$$

Substituting in the respective mean and fluctuating components of the pressure and velocity, and separating out the mean and fluctuating contributions, gives:

$$(1-b)\,\bar{p}_2 + \rho_u \bar{u}_2^2 + b\bar{p}_2 = \bar{p}_3 + \rho_b \bar{u}_3^2$$

and

$$(1-b)\left[p_2' + 2\rho_u \bar{u}_2 u_2' + \rho_u u_2'^2\right] = p_3' + 2\rho_b \bar{u}_3 u_3' + \rho_b u_3'^2$$

On linearization, the expressions for the fluctuating velocity and pressure at position 2 in terms of the velocity and pressure at position 1 can be introduced into the momentum equation, resulting in

$$(1-b)\left[p_1' + \rho_u \bar{u}_1 u_1' \left(1 + \frac{1}{(1-b)^2}\right)\right] = p_3' + 2\rho_b \bar{u}_3 u_3' \qquad (4.8)$$

The fluctuating velocity and pressure relationship downstream of station 3 can be treated in the same manner as in the unburnt gas region

ahead of position 1. It is assumed that this control volume behaves acoustically as an open ended pipe. Acoustic theory gives a general expression in the burnt gas zone of

$$\frac{p'}{u'} = j\rho_b c_b \tan k_b(L_2 - y) \qquad (4.4)$$

with $$u' = \bar{u}\tilde{V} \cos(\omega t + \phi_3)$$

where $\rho_b$ = burnt gas density

$c_b$ = local sound speed in the burnt gas

$k_b = \omega/c_b(1 - M_b^2)$

$L_2$ = total length of the burnt gas region

$y$ = distance from position 3 to any point in the burnt gas column

$M_b$ = Mach number of the burnt gas flow

$\bar{u}$ = mean burnt gas flow velocity

$\tilde{V}$ = relative amplitude of burnt gas velocity fluctuations, $|\hat{u}'/\bar{u}|$

$\phi_3$ = phase difference between fluctuating velocities of position 3 relative to position 2

The introduction of the phase angle $\phi_3$ accounts for possible differences between the velocities $u_1'$ and $u_3'$, which allow for mass storage in the combustion zone.

Applying the small pressure oscillation assumption to equation 4.9, the fluctuating pressure at position 3 (y = 0) becomes

$$p_3' = \rho_b \omega \frac{L_2}{(1 - M_b^2)} \bar{u}_3 \tilde{V} \cos(\omega t + \phi_3 + \frac{\pi}{2}) \qquad (4.10)$$

Substituting the fluctuating pressures defined by equation 4.10 and 4.4 into equation 4.8, on manipulation, two separate equations may be deduced. One equation is an amplitude relationship between the oscillation in the cold and hot sections, and the other is the phase relationship.

Reducing the amplitude equation by simple algebra, the result is,

$$\left(\frac{\tilde{U}}{\tilde{V}}\right)^2 = \left[\frac{\omega^2 \frac{L_2^2}{(1 - M_b^2)} + 4\bar{u}_1^{-2}\left(\frac{\rho_u}{\rho_b}\right)^2}{\omega^2(1 - b)^2 \frac{L_1^2}{(1 - M_u^2)} + \bar{u}_1^2\left(\frac{2 - 2b + b^2}{1 - b}\right)}\right] \qquad (4.11)$$

while the phase equation reduces to,

$$\phi_3 = -\tan^{-1}\left[\frac{\omega(1 - b)^2 \frac{L_1}{(1 - M_u^2)}}{\bar{u}_1(2 - 2b + b^2)}\right] - \tan^{-1}\left[\frac{\frac{\omega L_2}{(1 - M_b^2)}\left(\frac{\rho_b}{\rho_u}\right)}{2\bar{u}_1}\right] \qquad (4.12)$$

The phase equation is a simple expression that can be solved by direct substitution of the necessary flow and length parameters; however, the relative amplitudes, $\tilde{U}$ and $\tilde{V}$, cannot be solved separately, without prior knowledge of one of these values. This is a consequence, as noted in section 4.1 above, of the absence of a detailed energy balance equation in the present model.

If typical data values from an experiment are inserted into these equations ($L_c$ = 0.20 m, $L_n$ = 0.61 m, b = 0.3, $\bar{u}_1$ = 20 m/s, f = 64 Hz), $\tilde{U}/\tilde{V} = (u_1'/u_3')(\bar{u}_3/\bar{u}_1) \simeq 3.46$ and $\phi_3 \simeq -85.7^{\circ}$. Since $\bar{u}_3/\bar{u}_1 = \rho_u/\rho_b \simeq 7$, these numbers suggest that the peak value of the downstream velocity fluctuation is higher than that upstream of the flame, and the velocity downstream lags the upstream velocity by almost $\pi/2$. A more complete comparison of data to theory is explored in chapter 5.

## 4.4 Heat Release Rate Fluctuation - Theory

The next stage in the development of the model is to examine the fluctuating heat release rate in the combustion zone (between position 2 and 3), using the definitions for the fluctuating pressures and velocities at the two faces, presented in the previous section. As a simplification, the volume contained between station 2 and 3 is assumed to be small in comparison to the total duct volume. By fixing the location of station 2 and 3, a constant control volume is created, containing a mixture of burnt and unburnt gas. This volume can be expressed as,

$$V_T = V_u + V_b \tag{4.13}$$

where $V_T$ = total volume between position 2 and 3

$V_u$ = unburnt gas volume in $V_T$

$V_b$ = burnt gas volume in $V_T$

Three separate mass flow rates can be identified. There is a mass flow into the control volume at position 2 $\dot{m}_2 = \dot{m}_1$, a mass flow, $\dot{m}_3$, out of the control volume at position 3, and within the control volume, there is a mass flow through the flame front, $\dot{m}_f$, defined as the rate of combustion. All three mass flows can be separated into mean and fluctuating components:

$$\dot{m}_1 = \bar{\dot{m}}_1 + \dot{m}_1'$$
$$\dot{m}_f = \bar{\dot{m}}_f + \dot{m}_f'$$
$$\dot{m}_3 = \bar{\dot{m}}_3 + \dot{m}_3'$$

and from continuity

$$\bar{\dot{m}}_1 = \bar{\dot{m}}_f = \bar{\dot{m}}_3.$$

Since the total volume in the combustion region is assumed to be fixed, equation 4.13, and the individual burnt and unburnt gas volumes as the sum of mean and fluctuating components, then the derivative of the total volume with time is

$$\frac{dV_u'}{dt} + \frac{dV_b'}{dt} = 0.$$

However, the unburnt and burnt gas flows are both assumed incompressible, resulting in

$$\frac{dV_u'}{dt} = \frac{\dot{m}_1' - \dot{m}_f'}{\rho_u}$$

and

$$\frac{dV_b'}{dt} = \frac{\dot{m}_f' - \dot{m}_3'}{\rho_b}$$

Substituting and rearranging the above equations gives,

$$\dot{m}_f' = \frac{\dot{m}_3'\rho_u - \dot{m}_1'\rho_b}{(\rho_u - \rho_b)}$$

This expression indicates that the fluctuating mass flow rate through the flame can be expressed in terms of the fluctuating mass flow rates in and out of the control volume. Introducing into this equation, expressions for $\dot{m}_1'$ and $\dot{m}_3'$,

$$\dot{m}_1' = \rho_u S u_1',$$
$$\dot{m}_3' = \rho_b S u_3'$$

where S = duct cross-sectional area

gives

$$\dot{m}_f' = \frac{S\rho_u\rho_b}{(\rho_u - \rho_b)}(u_3' - u_1')$$

where $\bar{\dot{m}}_1 = S\rho_u\bar{u}_1$.

Since the heat release rate is proportional to the mass flow rate through the flame, it can be expressed as,

$$\bar{\dot{Q}} \propto \bar{\dot{m}}_1 \quad \text{and} \quad \dot{Q}' \propto \dot{m}_f'$$

such that

$$\dot{Q}'/\bar{\dot{Q}} = \dot{m}_f'/\bar{\dot{m}}_1$$

$$= \frac{\rho_b}{(\rho_u - \rho_b)}\left[\frac{u_3'}{\bar{u}_1} - \frac{u_1'}{\bar{u}_1}\right]$$

From continuity in an incompressible flow,

$$\bar{u}_3 = \rho_u\bar{u}_1/\rho_b$$

thus the fluctuating heat release rate ratio will be

$$\frac{\dot{Q}'}{\bar{\dot{Q}}} = \frac{\rho_b}{(\rho_u - \rho_b)}\left[\frac{u_3'}{\bar{u}_3}\left(\frac{\rho_u}{\rho_b}\right) - \frac{u_1'}{\bar{u}_1}\right] \qquad (4.15)$$

The terms on the right hand side of this equation have already been specified in section 4.3.1, while the terms on the left can be written in a similar form to the fluctuating velocity divided by the mean, as in equation 4.3,

$$\frac{\dot{Q}'}{\bar{\dot{Q}}} = \tilde{Q} \cos(\omega t + \phi_q)$$

where $\tilde{Q}$ = fluctuating intensity of the heat release rate $|\hat{\dot{Q}}'/\bar{\dot{Q}}|$

$\phi_q$ = phase difference between the heat release rate and upstream velocity fluctuations (induced through mass storage).

Substituting the fluctuating and mean velocities into equation 4.15, and separating into amplitude and phase equations, the resulting expressions are:

$$\frac{\tilde{Q}}{\tilde{U}} = \frac{\rho_b}{(\rho_u - \rho_b)} \sqrt{\left[\left(\frac{\rho_u}{\rho_b}\right)\frac{\tilde{V}}{\tilde{U}} - 1\right]^2 + \left[\left(\frac{\rho_u}{\rho_b}\right)\frac{\tilde{V}}{\tilde{U}} \sin\phi_3\right]^2} \qquad (4.16)$$

and

$$\phi_q = -\pi + \tan^{-1}\left[\frac{\sin\phi_3}{\cos\phi_3 - \left(\frac{\tilde{U}}{\tilde{V}}\right)\left(\frac{\rho_b}{\rho_u}\right)}\right] \qquad (4.17)$$

The phase of the heat release rate can be determined by substituting in the various experimental parameters, but the heat release rate fluctuation $\tilde{Q}$, can only be evaluated relative to $\tilde{U}$. However, it is worth inserting typical data from the experiments; and using the same data as the example in section 4.3.1, gives $\phi_q = -113.5^o$ and $\tilde{Q} = 0.37\tilde{U}$.

These results indicate that the heat release is roughly in phase with the upstream pressure fluctuation, in accordance with the Rayleigh criterion, and that a small relative amplitude $\tilde{Q}$ for the heat release rate fluctuations is associated with a three times greater relative amplitude of upstream velocity fluctuations.

## 4.5 Summary of Model

The expressions resulting from the model are of two kinds: (i) phase relationships between downstream velocity and heat release to the upstream velocity, and (ii) fluctuating amplitude ratios of downstream velocity or heat release to upstream velocity (i.e., $\tilde{V}/\tilde{U}$, $\tilde{Q}/\tilde{U}$).

As noted earlier, the model cannot predict the individual fluctuating amplitudes $\tilde{U}$, $\tilde{V}$ or $\tilde{Q}$, because no use has been made of an energy balance equation. If experimental conditions, such as inlet velocity, blockage ratio, duct lengths and gas density ratio are inserted into the equation, along with an additional piece of information or modelling assumption, then predictions can be made for phase and amplitude ratio, and the combustion driven oscillation frequency.

# CHAPTER 5

# DISCUSSION OF THEORETICAL AND EXPERIMENTAL RESULTS

## 5.1 Introduction

The theoretical model derived in this study provides a method of investigating possible controlling processes in low frequency oscillations. A portion of this chapter is used to test the model against experimental observations in order to determine the strengths and weaknesses of the proposed theory.

As the model requires additional information to close the set of equations, the first section of this chapter mentions the closure expression adopted for this study. Subsequent sections use the model and closure expression to determine the oscillation frequency and fluctuation intensities of the downstream flow velocity and heat release rate for the experimental conditions mentioned in Chapter 3.

The later sections focus on the model capabilities and the experimental results in two separate discussions. At the end of each discussion, possible future work, where deemed necessary, is mentioned to improve further the understanding of buzz.

## 5.2 Model Closure Term

In order to close the set of equations describing the low frequency oscillation theory, cf. Chapter 4, an additional piece of information, empirical or theoretical, is required. Examination of the experimental results indicated a number of possible closure hypotheses. The particular closure chosen to complete the theory was to prescribe a $90^{\circ}$ phase difference between upstream and downstream pressure fluctuations. Microphone traverses and fixed pressure transducers showed the downstream pressure fluctuations to lead the upstream pressure fluctuation by approximately $90^{\circ}$. In terms of fluctuating velocities, this closure then specifies that the upstream fluctuating velocity leads the downstream fluctuating velocity by $90^{\circ}$.

Alternative closures were considered and are discussed in section 5.4.1 in relation to the chosen closure.

## 5.3 Results from the Model of the Low Frequency Oscillation

Substitution of the closure expression into the model provides the necessary information to determine the oscillation frequency and relative amplitude ratios $\tilde{U}/\tilde{V}$ and $\tilde{Q}/\tilde{U}$+. To facilitate the interpretation of the two ratios, further experimental information is introduced in the form of the upstream flow velocity fluctuation intensity, $\tilde{U}$. Since pressure data is available from experiments involving the buzz amplitude measurements in the upstream section of the duct, cf. section 3.3.3, it is possible to derive the corresponding fluctuating velocity accompanying the pressure, using equation (A.8) from Appendix A.

Using the experimental conditions (i.e., flow conditions and duct geometry) invoked at the time the buzz pressure measurements were made, $\tilde{U}$ can be determined, and hence $\tilde{V}$ and $\tilde{Q}$ calculated from the theory. The results of the calculations are presented in the following subsections.

### 5.3.1 Frequency

The duct and flow conditions used in the model predictions correspond to those in the buzz experiments. The conditions are identified on the graphs showing the frequency and peak amplitude of buzz versus various parameters, Figs. 3.16 to 3.21. Plotted in Fig. 5.1a to e, are the results of the frequency predictions. Beside the theoretical calculations are the experimentally observed frequencies drawn from Chapter 3.

---

+Recalling from Chapter 4 that:

$\tilde{U} = |\hat{u}_1'/\bar{u}_1|$ relative intensity of upstream velocity fluctuation

$\tilde{V} = |\hat{u}_3'/\bar{u}_3|$ relative intensity of downstream velocity fluctuation

$\tilde{Q} = |\hat{\dot{Q}}/\bar{\dot{Q}}|$ relative intensity of heat release rate fluctuation

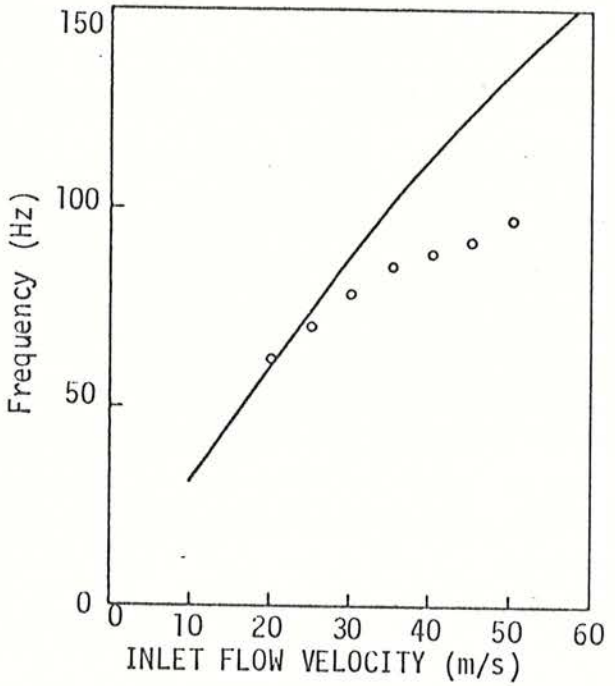


a. ($L_c$ = 0.05 m, $L_h$ = 0.66 m, 30% blockage, $\phi$ = 1.15)

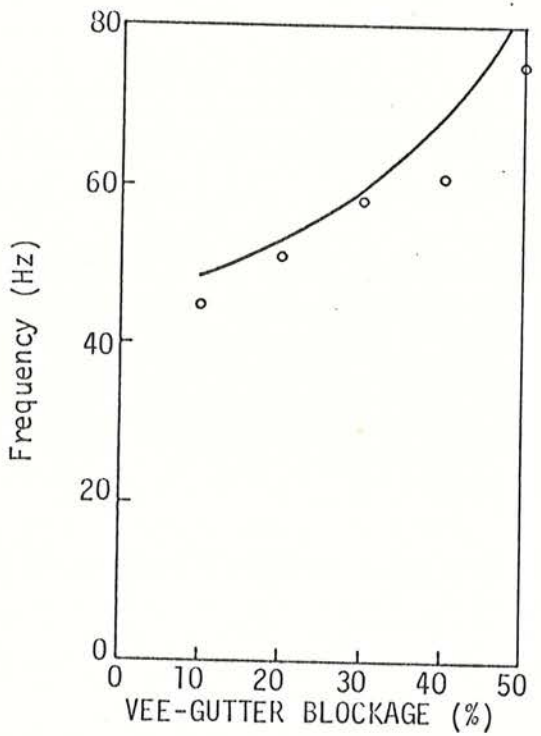


b. ($L_c$ = 0.05 m, $L_h$ = 0.66 m, $U_o$ = 20 m/s, $\phi$ = 1.15)

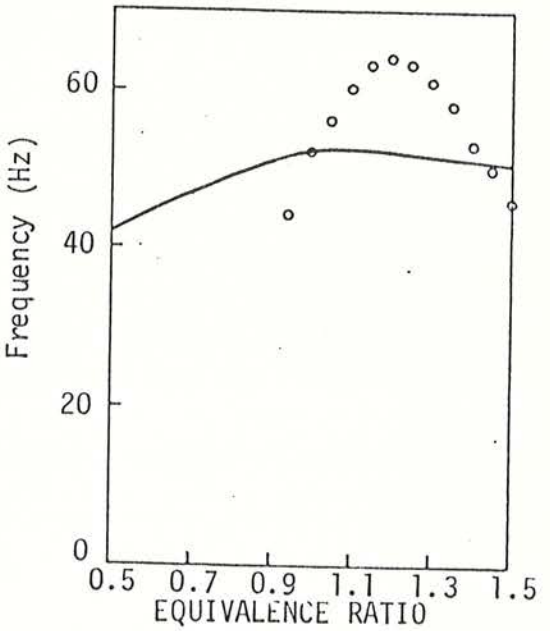


c. ($L_c$ = 0.05 m, $L_h$ = 0.81 m, $U_o$ = 20 m/s, 30% blockage)

Fig. 5.1 Predictions of the buzz frequency versus various duct and flow parameters (experimental results represented by open circles).

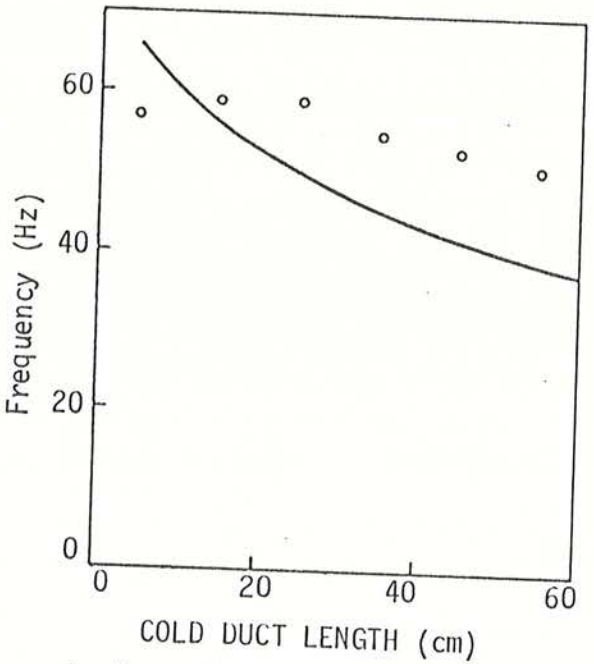


d. ($L_h$ = 0.56 m, $U_o$ = 20 m/s, 30% blockage, $\phi$ = 1.15)

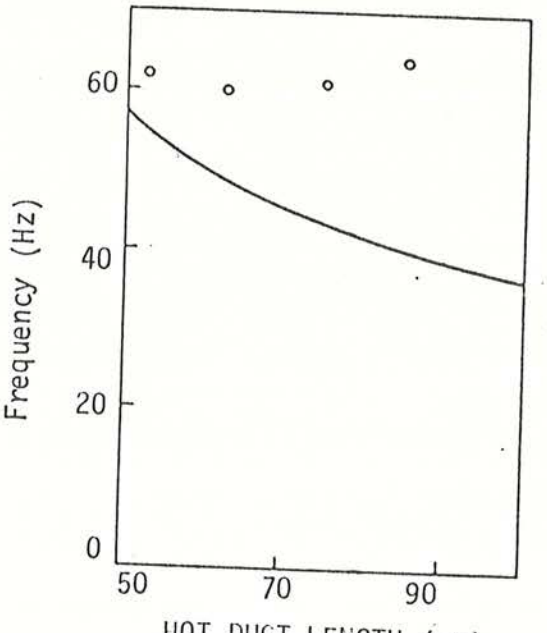


e. ($L_c$ = 0.20 m, $U_o$ = 20 m/s, 30% blockage, $\phi$ = 1.15)

Fig. 5.1 continued.

### 5.3.2 Relative intensity of downstream velocity fluctuations, $\tilde{v}$

Under the same flow and duct geometry conditions employed for the frequency predictions, the relative amplitude ratio $\tilde{u}/\tilde{v}$ can be determined. To facilitate the interpretation of this ratio, experimentally derived values of $\tilde{u}$, the upstream flow velocity fluctuating intensity, are substituted into the ratio. $\tilde{u}$ in this case represents an experimental result specified as the RMS value of the velocity fluctuation, whereas in the theory, $\tilde{u}$ is normally referred to as a peak velocity fluctuation. Upon substitution of the experimental data into the theory, $\tilde{v}$, the downstream flow velocity fluctuation intensity also becomes an RMS value.

Both the calculated value of $\tilde{v}$ and the experimentally determined value of $\tilde{u}$ are plotted together in Figs. 5.2a to e. The experimental conditions for these plots are identical to their counterparts for the preceding frequency plots, Fig. 5.1. If the two fluctuating intensities are multiplied by the respective mean flow velocities, then in all the cases presented, $u_3' > u_1'$, i.e., the magnitude of the fluctuating downstream velocity is larger than the fluctuating upstream velocity.

### 5.3.3 Relative intensity of heat release rate fluctuations, $\tilde{Q}$

Substitution of the inlet fluctuating velocity intensity $\tilde{u}$, into the predicted relative amplitude ratio for the heat release rate $\tilde{Q}/\tilde{u}$, gives a direct measure of the intensity of the fluctuating heat release rate. Plotted in Fig. 6.3a to c are the predicted $\tilde{Q}$ against the standard duct and flow parameters.

It is worth noting that the fluctuation intensities in upstream and downstream flow velocities and the heat release rate exhibit similar trends.

The phase difference between the heat release rate and upstream pressure fluctuation was predicted to vary from a minimum of $16^{o}$ to a maximum of $32^{o}$; heat release rate lagging the pressure.

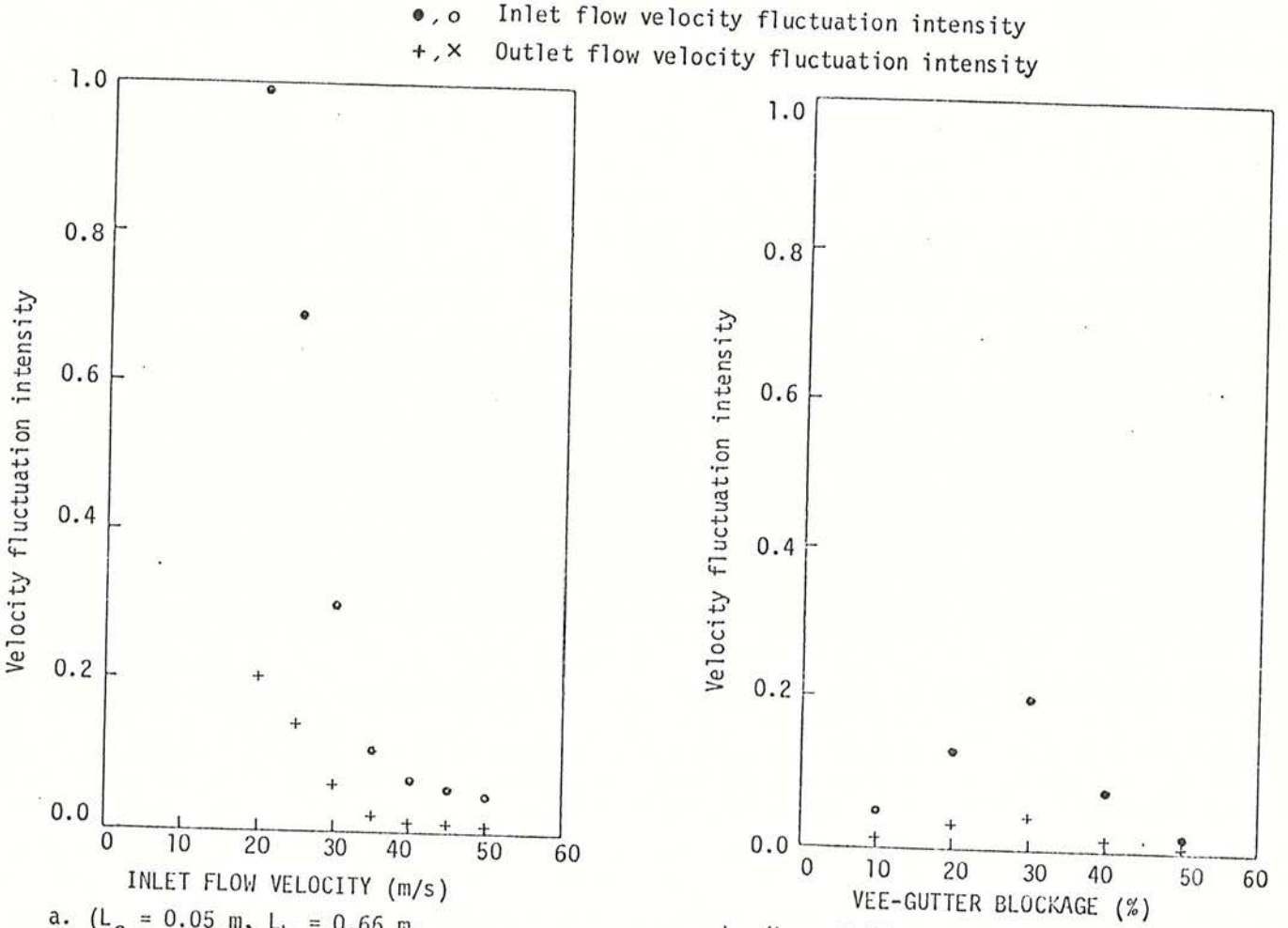


a. ($L_c$ = 0.05 m, $L_h$ = 0.66 m, 30% blockage, $\phi$ = 1.15)

b. ($L_c$ = 0.05 m, $L_h$ = 0.66 m, $U_o$ = 20 m/s, $\phi$ = 1.15).

Fig. 5.2 Experimentally determined values of inlet flow velocity fluctuation intensity, $|u_1'/\overline{u_1}|$ and predictions of outlet flow velocity fluctuation intensity, $|u'_3/\overline{u_3}|$ versus various duct and flow parameters.

SOUTHAMPTON UNIVERSITY LIBRARY

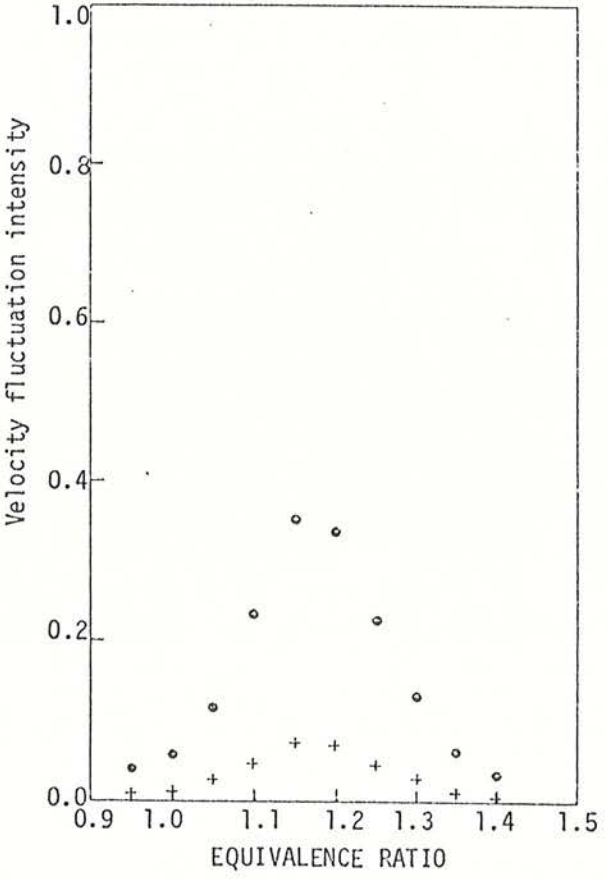


c. ($L_c$ = 0.05 m, $L_h$ = 0.81 m, $U_o$ = 20 m/s, 30% blockage)

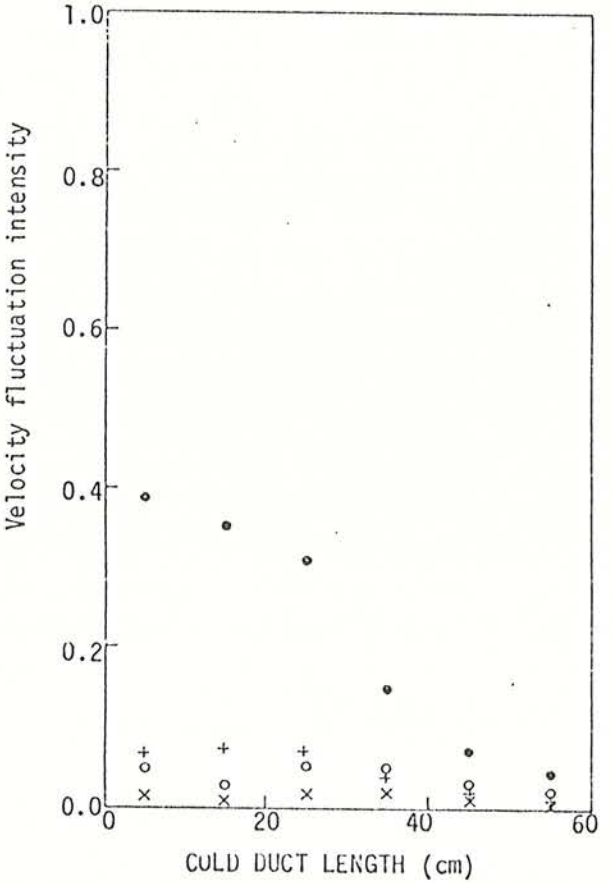


d. ($L_h$[o, x = 0.56 m; •, + = 0.86 m], $U_o$ = 20 m/s, 30% blockage, $\phi$ = 1.15)

Fig. 5.2 continued.

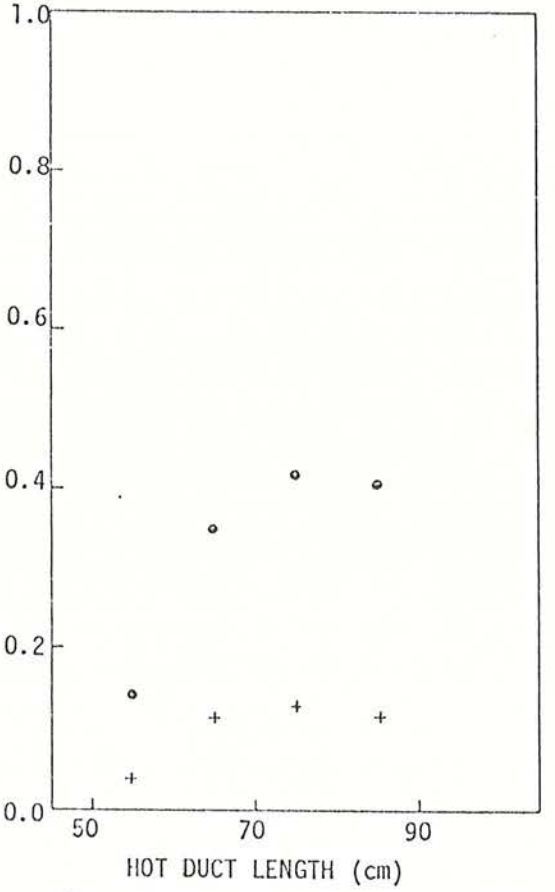


e. ($L_c$ = 0.20 m, $U_o$ = 20 m/s, 30% blockage, $\phi$ = 1.15)

Fig. 5.2 continued.

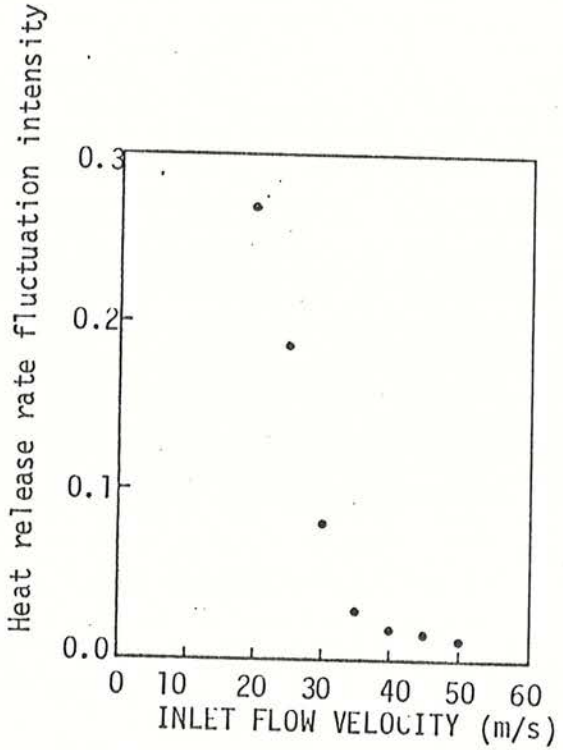


a. ($L_c$ = 0.05 m, $L_h$ = 0.66 m, 30% blockage, $\phi$ = 1.15)

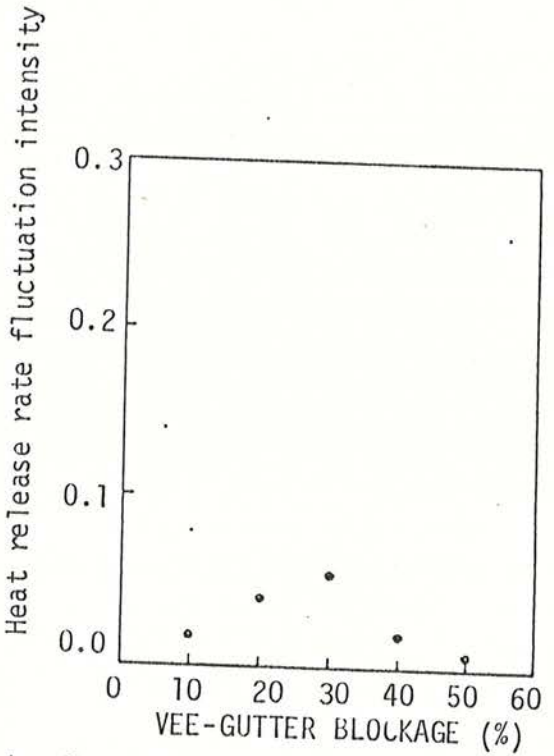


b. ($L_c$ = 0.05 m, $L_h$ = 0.66 m) ($U_o$ = 20 m/s, $\phi$ = 1.15)

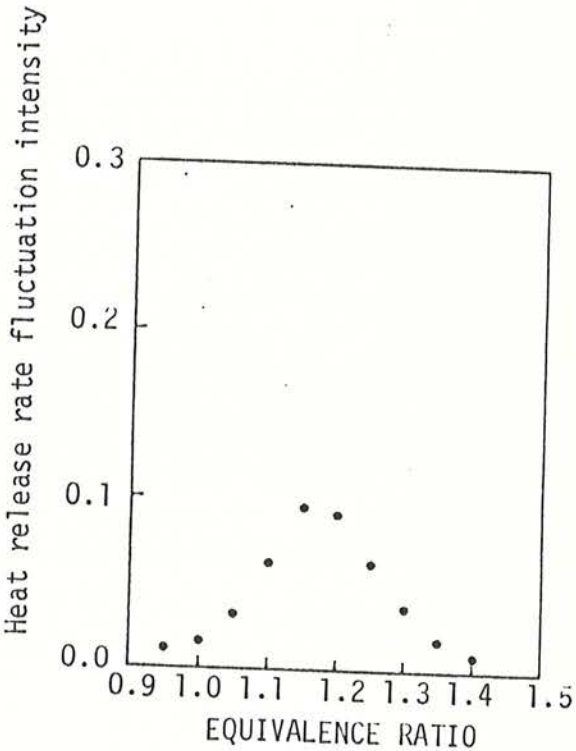


c. ( $L_c$ = 0.05 m, $L_h$ = 0.81 m, $U_o$ = 20 m/s, 30% blockage)

Fig. 5.3 Predictions of the heat release rate fluctuation intensity, $|\dot{Q}'/\bar{\dot{Q}}|$, versus various duct and flow parameters.

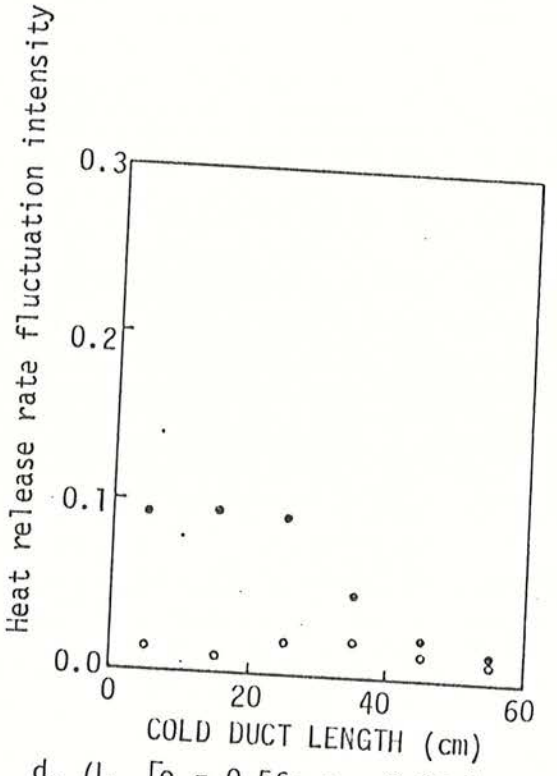


d. ($L_h$ [o = 0.56; ● = 0.86m], $U_o$ = 20 m/s, 30% blockage, $\phi$ = 1.15)

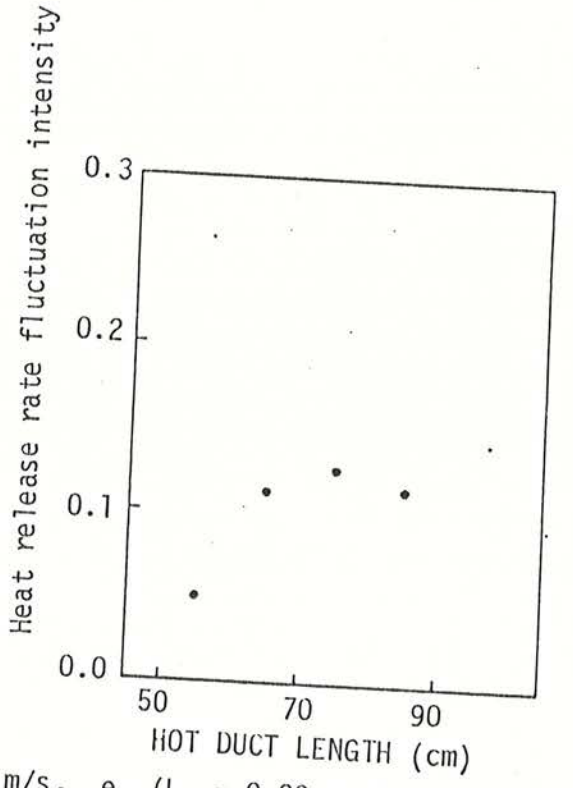


e. ($L_c$ = 0.20 m, $U_o$ = 20 m/s, 30% blockage, $\phi$ = 1.15)

Fig. 5.3 continued.

## 5.4 Discussion of the Model

The first part of this discussion examines some alternative closure strategies, while the latter part discusses the model capabilities.

### 5.4.1 Alternative model closures

As previously mentioned, there are a number of possible closure techniques available to complete the model. Three major approaches under consideration were:

(i) equating the RMS pressure fluctuations across the combustion zone between the unburnt and burnt gas columns (experimental observation, cf. section 3.3.2).

(ii) Synchronizing the peak heat release rate and peak upstream pressure to maximise heat addition (theoretical - Rayleigh criterion (4)).

(iii) Settling a phase difference between the inlet and outlet pressure fluctuations of $90^{o}$, with the downstream pressure leading (experimental observation, cf. section 3.3.2).

The closure involving the equating of the RMS pressure amplitudes on both sides of the combustion control volume appeared to be a valid closure considering the results of a microphone traverse in a combusting flow. However, implementation of this closure tended to yield frequencies in the range 10 to 20 Hz with the fluctuating upstream and downstream velocities nearly in phase, and the corresponding fluctuating pressure nearly $180^{o}$ out of phase. These results did not match the observed results, thus this closure was not used.

Implementation of the Rayleigh criterion in the model by removing any phase difference between the heat release rate and upstream pressure fluctuations also closed the model. Unfortunately the theoretical predictions for the oscillation frequency were low. For example, using the following experimental conditions: $L_c$ = 0.15 m, $L_h$ = 0.56 m, an inlet flow velocity of 20 m/s at an equivalence ratio of 1.15, the calculated frequency for buzz was 13 Hz, whereas the experimental frequency was 58 Hz. The predicted phase difference between upstream and downstream pressure fluctuations was $147^{o}$ with the downstream pressure leading. This phase

difference was unusually high compared to the experimental value of 70-90°. Thus, whilst intuitively attractive, this closure also appears to be incompatible with the underlying assumption regarding the heat release zone.

The third closure incorporated an experimental observation that a phase difference of approximately 90° existed between the upstream and downstream pressure fluctuations. An example of the result of employing this closure is as follows. Under the same experimental conditions as above, the predicted frequency was 54 Hz compared with that observed of 58 Hz; in addition, the phase difference between the heat release rate and upstream pressure was 24°, which was within the 90° phase difference deemed necessary to maintain the amplification of the oscillation (21 ). Slight changes in the phase relationship between pressure and heat release rate induce large changes in the buzz frequency. This shows the model to be sensitive to phase changes, notably through the difference in the results of the Rayleigh criterion and the 90° phase difference closures.

Further comparisons between theoretical predictions and experimental observation increase the support for the pressure phase difference closure. In a group of experiments, pressure fluctuations were simultaneously recorded near both ends of the combustion chamber. These measurements and those of Lee (47) allowed the phase difference and relative amplitudes of the fluctuating velocity intensity $\tilde{U}$ and $\tilde{V}$ to be determined. The results of these experiments and the accompanying theoretical predictions are tabulated in Table 5.1.

The predictions using this closure compare favourably with observations in frequency, and heat release phasing, but are generally poor for the amplitude ratio $\tilde{U}/\tilde{V}$. From Table 5.1, if the observed 75-80° phase difference was imposed by way of the closure, then the predicted frequencies would rise by 10-20% without affecting the predicted trends. It was felt that of the three closures, this last method gave the most consistent predictions and compared satisfactorily with the experimental results.

| DUCT LENGTHS $L_c$ (m) | $L_h$ (m) | RESULTS | FREQUENCY (hz) | PHASE RELATIONSHIP ($^o$) | $\tilde{U} / \tilde{V}$ |
|---|---|---|---|---|---|
| 0.05 | 0.736 | EXPERIMENTAL | 60 | 76 ± 1 | 3 ± 1.5 |
| | | THEORETICAL | 50.4 | 90 | 4.52 |
| 0.05 | 0.609 | EXPERIMENTAL | 62 | 79 ± 1 | 0.75 ± 0.05 |
| | | THEORETICAL | 50 | 90 | 3.62 |
| 0.38 | 0.79 | EXPERIMENTAL | 72 | 79 ± 1 | 0.56 ± 0.05 |
| | | THEORETICAL | 34 | 90 | 3.134 |

Table 5.1 Experimental and predicted results of buzz frequency, phase relationship between upstream and downstream velocity fluctuations, and the ratio of fluctuation intensity between upstream and dowmstream velocities.

### 5.4.2 Discussion

The model predictions for both buzz frequency and amplitude ratios are based on a fluctuating momentum balance between the cold and hot gas columns on either side of a combustion zone. A change in a duct or flow parameter (i.e., inlet flow velocity, equivalence ratio, etc) varies the momentum which in turn requires a frequency and/or amplitude change to re-establish a momentum equilibrium, cf. section 4.3.

Interwoven with the momentum balance is a model of the heat release rate. The model describes the heat release by the mass flux through the boundaries of the combustion zone developed by the two gas columns, cf. section 4.4.

Model predictions are encouraging and have reproduced satisfactorily certain aspects of the low frequency oscillation. Generally, the results show that for changes involving the inlet gas column parameters, both the trend and numerical values for the frequencies were closer to the experimental results than those for changes in the hot gas parameters. Correct trends in the buzz frequencies were predicted for increases in the inlet flow velocity, flame stabilizer blockage and cold duct length. On the other hand, poor numerical prediction, albeit with the correct trends, were shown for the influence of the equivalence ratio changes. However, the model failed completely in predicting the effect of the hot duct length on the buzz frequency. These failures in the model directly reflect the incomplete and unsatisfactory description of the turbulent combustion processes.

While frequency predictions can be evaluated against experimental observations, the relative velocity amplitude ratio $\tilde{u}/\tilde{v}$ and the heat release ratio $\tilde{Q}/\tilde{u}$ predicted by the model generally can not be adequately tested to access their accuracy. For the few cases where pressure measurements along the duct gave sufficient information to estimate the ratio $\tilde{u}/\tilde{v}$, the theoretical values were two to five times larger than those measured. Unfortunately, no comparisons can be made for the heat release rate ratio since there are no experimental measurements available.

The results obtained by introducing $\tilde{u}$ into the ratios $\tilde{u}/\tilde{v}$ and $\tilde{Q}/\tilde{u}$, of section 5.3, gave values for the intensities of the downstream velocity and heat release rate fluctuations, $\tilde{v}$ and $\tilde{Q}$, respectively.

In all cases when the inlet velocity fluctuation ratio fell, both the downstream velocity and heat release rate fluctuation intensity also dropped. However, while these predicted values of $\tilde{V}$ and $\tilde{Q}$ appear plausible, they cannot be checked against experiments.

In contrast to other models, for example Marble (44,55) or Stewart (36), cf. section 1.3.2, the present theory has attempted to model the response of the flow at the level of an assumed excitation mechanism in the combustion zone. Marble's theory provides a method of calculating the time varying flame shape in response to imposed upstream pressure changes.

Stewart's suggestion of reflecting waves interfering with the fuel flow was reasonable for his particular burner, but was not relevant in this investigation. For the present burner, the time required for a flow disturbance to travel back upstream and affect the fuel injection was at least an order of magnitude longer than observed in the oscillations. It is also likely that the disturbance mechanism proposed by Stewart would be attenuated in the upstream section of the present rig.

The theoretical model developed for this study has a number of shortcomings, and thus offers scope for further improvements. The absence of a sound theoretical description of the coupling between heat release rates and pressure or velocity fluctuations remains the principal model shortcoming. Addition of a complete energy balance equation incorporating a fluctuating heat release rate would partly alleviate the need for a closure expression. Similarly, introducing momentum and energy storage into the combustion zone would allow a phase shift to occur between upstream and downstream control volumes and so complete the closure expression.

More ambitious programs could introduce two dimensional flow, ultimately leading to the insertion of a heat release distribution along the length of the flame front.

## 5.5 Discussion of the Experiments

The objective of the experiments was to identify and differentiate between types of combustion driven oscillations in a ducted burner. During the investigation, the behaviour of the oscillations was found to be divisible into two groups; those associated with acoustic resonances of the combustion chamber, and those of lower frequencies independent of the chamber resonances.

Experiments have revealed two major differences between the types of oscillations. Firstly, the fundamental resonant frequencies are consistently higher than those of buzz. Secondly, whereas the acoustic resonances are present in cold or combusting flows under any geometric arrangement of hot and cold duct lengths, buzz oscillations only existed in combusting flows where the hot duct length of the combustion chamber exceeded 0.5 m (there is no indication that this is a standard length for any other ducts).

As a prelude to understanding combustion resonances it is important to grasp the fundamentals of chamber resonances in simple cold flow conditions. An investigation into the resonances in cold flow produced a self-contained study, cf. Section 3.2 and Appendix A. The measured peak frequencies from a fixed pressure transducer corresponded to within 5% with the predicted resonances. The RMS fluctuating pressure profile for the fundamental mode, measured by a traversing microphone probe, was similar in shape to that predicted by the acoustic model. This gave a rudimentary understanding of the interactions between fluctuating velocity and pressure in a duct and a basis on which to examine acoustic resonances in combusting flows.

Measurements in combusting flows, without buzz, showed that the resonant frequencies recorded in this chamber could be fairly accurately determined from calculations of the time taken for a disturbance to travel the length of the burner through both cold and hot flows, subsequently returning to the point of origin. It was encouraging to note that other investigators had derived similar expressions and used them successfully on their data for resonances in ducted burners (6 ,21).

The RMS pressure profiles for the resonances in the combusting flow were similar in shape to the cold flow traverses (i.e., rectified sine waves starting and ending at the ends of the duct with approximately zero

amplitude). Phase changes in the pressure fluctuation with duct length appeared to be consistent with expected phasing when viewed through an analogy to the cold flow theory. The first mode, disregarding the slow phase change along the duct length believed due to a velocity modulation, had only small pressure phase differences between any two points in the duct. While the second mode showed a $180^{o}$ phase change at the first internal pressure node in the chamber. These results were consistent with a number of investigators who had hypothesised standing waves in burners. However, only a few investigations had measured the standing waves amplitude profile (6 ) and only one determined the phase changes due to induced noise (58).

Flame motion revealed by spark and cine schlieren photographs pointed out part of the heat exchange mechanism between the flame and pressure. The flame front was observed to wrinkle at some of the chamber resonances, cf. section 3.2.3. It appeared that the velocity disturbances at the stabilizer distorted the flame profile by inducing synchronous vortex formation off both trailing edges of the vee-gutter. The vortices introduced a bubbling into the flame front that appeared to increase the surface area, thus affecting heat release of the flame. Through inference with cold flow theory the velocity disturbances corresponding to the pressure fluctuation of the resonant standing waves were responsible for the flame wrinkling. The pressure oscillations induced velocity changes of up to several meters per second at the vee-gutter. If a node in the fluctuating velocity lay near the flame stabilizer, then for that particular resonant frequency the flame front would not be affected. This did not preclude the corresponding resonant pressure fluctuation existing in the chamber. However, if a pressure node lay near the stabilizer then there was a strong influence of that frequency on the flame shape. Further, the bubbling flame could produce a strong well-defined resonance by coupling with the fluctuating pressure at the same frequency.

As previously mentioned the acoustic oscillations were present in the combustion chamber for any duct and flow setting; however, once the hot duct length exceeded 0.5 m the flame oscillations became a mixture of buzz oscillation and acoustic resonances.

High speed schlieren cines of buzz oscillations in a ducted burner by the author, cf. section 3.3.1, and Smart (37) have revealed the flame motion accompanying both acoustic and buzz oscillations. Using pressure transducers and hot wire or Laser doppler anemometry, the flame motion could be correlated to the upstream fluctuating pressure and flow velocity (47). The motion of the flame can be interpreted as an interplay between inlet flow velocity and pressure, and heat release by the flame. Starting from the quiescent state of the flame spreading out behind the vee-gutter, the flame swells or "balloons". The swelling accompanies an increase in the downstream pressure resulting from an increased heat release. This leads to the flow downstream accelerating and the upstream flow decelerating. The precise phase of these events remains unclear. However, as the inlet flow velocity starts to decrease and the flame pushes forward towards the stabilizer, its surface area decreases and the amount of fuel intake into the combustion zone is reduced. A reduction in the energy released by the flame cannot then sustain the high downstream pressure which results in the arresting of the forward motion of the flame and the subsequent pushing of the flame downstream by an increasing inlet velocity and decreasing outlet velocity. As the flame front stretches out behind the stabilizer the flame area is increased, allowing more fuel to be burned, increasing the downstream pressure and re-establishing the cyclic motion of the flame front.

The microphone traverse along the chamber length during a buzzing flow showed the RMS pressure fluctuation distribution to have three distinct sections, fig. 3.14. From the duct inlet the RMS fluctuating pressure rose from an approximately zero amplitude to a maximum (in near linear rise) at the vee-gutter. Behind the vee-gutter for approximately 10-20 cm the amplitude remained constant, after which the pressure amplitude fell to zero at the duct exit. Using the fluctuating pressure-velocity relationship, the fluctuating velocity could be estimated to start with maximum amplitude at the duct ends and decreased slowly towards the combustion zone (region of highest RMS fluctuating pressure). The amplitude of the velocity fluctuations in the combustion region would be dependent on the strength of the buzz.

Whilst the data accumulated from the experiments could not definitively identify the complex mechanism that controlled the buzz process, the foregoing description appears plausible and inter-relates most of the quantitative data available. The volume of data required to complete the description, bearing in mind the necessary spatial and temporal resolutions is formidable and possibly prohibitive.

The flame in a quiescent state spreads out in a wedge shape behind the vee-gutter ($L_h$ < 0.5 m). The area of the flame is approximately constant, as would be the heat release, and the pressure drop through the burnt region of the chamber. Experiments indicate that if the hot length of the duct is extended, then burning becomes unstable. The pressure developed because the burning gas is prevented from expanding sufficiently in a longer duct ($L_h$ > 0.5 m) is unable to be released without oscillation. The momentary overpressure in the duct slows the approach flow down allowing the burnt gas to exit the chamber. As the approach flow decreases, the flame is pushed forward, reducing the flame surface area and therefore slowing the rate of fuel consumption. The resulting reduction of combustion lets the downstream pressure drop, leading to an increase in the inlet flow velocity, ultimately driving the flame back down the duct. This is an oversimplified view neglecting the observed variation of mass flow per unit area through the flame during a cycle (47, 57) of the process, but it does represent a plausible sequence of events. Any change in the parameters of the flow or duct geometry can alter the oscillations.

Increasing the hot duct length beyond a threshold length entraps proportionally more of the expanding gas, building up the oscillating pressure, resulting in large flame movements and heat release fluctuations through the flame area changes. The fluctuating pressure can, with sufficient hot duct length, stop the inlet flow, i.e., when $P' \geq \frac{1}{2}\rho U_o^2$.

Stepping up the inlet flow velocity appears to have a number of possible effects on the oscillation. Firstly, the turbulence of the flow increases, enhancing the burning rate to an unknown extent, and secondly, the higher the inlet velocity the faster the burning slugs of gas move through the duct. The result of the second condition is that gas not completely burnt in the duct will not develop as large a pressure as it could, thus reducing the tendency for strong oscillations. If, as a

result of the first condition the fluctuating heat release only increases slightly, with velocity, then the fluctuating pressure developed will also only increase slightly. The result of this may then be a marginal increase in the fluctuating velocity, but in comparison to the increased mean flow, $u'/\bar{u}$ can decrease as observed, and thus reduce the flame area change, hence heat release rate, which feeds back into the pressure fluctuations. This argument attempts to explain the observed decrease in the buzz amplitude with velocity increase.

Altering the equivalence ratio from a value of 1.0 should reduce the energy release by the flame, resulting in a reduction in the pressure of the hot duct length. The lowering of the downstream pressure then reduces the amplitude of the oscillations.

Extending the cold duct length does not alter the combustion as the other parameters might, but could well change the heat release rate fluctuations through the velocity fluctuations. If the combustion process is not altered by the cold length extension then it can be assumed that the pressure amplitude of the oscillation will not alter, thus the corresponding velocity fluctuations will drop as the distance from the duct inlet to the combustion zone increases. A drop in the fluctuating velocity $u'$ results in lower area changes and thus lower heat release rate fluctuations. The outcome being a general reduction in the buzz oscillation amplitude as observed.

Blockage ratio changes could have two competing effects occurring. At low blockage the flame spreads out from effectively the centreline of the duct, which extends the flame further down the duct before the pressure blockage takes effect. As the blockage goes up the flame starts closer to the wall of the duct shortening the flame length. However, as the blockage is increased the flow velocity around the vee-gutter increases, making it more difficult for a velocity oscillation due to the pressure to change the flame shape.

As previously mentioned, the mechanism is too complex at the moment to describe, but further work could resolve this type of oscillation. Further experimental exercises should be directed towards establishing methods of determining heat release rates in the combustion region. Initially, some version of the infra-red monochromatic radiation absorption (IMRA), used by Lee (47) in his experiments on temperature fluctuations,

coupled with high speed schlieren photography of the combustion, could start to give useful information on heat release. Connect this with local pressure and flow velocity in the combustion region and the basic details of the heat release coupling might begin to appear. If this is successful in at least a rudimentary way, then mapping of the various fluctuating parameters along the duct length would be useful in locating and characterizing the source.

Away from the large scale experimentation previously mentioned, attention should also be placed on attempts at measuring the flame speed changes during the buzz cycle as part of the heat release rate investigation. Work should also be addressed to the two end impedances of the combustion chamber (under flow conditions) to determine the respective energy losses and reflections of the acoustic field. The temperature profile across the duct in the hot region might show the extent of boundary layer burning present in the flame.

In conclusion, future investigations should be directed towards the heat release problem and its interaction with the fluctuating parameters in the flow, both experimentally and theoretically.

# CHAPTER 6

## CONCLUSIONS

An extensive parametric investigation of oscillatory burning in a ducted premixed flame is reported. Important distinctions are observed between oscillations at frequencies which correspond to the principal longitudinal acoustic resonances for the duct, and the violent, large amplitude flame motion which accompanies the low frequency buzz.

Acoustic disturbances were observed under all flow conditions and duct geometries. Whilst the measured frequencies were strongly influenced by changes in duct length, they were only weakly influenced by equivalence ratio and flow velocity. These frequencies are readily predicted by a knowledge of the duct configuration and cover the range of $\sim$150 to $\sim$1000 Hz for the present investigation. Resonant coupling with the flame motion is observed to rely to some degree on the stabiliser position in the duct . Velocity fluctuation at the stabiliser gives rise to cellular disturbances on the flame front, which are discernible in high speed schlieren photography. There does not appear to be any significant connection between these 'high frequency' acoustic oscillations and the more violent and disruptive buzz.

Low frequency ($\lesssim$ 100 Hz) buzz oscillations are initiated only when a minimum length of burning is attained; at least 0.5 m at a flow velocity of 20 m/s. Under such conditions the transient pressure rise cannot be released by flow acceleration and a strong cyclical interaction between approach flow velocity, flame shape and hence heat release rate, is established. With the aid of a detailed frame-by-frame analysis of the high speed cine schlieren, the essential features of this interaction have been diagnosed.

The parametric variation of buzz frequency and amplitude has been systematically explored using pressure measurements from both wall mounted pressure transducers and a travelling microphone probe, as the principal experimental techniques. Buzz frequency was observed to increase when:

- the inlet flow velocity was increased
- the flame stabilizer blockage was increased
- the heat release through the equivalence ratio was maximized
- the cold duct length was decreased.

The amplitude of the disturbance increased when:

- the inlet flow velocity was decreased
- the flame stabilizer reached 30% blockage
- the heat release was maximized by equivalence ratio changes
- the cold and hot duct lengths were increased

These summary observations of the dependence of buzz amplitude and frequency on a wide range of rig and flow parameters are described and discussed fully in Chapters 3 and 5. Taken in conjunction with the finely resolved flow visualisation possible with high speed Schlieren photography, they permit the identification and detailed description of a representative buzz cycle. Buzz emerges to be a strongly coherent phenomenon lending itself to cycle analysis. The observations and measurements support the interpretation of buzz oscillations as comprising a sequence of events in which pressure disturbances influence reactant approach flow velocity, so modifying flame shape and mass burning rate or heat release, changes which result, in turn, in the non-steady influence of confined burning on the pressure field. Some important features of this cyclic behaviour are incorporated in the mathematical model described in Chapter 4.

This simple control volume model of oscillatory burning plausibly predicts most of the principal parametric variations observed experimentally. It describes the conservation of mass and momentum in two linked homogeneous columns of fully burnt gas and unburnt reactant mixture. The burning zone is treated as a narrow, geometrically simple interface, separating the columns. The formulation is closed with the aid of an empirical relationship between fluctuating pressure at the entry to the working section and that at the duct exit. Solution of the energy equation, involving the complex interaction between flow field and heat release is thus avoided but this in turn restricts the details available in comparison with experiments in relation to disturbance amplitude.

The agreement between prediction and experiment is particularly encouraging in respect of the variation of frequency with flow velocity and blockage ratio whilst further possible model refinements are suggested with the insights gained from the wide range of time resolved diagnostics employed in this study.

## REFERENCES


1. S.L. Bragg
*Combustion Noise*
J. of the Institute of Fuel, Jan. 1963, 12.

2. M. Barrère, F.A. Williams
*Comparison of Combustion Instabilities Found in Various Types of Combustion Chambers*
Twelfth Symposium (International) on Combustion, The Combustion Institute, 1969.

3. F.L. Rijke
*On the Vibration of Air in a Tube Open at Both Ends*
Philosophical Magazine, 1859, 17(4), 419.

4. J. Rayleigh
*The Theory of Sound, Volume II*
Dover Publications, second edition, 1945 re-issue.

5. A.A. Putnam, W.R. Dennis
*Organ Pipe Oscillations in a Flame-filled Tube*
Fourth Symposium (International) on Combustion, Williams and Wilkins, 1953.

6. J.K. Kilham, E.G. Jackson, T.J.B. Smith
*Oscillatory Combustion in Tunnel Burners*
Tenth Symposium (International) on Combustion, The Combustion Institute, 1965.

7. P.L. Blackshear
*Driving Standing Waves by Heat Addition*
Fourth Symposium (International) on Combustion, Williams and Wilkins, 1953.

8. P. Morcau, S. Candel, J.M. Piquemal, R. Borghi
*Phenomene d'Instabilite dans un foyer Turbulent*
First Specialists Meeting (Int.) of the Combustion Institute, Bordeaux, July 1981, 13.

9. D. Gorter
*Combustion-driven Oscillation in a 600 MW Power Plant*
Gas Warme International, 1979, 28(1), 24.

10. E.W. Price
*Experimental Solid Rocket Combustion Instability*
Tenth Symposium (International) on Combustion, The Combustion Institute, 1965.

11. L. Crocco
*Research on Combustion Instabilities in Liquid Propellant Rockets*
Twelfth Symposium (International) on Combustion, The Combustion Institute, 1969.

12. H. Ellis, I. Odgers, A.J. Stosick, N. Van de Verg, R.S. Wick
*Experimental Investigation of Combustion Instabilities*
Fourth Symposium (International) on Combustion, Williams and Wilkins, 1953.

13. K. Berman, S.H. Cheney
*Combustion Studies in Rocket Motors*
Jet Propulsion, 1953, 23, 89.

14. L.J. Parker, R.F. Sawyer, A.R. Ganji
*Measurements of Vortex Frequency in a Lean, Premixed Prevaporized Combustor*
Western States Section - Combustion Inst., No. 79-25, Utah, April 1979.

15. P.W. Pitz, J.W. Daily
*Experimental Study of Combustion in a Turbulent Free Shear Layer Formed at a Rearward Facing Step*
AIAA 19th Aerospace Sciences Meeting, Missouri, January 1981.

16. J.O. Keller, L. Vaneveld, D. Korschett, A.F. Ghonivm, J.W. Daily, A.K. Oppenheim
*Mechanism of Instabilities in Turbulent Combustion Leading to Flashback*
AIAA 19th Aerospace Sciences Meeting, Missouri, January 1981.

17. K.D. Mach
*System Aspects of Augmentor Combustion*
AIAA/SAE 7th Propulsion Joint Specialist Conference, Utah, June 1971.

18. J.M. Bonnell, R.L. Marshall, G.T. Riecke
*Combustion Instabilities in Turbojet and Turbofan Augmentors*
AIAA/SAE 7th Propulsion Joint Specialist Conference, Utah, June 1971.

19. G.D. Lewis, G.D. Garrison
*The Role of Acoustic Absorbers in Preventing Combustion Instabilities*
AIAA/SAE 7th Propulsion Joint Specialist Conference, Utah, June 1971.

20. J.S. Lewis
*The Effect of Local Fuel Concentration on Reheat Jet Pipe Vibrations*
Proceedings of International Propulsion Symposium, England, April 1967.

21. A.A. Putnam, W.R. Dennis
*A Study of Burner Oscillations of the Organ Pipe Type*
Transactions of the ASME, January 1953, 15.

22. R.H. Sabersky
*Effect of Wave Propagation in Feedlines on Low Frequency Rocket Instabilities*
Jet Propulsion, 1954, 24, 172.

23. J.M. Pariel, L. De Saint Martin
*Contribution to the Study of Non-steady Combustion in Industrial Hearths*
Twelfth Symposium (International) on Combustion, The Combustion Institute, 1969.

24. H.J. Merk
*An Analysis of Unstable Combustion of Premixed Gases*
Sixth Symposium (International) on Combustion, Reinhold Publishing Co., 1957.

25. F. Mauss, E. Perthuis, B. Salé
*A Contribution to the Study of Low Frequency Oscillations in Fuel-Oil Boilers*
Tenth Symposium (International) on Combustion, The Combustion Institute, 1965.

26. S. Hadvig
*Combustion Instabilities - System Analysis*
J. of the Institute of Fuel, Oct. 1971, 550.

27. N. Fricker, C.A. Roberts
*An Experimental and Theoretical Approach to Combustion Driven Oscillations*
Gas Wärme International, 1979, 28(1), 13.

28. H.J. Merk
*Analysis of Heat Driven Oscillations of Gas Flows*
Part I: Appl. Sci. Res., 1957, A6, 317
Part II: 1957, A6, 402
Part III: 1958, A7, 175
Part IV: 1958, A7, 192
Part V: 1959, A8, 1

29. R. Becker, R. Günther
*The transfer function of Premixed Turbulent Jet Flames*
Thirteenth Symposium (International) on Combustion, The Combustion Institute, 1971.

30. M.W. Thring
*Combustion Oscillations in Industrial Combustion Chambers*
Twelfth Symposium (International) on Combustion, The Combustion Institute, 1969.

31. E.W. Price
*Recent Advances in Solid Propellant Combustion*
Twelfth Symposium (International) on Combustion, The Combustion Institute, 1969.

32. B.D. Mugridge
*Combustion Driven Oscillations*
J. of Sound and Vibration, 1980, 70(3), 437.

33. B.T. Chu
*Analysis of a self-sustained Thermally Driven Non-linear Vibration*
The Physics of Fluids, Nov. 1963, 6(11), 1638.

34. H. Jones
*The Mechanics of Vibrating Flames in Tubes*
Proceedings of the Royal Society, London, 1977, A353, 459.

35. A.A. Putnam, W.R. Dennis
*Some Stability Tests on an Axially Symmetric Combustor*
Sixth Symposium (International) on Combustion, Reinhold Publishing Co., 1957.

36. D.G. Stewart, M.V. Nesbitt
*An Investigation of Oscillations of the Type Found in Ram Jet and Reheat Combustion Chambers*
National Gas Turbine Establishment, Report No. R134, April 1953.

37. A.E. Smart, B. Jones, N.T. Jewell
*Measurements of Unsteady Parameters in a Rig Designed to Study Reheat Combustion Instabilities*
AIAA 14th Aerospace Sciences Meeting, Washington DC, January 1976.

38. K.G.G. Wales
*Model Tests Concerning the Influence of Burning Length on Reheat Combustion Instability*
National Gas Turbine Establishment, Note No. NT 1075, June 1977.

39. H. Clare
*Combustion Roughness with Single Gutterbuilds and Varying Lengths of Reheat Tailpipe*
National Gas Turbine Establishment, Note No. NT 923, March 1974.

40. J.D.P. Hakluytt, J.R. Tilston, M.E. Hussey
*Acoustic Nature of High Amplitude Combustion Oscillations*
National Gas Turbine Establishment, Report No. NT 951, January 1975.

41. M.W. Thring
*A Non-acoustic Theory of Oscillations in Pressure-Jet Oil-Fired Combustion Chambers*
Seventh Symposium (International) on Combustion, Butterworth Scientific Publications, 1959.

42. P.H. Kydd
*Analysis and Experiments on Unsteady Flow in Gas Turbine Main Combustors*
Twelfth Symposium (International) on Combustion, The Combustion Institute, 1969.

43. D.M. Dix, G.E. Smith
*Analysis of Combustion Instabilities in Aircraft Engine Augmenters*
AIAA/SAE 7th Propulsion Joint Specialist Conference, Utah, June 1971.

44. F.E. Marble, S.M. Candel
*An Analytical Study of the Non-Steady Behaviour of Large Combustors*
Seventeenth Symposium (International) on Combustion, The Combustion Institute, 1979.

45. K.J. Lewis, J.B. Moss
*Time Resolved Scalar Measurements in a Confined Turbulent Premixed Flame*
Seventeenth Symposium (International) on Combustion, The Combustion Institute, 1979.

46. A.J. Munday, R.A. Farrar
*An Engineering Data Book*
The MacMillan Press Ltd., 1979.

47. O.K. Lee
*Ph.D. Thesis, to be published.*

48. F.C. Weller
*An Investigation of Ammonia Dissociation in the Platinum Gauze Catalyst Packs of Electrothermal Hydrazine Fuelled Thrusters*
Ph.D. Thesis, Southampton University, 1980.

49. D.W. Holder, R.J. North
*Schlieren Methods*
Notes on Applied Science No. 31, National Physical Laboratory, London, 1963.

50. A. Ballantyne, D.J. Boon, J.B. Moss
*Measurements of Fluctuating Temperature in Open Diffusion Flames Employing Fine Wire Thermocouples*
Southampton University, AASU Memo. No. 76/3, August 1976.

51. H. Schlichting
*Boundary Layer Theory*
Fourth edition, McGraw-Hill Book Co. Ltd., 1960.

52. B.S. Massey
*Mechanics of Fluids*
Third edition, Van Nostrand Reinhold Co., 1975.

53. L.E. Kinsler, A.R. Frey
*Fundamentals of Acoustics*
Second edition, Wiley Ltd., 1962.

54. L.L. Beranek
*Acoustics*
McGraw-Hill Book Co. Ltd., 1954.

55. F.E. Marble, M.V. Subbaiah, S.M. Candel
*Analysis of Low Frequency Disturbances in Afterburners*
AGARD-CP-275 Specialist Meeting, Köln, October 1979.

56. A.F. Seybert, D.F. Ross
*Experimental Determination of Acoustic Properties Using a Two-microphone Random-excitation Technique*
J. Acoustic Society of America, 1977, 61(5), 1362.

57. I.G. Campbell, K.N.C. Bray, J.B. Moss
*Combustion Oscillations in a Ducted Premixed Flame*
Paper submitted to the Inst. Mechanical Engineers International Conference on "Combustion Engineering", April 1983.

58. M. Salikuddin, B.T. Zinn
*Adaption of the Impedance Tube Technique for the Measurement of Combustion Process Admittances*
J. of Sound and Vibration, 1980, 68(1), 119.

## APPENDIX A. Duct Resonances

In this appendix, theoretical and graphical approaches to acoustic resonances in the burner are examined in terms of fluctuating pressure and velocity in both cold and combusting flows.

### A.1 End Conditions of the Duct.

A theoretical expression for the impedance, or pressure-velocity relationship at the ends of the combustion chamber is developed in this section. Figure A.1 presents a schematic diagram of the burner inlet, with cold flow entering the duct in a direction which is defined as positive. Two pressure waves, $p^+$ and $p^-$, represent incident and reflected waves in the end region, where

$$p^+ = Be^{j\omega t_e - j\omega x/c(1 + M)} \tag{A.1}$$

$$p^- = Ae^{j\omega t_e + j\omega x/c(1 - M)} \tag{A.2}$$

where $\omega$ is the oscillation frequency (in radians), $x$ is the distance from the duct entrance, $c$ is the local speed of sound, and $M$ is the Mach number of the inlet flow.

These two pressure waves are of arbitrary frequency $\omega$, and amplitudes A and B. They are both affected by the mean flow in the duct as represented by the modification (Doppler effect) to the speed of sound.

The total fluctuating pressure at any location at the duct inlet for a given frequency is,

$$p' = p^+ + p^- \tag{A.3}$$

while the corresponding fluctuating velocity induced by the pressure is ( ),

$$u' = \frac{p^+}{\rho c} - \frac{p^-}{\rho c} \quad . \tag{A.4}$$

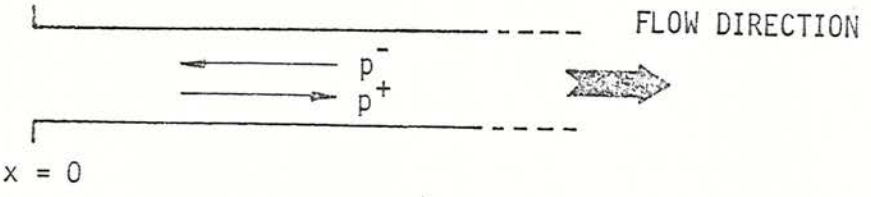


Fig. A.1 Schematic diagram of the duct entrance with pressure waves indicated

Given the large area change between the settling chamber and burner at the duct inlet, the fluctuating pressure is approximately zero for low frequencies satisfying the condition $f < c/4\pi D$ (53) where $c$ is the local speed of sound and $D$ is effective duct diameter. This implies that at $x = 0$, the amplitudes of the two pressure waves sum to zero, thus from equations (A.1) to (A.3),

$$A = -B.$$

Moving into the duct away from the inlet, the pressure fluctuation becomes non-zero, in particular for any value of $x$,

$$p' = A2j \sin \frac{\omega x}{c(1 - M^2)} e^{j\omega t_e + j\omega xM/c(1 - M^2)} \tag{A.5}$$

using equations (A.1) to (A.3). Similarly the fluctuating velocity becomes

$$u' = - \frac{A2}{\rho c} \cos \frac{\omega x}{c(1 - M^2)} e^{j\omega t} e^{+j\omega xM/c(1 - M^2)} \tag{A.6}$$

The impedance, $p'/u'$, generally expressed as

$$\frac{p'}{u'} = \rho c \left(\frac{p^+ + p^-}{p^+ - p^-}\right) \tag{A.7}$$

becomes

$$\frac{p'}{u'} = -j\rho c \tan \frac{\omega x}{c(1 - M^2)} \tag{A.8}$$

for the inlet end of the duct.

The effect of the mean flow on the impedance is to modify the wave number, $\omega/c$, in equation (A.8). At low Mach numbers, $< 0.2$, there are only small modifications to the impedance, however, there is a noticeable Mach number effect on the fluctuating pressure and velocity. The last exponential term in equations (A.5) and (A.6) is dependent on the Mach number and location in the duct. Comparing the phase difference of the pressures at two locations in the duct for a no flow condition, both theory

and experiments show that the two fluctuating pressures will be in phase. However, with flow, analysis reveals that the phase difference between two displaced pressure measurements will increase with increasing Mach number, downstream pressure leading upstream pressure. An example of this can be seen in Fig. 3, where approximately half of the observed phase difference along the duct length can be attributed to "flow" phase shifting.

At the exit of the duct, the same procedure is applied to derive the impedance. The large area change between the duct and open space beyond the burner exit, again defines the pressure fluctuations as zero at $x = L$. Figure A.2 shows a schematic view of the duct exit containing two pressure waves $p^+$ and $p^-$. In this case the mean flow defines a positive direction going out of the duct into atmosphere. Reworking equations (A.1) and (A.2) under these conditions at some position $x$ relative to the duct exit and then substituting the results into equation (A.8) for the impedance, gives:

$$\frac{p'}{u'} = j\rho c \tan \frac{\omega(L - x)}{c(1 - M^2)} . \qquad (A.9)$$

In these two cases the impedance shows the amplitude and phase of the velocity and pressure fluctuations at a single point. The major difference between equations (A.8) and (A.9) is the phase relationship between the fluctuating pressure and velocity. At the duct inlet, the pressure lags velocity by $90^\circ$, while at the duct exit, pressure leads velocity by $90^\circ$. This result reflects the fixed definition of positive flow direction.

These relationships are of particular interest in that they can be used to derive velocity fluctuations from the pressure fluctuations and visa versa. To illustrate this facet of the theory and to show that the equation is correct in the cold gas column, an example is shown in Fig. A.3. The details of the particular experimental conditions are given on the fiqure, together with pressure and velocity spectra, and the phase difference between the two.

Velocity and pressure signals were simultaneously recorded 7.6 cm from the duct inlet during a buzz experiment. The pressure spectrum (plot a) is used to derive the velocity spectrum (plot c), and the results are shown as a dashed line on the velocity spectrum. Also plotted as a dashed line is the theoretical phase difference between the two signals in comparison with the measured phase (plot b).

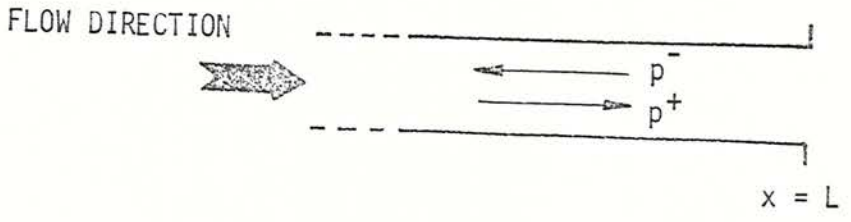


Fig. A.2 Schematic diagram of the duct exit with pressure waves indicated

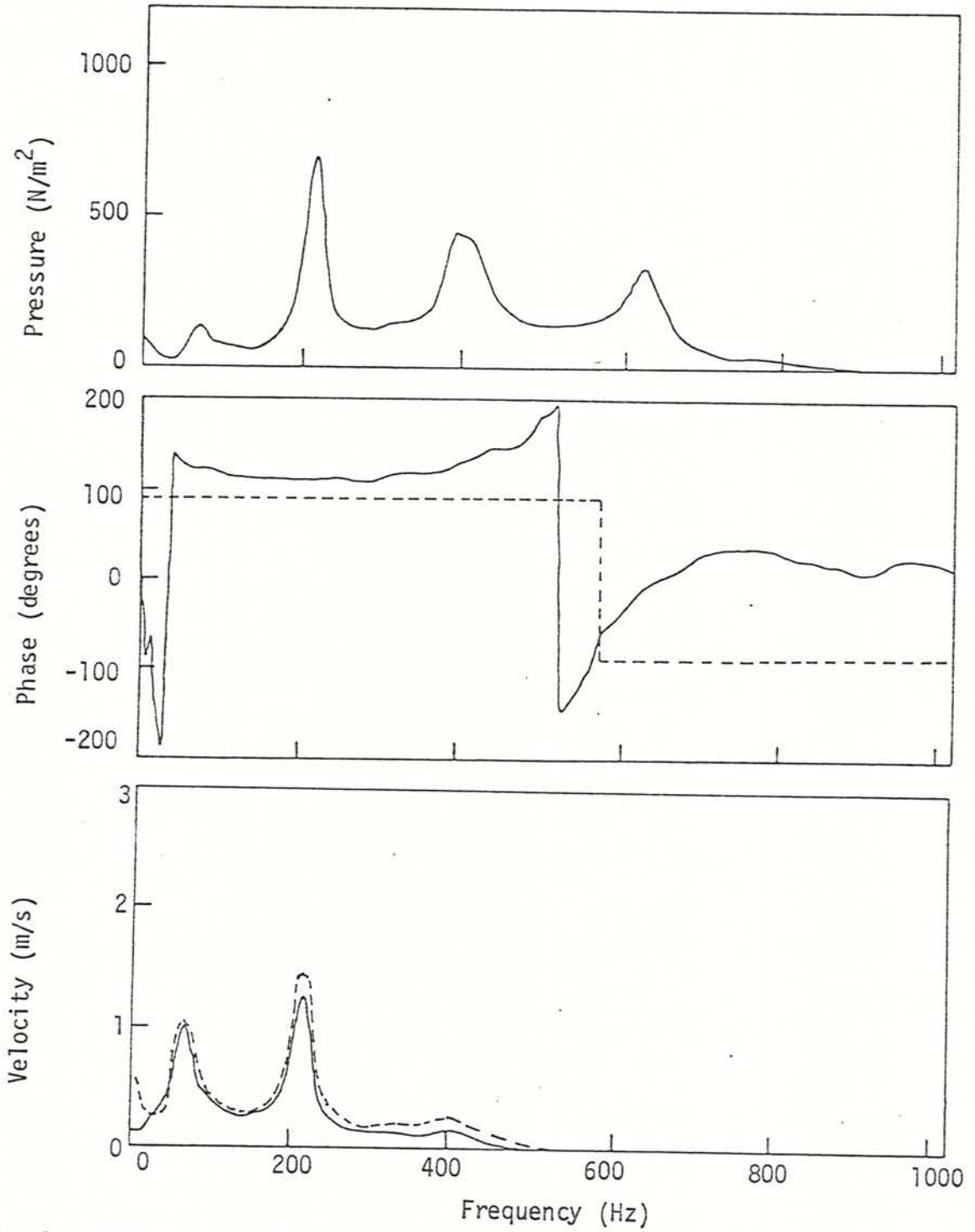


Fig. A.3 Simultaneous RMS inlet pressure and velocity spectra with the phase difference between velocity and pressure (using pressure as reference).
($L_c$ = 0.38 m, $L_h$ = 0.78 m, $U_o$ = 20 m/s, 30% blockage, $\phi$ = 1.15)

The results show a good agreement between the measured and calculated velocity fluctuation. Unfortunately, beyond a frequency of ∿500 Hz, the phase difference begins to show a substantial deviation from theory, and the use of these expressions beyond this frequency is not recommended. The reason for the discrepancy is that at higher frequencies, the shortened wavelength of the oscillation begins to act as a non-plane wave at the duct exit, thus these relationships begin to break down.

## A.2 Cold Flow-Resonances.

Most text books on acoustics give examples of resonant conditions in tubes or ducts in some detail (54). In this section of the appendix, the longitudinal acoustic resonances in the duct with cold flow are briefly reviewed.

Shown in Fig. A.4 is a schematic diagram of a duct, L in length, with a mean gas flow from left to right (flow direction is defined as positive). In the duct are two pressure waves, $p^+$ and $p^-$, defined in section A.1 by equations (A.1) and (A.2). The total fluctuating pressure for any given frequency at either end of the duct is zero.

Following an approach similar to the previous section, application of the condition of zero pressure fluctuations at the duct inlet results in the amplitudes of the two pressure waves being equal but of opposite sign, i.e., A = -B. The second condition of zero pressure fluctuations at the duct exit gives

$$e^{\frac{j\omega L}{c(1-M)}} - e^{\frac{-j\omega L}{c(1+M)}} = 0,$$

This expression is valid only for specific frequencies, i.e., when the frequency satisfies,

$$2j \sin \frac{\omega L}{c(1-M^2)} = 0.$$

This specifies a set of frequencies that comply with the requirement for zero fluctuations at the open ends of the duct.

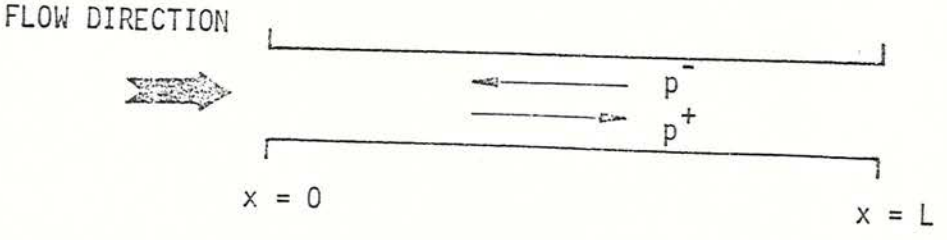


Fig. A.4 Schematic diagram of entire duct with pressure waves indicated

These frequencies are

$$f_n = \frac{nc(1 - M^2)}{2L} \qquad \text{for} \quad n=1, 2, 3 \qquad (A.10)$$

which represent the resonances for a particular duct length and flow velocity, with $n = 1$ being the first harmonic, $n = 2$, the second harmonic, etc.

As an example to confirm this equation, a series of experiments were conducted that involved measuring the pressure fluctuations, in ducts of various lengths, stimulated by a 20 m/s air flow. In Fig. A.4 are displayed the results of the experimental observations and the theoretical predictions. The agreement is good with a variation between experiments and theory of less than 5%.

At these resonant conditions the RMS pressure and velocity amplitudes can be plotted against duct length. Using equations A.5 and A.6, for the first and second harmonics in an arbitrary length duct, the resulting pressure and velocity amplitudes are plotted in Fig. A.6. The flow rate in this case is zero. For both harmonics the amplitude profile shows a rectified sine or cosine wave. The maximum RMS amplitude of one signal always corresponds to the minimum of the other.

## A.3 Combusting Flow.

This section deals with a graphical interpretation of acoustic resonances in a duct with combusting flow. This involves following the path of a pressure wave through the combustion chamber subsequently returning to the origin of the wave.

Referring to the time-distance diagram, Fig. A.7, a pressure wave leaves the entrance to the chamber and travels down the length of the duct at a speed enhanced by the mean flow. The time it takes to travel through the cold and hot lengths of duct are $t_1$ and $t_2$, respectively, given by

$$t_1 = \frac{L_1}{c_u(1 + M_u)}$$

and

$$t_2 = \frac{L_2}{c_b(1 + M_b)}$$

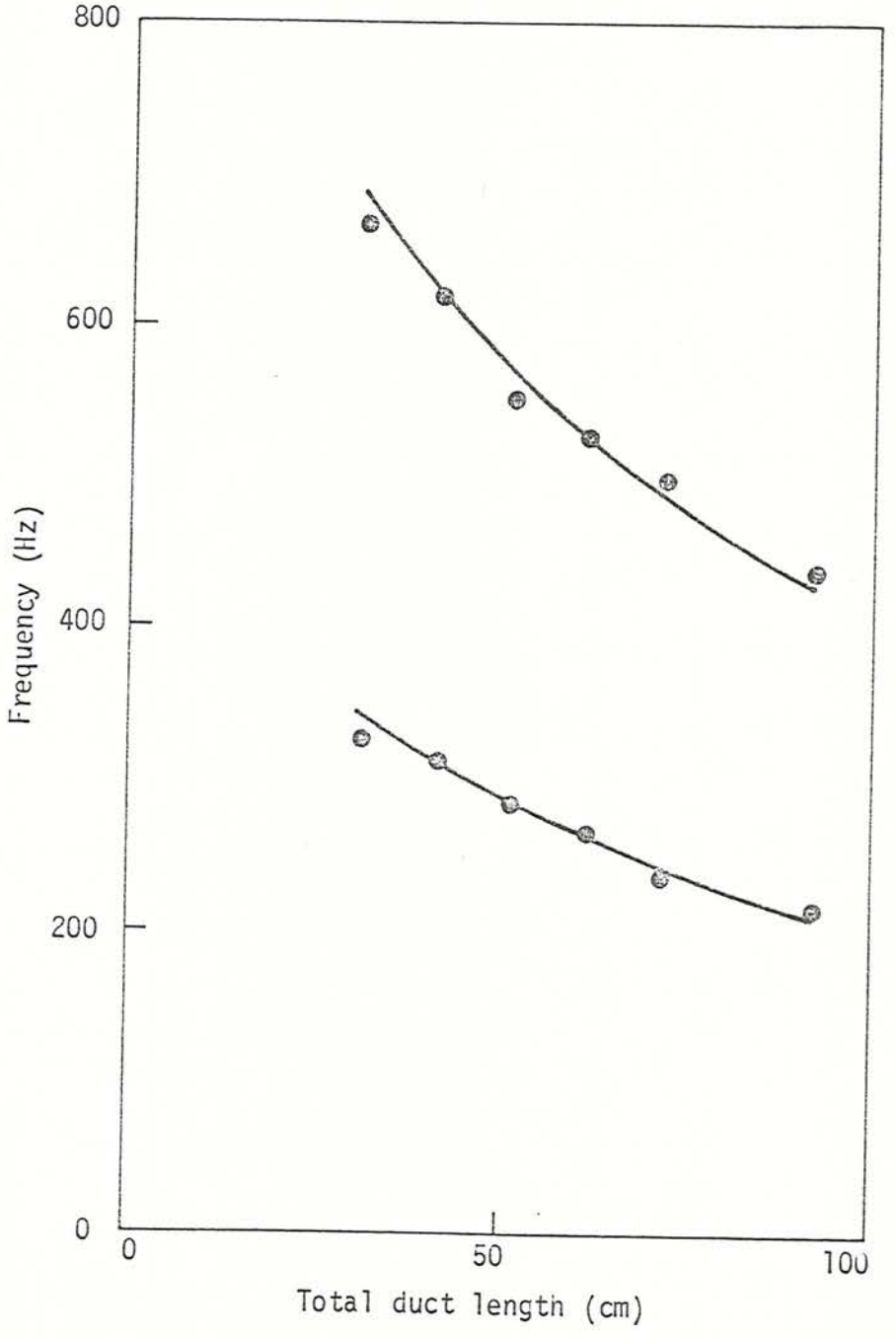


Fig. A.5 Peak frequencies in pressure spectrum for various total duct lengths
($L_h$ = 0.36 m, $U_o$ = 20 m/s, 30% blockage, $\phi$ = 0.0)

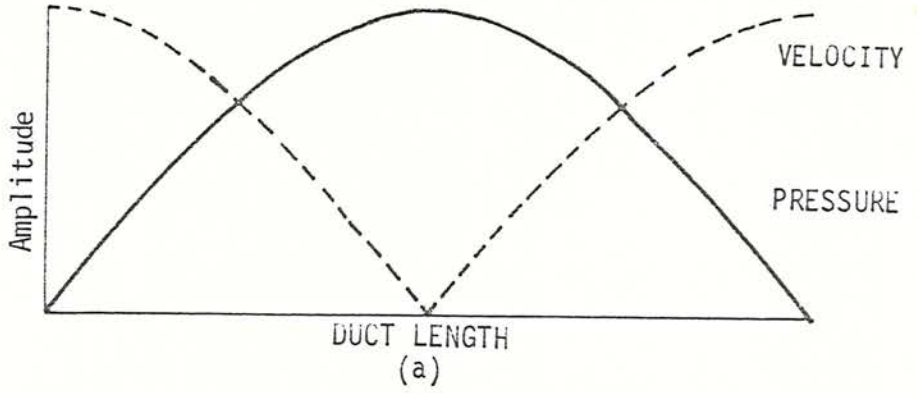


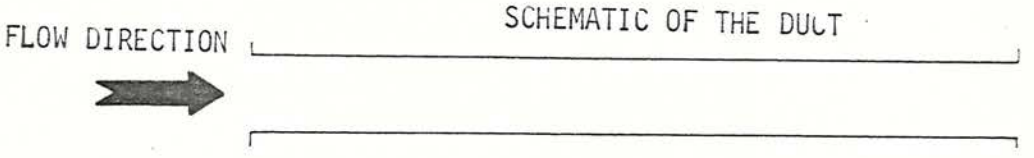


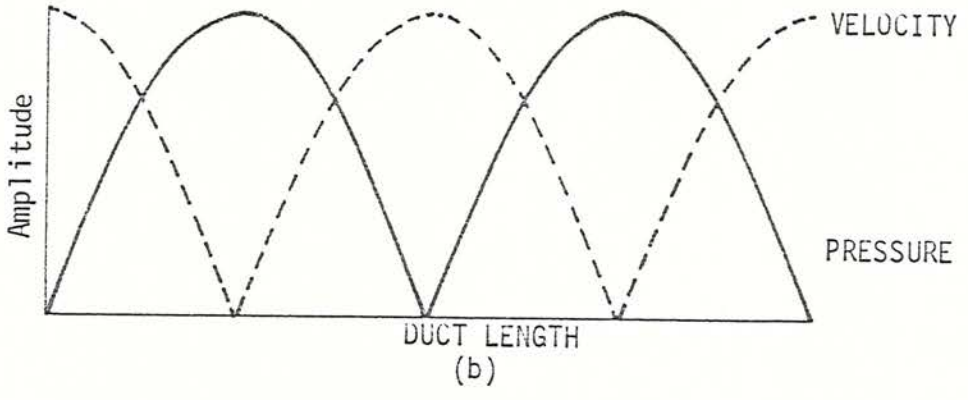


Fig. A.6 Schematic diagram of the duct, subjected to a cold flow, showing the relative RMS pressure and velocity standing waves; (a) first duct harmonic, (b) second duct harmonics.

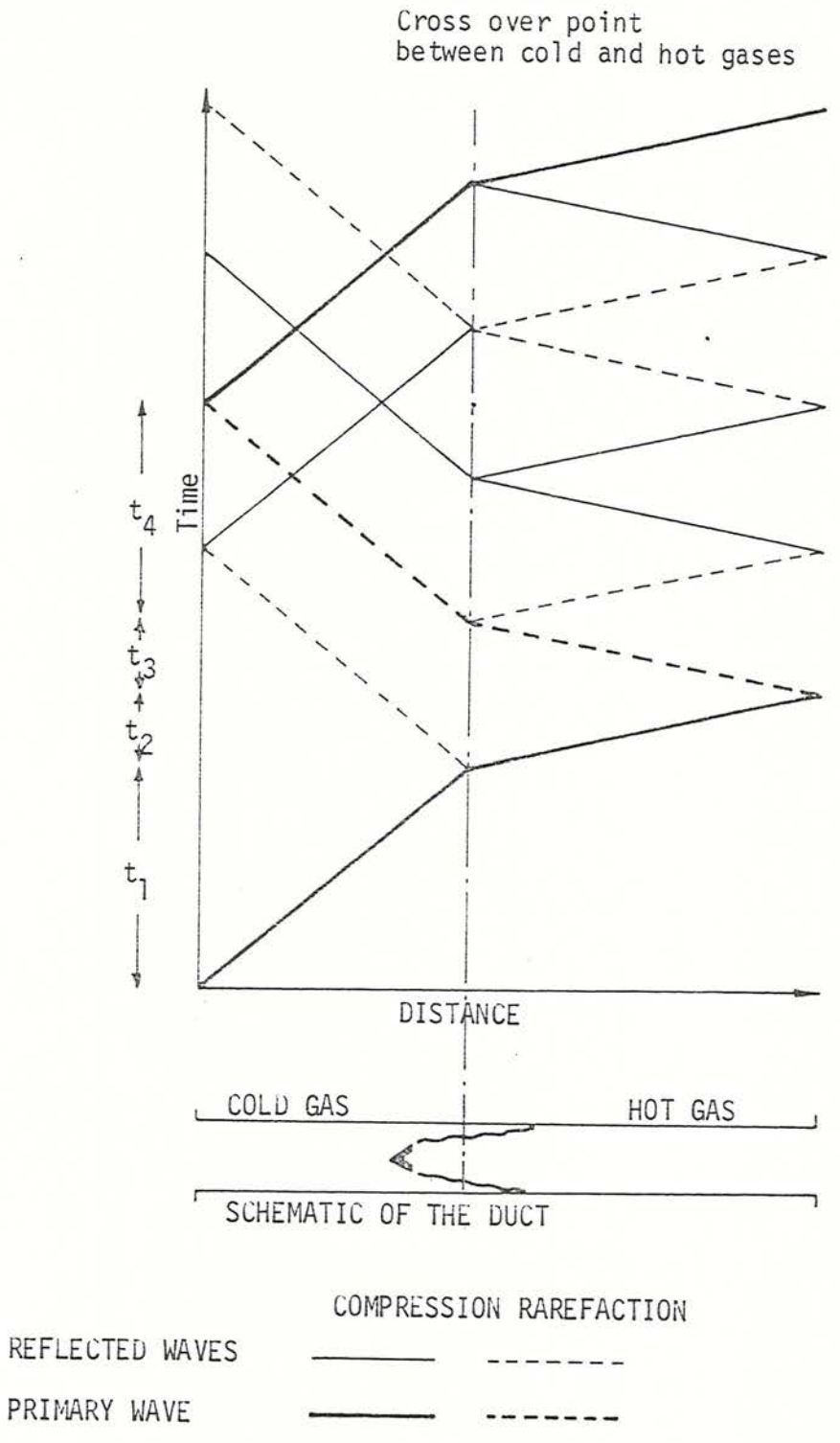


Fig. A.7 Time-distance diagram of pressure waves in a combusting flow

where $L_1$ is the cold length of the duct,

$L_2$ is the hot length of the duct,

$c_u$ is the speed of sound in the cold gas,

$c_b$ is the speed of sound in the hot gas,

$M_u$ is the Mach number of the cold flow,

and $M_b$ is the Mach number of the hot flow.

The passage of the pressure wave through the flame front is assumed to have no effect on the phase of the wave in this type of analysis. However, the amplitude must be affected since part of the wave is reflected back into the cold gas with a phase change of $180^{\circ}$, due to the density change between the two gas columns. With every passage of a pressure wave through the flame front a reflected and transmitted wave are generated.

The return journey of the pressure wave brings it back through the oncoming flow to its point of origin. The times taken to travel back through the hot and cold gas columns are,

$$t_3 = \frac{L_2}{c_b(1 - M_b)}$$

and

$$t_4 = \frac{L_1}{c_u(1 - M_u)} .$$

The total time for a single cycle, not taking into account any possible effects due to the heat release of the flame, is

$$t = \sum_{i=1}^{4} t_1$$

$$= \frac{2L_1}{c_u(1 - M_u^2)} + \frac{2L_2}{c_b(1 - M_b^2)} .$$

Recasting this time of travel as a frequency gives,

$$f_1 = \frac{1}{t} = \tfrac{1}{2} \left[ \frac{1}{\frac{L_1}{c_u(1 - M_u^2)} + \frac{L_2}{c_b(1 - M_b^2)}} \right] \qquad (A.11)$$

with the harmonics of this wave being,

$$f_n = nf_1 \qquad \text{for} \quad n = 1, 2, 3, \ldots.$$

It can be seen that equation (A.10) of the previous section which specified the resonant frequencies in the cold flow, can be derived from equation (A.11), by setting $L_h = 0$. Predictions using equation (A.11) for comparison with observed frequencies in a combusting flow are shown in Fig. 3. . The difference between the experimental points and the calculated frequencies are <20% which is encouraging when it is recalled that the heat release by the flame has not been taken into account in this model.

In order to predict the effect of the flame on the oscillations in a more rigorous manner, the full set of conservation equations coupled with an expression for the heat release rate must be used to link the two gas columns together. The problem, however, remains that some model for the heat release has to be derived before this type of theoretical study is more useful than that used in deriving equation (A.11).